Asymptotic Analysis of Wave Propagation in Regular and Perturbed Helical Springs

Master's Thesis
by
Rasmus Bruus Nielsen
Design of Mechanical Systems
Group 29b, Spring 2011

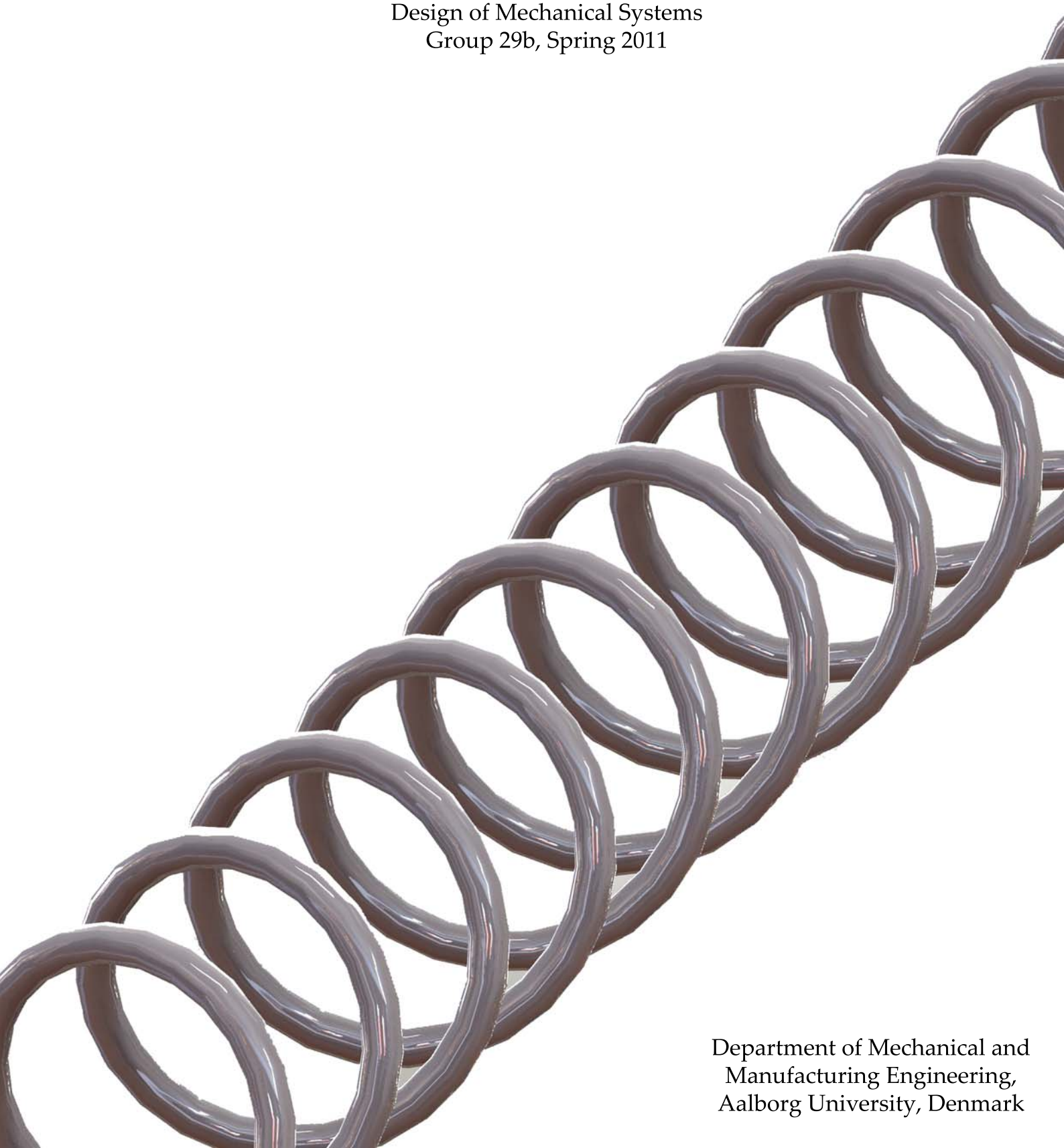

Department of Mechanical and
Manufacturing Engineering,
Aalborg University, Denmark

Aalborg University
Department of Mechanical
& Manufacturing Engineering
Pontoppidanstræde 105
9220 Aalborg Ø
Tel (+45) 9940 9300
Fax (+45) 9815 1675
http://www.m-tech.aau.dk/

Title:

Asymptotic Analysis of Wave Propagation in Regular and Perturbed Helical Springs

Semester theme:
Industrial development work

Project period:
The M-sectors tenth semester
February 1st 2011 – May 31st 2011

Project Group:
29b, DMS10

Participants:
Rasmus Bruus Nielsen

Supervisor:
Professor, Ph.D. Sergey V. Sorokin

Copies: 5

Number of Pages: 69

Rasmus Bruus Nielsen

Preface

This Master's thesis is the result of the work carried out in the period of February 1st to May 31th at the Department of Mechanical and Manufacturing Engineering, Aalborg University. The thesis constitute the 10th semester on the engineering curriculum *Design of Mechanical Systems* offered by the department.

Reaching this final stage of the project has been a fascinating yet challenging exercise where tools and methods has been employed that was new to me. Some of the results, findings, and conclusions in the last few chapters has been obtained in eleventh hour and consequently have not been given the time it really deserves. Nevertheless the I am for sure encourage to further study the topic and carry on with the methodology utilised in this report.

During the project work code and guidance has been received from Alf Søe Knudsen to facilitate the use of the Waveguide Finite Element method which is greatly appreciated.

Some reference are given to the content on the CD in appendix (C) mainly to derivations implemented in Mathematica. A free program that allows for viewing Mathematica notebooks called *CDF Player* can be downloaded from:

`http://www.wolfram.com/cdf-player/`

Aalborg, May 2011

Rasmus Bruus Nielsen

Abstract

This report presents how elastic wave propagation in infinite helical springs of regular and irregular shape can be analysed. In the report focus is given to the understanding and insight in the nature and mechanisms of wave propagation and modal coupling, and consequently analytical tools are mainly utilised to derive explicit formulas and expressions.

Initially the theory of the dynamics of a rod is presented, starting from deriving the Frenet-Serret equations of a spatial curve and a definition of the natural coordinate system. Next geometrical, constitutive, and equilibrium relation are established which are combined to give six governing linear differential equations of second order. The kinematics from the the Timoshenko beam theory will be employed in the derivation, and finally the six general governing equations are found.

Part one of the study constitutes an analysis of free vibrations in a regular helical spring. A dispersion relation is derived which provides the relation between frequency and wave number. In this context nondimensional variables are introduced to overcome difficulties on ill-conditioning. The results presented are regarded as exact, since the governing equations are solved in strong form, even though the roots of the dispersion polynomial is approximated by a polynomial solver.

A study of modal coefficients is presented to identify different modes, and assess the amount of coupling between them. It is found that a helical spring has coupling of modes at low frequencies, but also that these couplings are broken at high frequencies. Additionally the dispersion relation is subjected to an asymptotic analysis to retrieve approximate explicit solutions to cut-on frequencies and wave numbers at high and low frequencies. The result from this analysis facilitates the an assessment of dominant quantities. Consequently it is concluded that asymptotic analysis is a strong tool to gain understanding of the influence of the parameters on the wave propagation in the spring.

Part two presents a study of a corrugated helical spring which entails some peculiarities on the geometrical description of the helix. Different candidate methods for solving the problem is presented and shortly discussed. Namely the Method of Multiple scales and the WKB-approximation both known from classical Perturbation Methods. It is found that certain restrictions needs to be imposed on the corrugation for the problem to be solved by the method of multiple scales. An approach for provoking a solvability condition is presented and a solution is stated in general terms since the explicit version is much too cumbersome to be presented. The solution to the regular helix appears in some sense as the leading order solution to the corrugated helical spring. It is finally concluded that the solution, to the leading order, can only be expected to approximate the real solution within a narrow perturbation range.

Part three briefly presents the basics in the Waveguide Finite Element Method (WFE method) in which advantage is taken on the robustness of the FE method to determine stiffness and inertia properties of geometrically complicated structures and how this is exploited to predict the wave propagation in infinite periodic structures. The purpose is to make comparison to the analytical solutions. A FE model is generated in *ANSYS* and the stiffness and mass matrix is imported into *MatLab* where the calculations are performed. The results from the analytical methods are lastly compared to the results from the WFE analysis. Good agreement is found between the analytical method and the WFE for the conventional helix, while it turns out to be more troublesome to assess the validity of the analytical solution for the perturbed helix due to the narrow perturbation range.

Contents

Chapter

1

Introduction

This masters thesis presents methods and results for analysing the dynamics of rods with spatial curvature. The dynamics of rods is a classic study in mechanical engineering, and the subject has received much attention and particularly the case of straight rods is well understood and can be managed analytically, Rao [2004]. Also many publications exist on both planar and spatial curved rods. However, it seems that a numerical approach is preferred over an analytical approach, B. Tabarrak [1988], G. Karami [1990], Mottershead [1980]. The aim of the work presented in this report is to gain insight and understanding of how waves propagate and couple in a spatially curved rod. This motivates for putting emphasis on analytical methods and tools prior to numerical. The advantages of gaining knowledge on the topic are relevant in many engineering applications where fatigue and acoustic properties of rods subjected to time-dependent loading are essential. For instance in suspension systems where helical springs are used as vibration isolator in e.g. cars, compressors, and pumps, but also in thick-walled piping systems, or any other application where vibrating machinery is connected to the surroundings via long slender curved structural elements.

The project is suggested by Christian Svendsen, R&D Manager at SECOP GmbH, who manufactures household compressors where helical springs serve as a vibration isolator between the oscillating parts and a hermetic shell. In this industry a low noise level is a direct sales parameter which makes the project industrially relevant. The project does not aim at completely solving the problem, but merely, roughly speaking, supply the first half of the result, namely the free field solution.

A rod as a structural element should be thought of as a long slender element—a well known item from basic mechanics of materials that supports flexural, torsional, axial, and shear deformation. It utilises the plane cross-section assumption which reduces the complexity of the governing equations, as compared to the general elastodynamics. Indeed this is in good agreement with the fact that analytical methods are preferred prior numerical, since the simpler governing equations, most likely, will facilitate analysis of more complex cases.

The cases of spatial rods to be handled will be helical springs of regular and irregular shape like shown in figure 1.1 and 1.2. A conventional helical spring is indeed a case of a spatially curved rod, but of regular shape. I.e. the geometry does not change with any spatial coordinate, while for a helical spring of irregular shape, say for instance a conical or corrugated spring, the geometry changes with a spatial coordinate. Both kinds can be considered as helical springs, but they the represent two different levels of complexity when it comes to irregular geometry.

Several papers exist on the dynamics of helical springs. In Wittrick [1966] an analogy to an helical spring is made and analysed for low frequencies, and also the case of a helical spring, but with small pitch angles. In Sorokin [2009] the dispersion diagram is studied where the rod has been given both Bernoulli-Euler kinematics and the more general Timoshenko kinematics. Comparison is made on the exact solutions of these theories and it is concluded that the Tim-

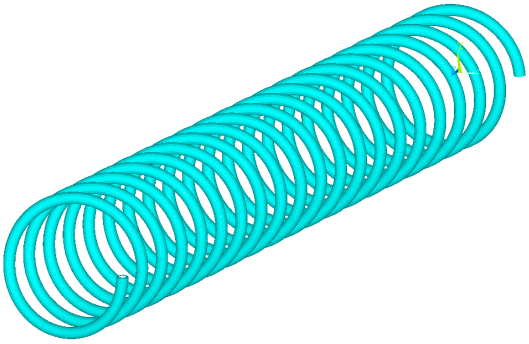

Figure 1.1: *Helical spring of regular shape.*

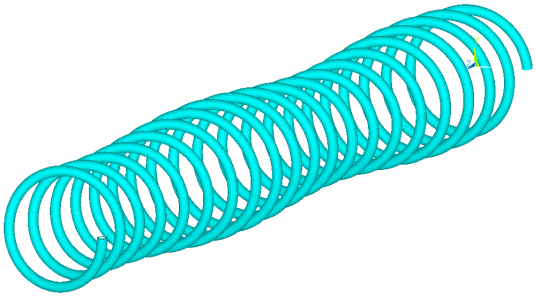

Figure 1.2: *Helical spring of irregular shape*

oshenko beam theory in general is the most accurate. The work presented in this report will be in line with Sorokin [2009], but solely utilise Timoshenko beam kinematics.

1.1 Preliminary considerations

A spatial rod is modelled by a centerline described by a parametric curve just as for the conventional beams. The rod will be given the Timoshenko beams kinematics c.f. the discussion in the previous section since this will provide the most general deformation state within rod theory utilising the plane cross-section assumption.

One restriction imposed on the governing equations for the spatial that the cross-section do not twist along the parametric curve. The effect of twisted rod could also constitute an interesting topic, however, in the context of studying impact of spatial curvature on wave propagation it is not considered as relevant.

Regarding boundary conditions it is chosen to study springs with infinite length. This will have the implication that the waves will be either travelling or evanescent and not standing. I.e. the *free field solution* will be studied. This can be seen as the first part of finding the response of a finite structure where the second part is the *boundary integral equations methods*. This method uses the free field solution to accounts for the boundary conditions. So effectively it builds the standing waves based on the solution for the travelling waves. This also means that this study effectively is a study of free vibrations of a conservative system and that the excitation happened infinitely long time ago. Consequently no transient effects will be captured and also no absolute values of oscillations can be determined, but only the magnitude of a wave amplitude relative to another wave amplitude.

Chapter

2

Project Outline

This chapter states the main questions that must be answered through the project and what approach will be taken to accomplish this.

Based on the discussions in the introduction the following questions is articulated to initiate the work. Through the analyses presented in the succeeding chapters the following must be answered:

For helical springs of regular and irregular shape:

- *How can wave propagation be predicted using analytical methods?*
- *What impact does the spatial curvature have on the dispersive properties of the elastic waves and their modal coupling?*
- *What analytical methods are available for studying wave propagation in the spring of irregular shape and what restrictions needs to be imposed?*
- *How can finite element software be exploited to study wave propagation in infinite periodic structures and how does the results compare with the analytical methods?*

Wave propagation in elastic structures is an extensive subject and the work presented in this thesis is in no way exhaustive. It is therefore pointed out that the thesis more aims at presented analytical methods for assessing like problems, what results and conclusions can be retrieved, and how the results can be compared to numerical results in order to assess the validity of the mathematical models.

2.1 Overall approach

Before proceeding to the mathematical analysis the overall approach and content of the report is briefly presented and discussed in words. The content can be summarised by the following main points:

- The dynamics of any spatial rod can be described by the solution to six governing differential equations. These will be derived since they are the basis for the analysis. A brief inspection of these shows that for spatial rods of regular shape the governing equations

have constant coefficients, while for spatial rods of irregular shape they will have spatially varying coefficients.

- The problem of wave propagation in a conventional helical spring (considered a case of regular shape) can be solved using standard methods for solving differential equations. The solution describes free vibrations of an infinitely long helical spring at varies frequencies. The main result from this analysis is the *dispersion equation* which constitutes a relation between frequency and wave number.
- The dispersion equation is subjected to *asymptotic analysis* which is a tool to identify dominant parameters and thereby obtain approximate explicit solutions. The results from the application of this highly facilitates the understanding of wave propagation.
- A perturbed helical spring (a case of irregular shape) will be analysed afterwards. The exact analytical solution is not available for this case, but approximate solution can be found using *methods of multiple scales*.
- Finally some comparison is done via results determined from a finite element approach.

Chapter

3

Governing equation for spatial rods

This chapter is devoted to derive and give and appropriate overview over the governing equations for a spatially curved rod. The derivation is completely general in terms of geometry. After the governing equations are derived they are recast into Lamé-type *equations since this is convenient for the following chapters.*

The governing equations for spatially curved are derived from geometric relations, constitutive relations, and equilibrium equations, just as in any other problem related to elasticity.

The primitive variables are forces, moments, displacements and rotations and in general there will be three of each which requires 12 governing equations. The corresponding relations that must be derived can be listed as follows:

- 3 moment constitutive equations: these links changes in curvature to internal moments
- 3 force constitutive equations: these links strains to internal forces
- 3 moment equilibrium equations: these links internal moments to rotations
- 3 force equilibrium equations: these links internal forces to displacements

Since the geometry is complex attention will first be drawn to determine two auxiliary equations that relates curvature changes and strains to displacements and rotations. This requires a preliminary study of spatial curves.

A spatial curve can be represented by either an equation or a parameterised vector function. It seems to be the common choice to choose a parameterised vector function representation where the arc length is the parameter, since this is a physically measurable quantity.

An essential ingredient in the study of spatial curves is the choice of coordinate systems. Three different systems are useful here. These are:

Frenet Frame: A local coordinate system located on the curve and controlled by the curvature and twist of the curve. Has the base $\vec{t}$, $\vec{n}$, and $\vec{b}$.

Principal Frame: A local coordinate system located on the curve and follows the inertial axis of the rod. Has the base $\vec{i}$, $\vec{j}$, and $\vec{k}$, and the origin coincides with the origin of the Frenet frame.

Global Frame: The coordinate frame in which the curve is drawn. Has the axis x, y, and z.

The inertial properties (i.e. moment of inertia, cross sectional area, etc.) of a spatial rod are most easily dealt with in the local principal coordinate system since these are constant along the rod as long as the cross-section is kept constant. This motivates for defining displacements and rotations in the principal frame as well. However, as will be discussed later in this chapter, the Frenet frame and the principal frame coincides as long as the cross-section is circular, which simplifies matters.

3.1 Geometrical relations for spatial parametric curves

To describe the geometry and kinematics for any spatially curved parametric function, the arbitrary vector function $\vec{r}(s)$ where s is the arc length is considered in this section. A representation is illustrated in figure 3.1.

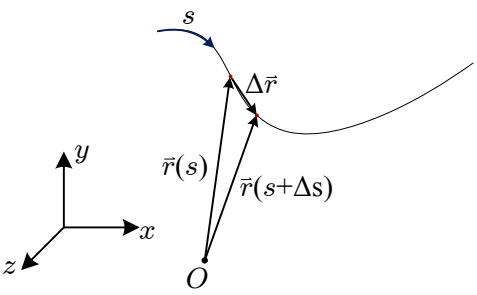

Figure 3.1: *Spatial curve and how the tangent vector is constructed.*

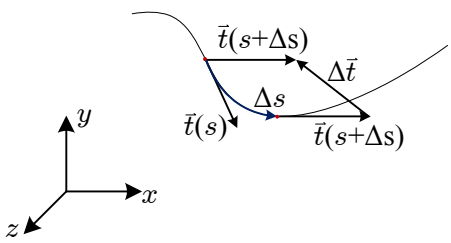

Figure 3.2: *The tangent vector at two different locations separated by the distance Δs. The tangent vector at $s+\Delta s$ is transferred to s.*

For the spatial parametric vector function the tangential vector, referring to figure 3.1, is defined as the derivative of the function:

$$\lim_{\Delta s \to 0} \frac{\Delta \vec{r}}{\Delta s} = \frac{d\vec{r}}{ds} = \vec{t} \tag{3.1}$$

where: $\vec{t}$ Tangential vector.

By definition $\vec{t}$ is unity since the length of $\Delta\vec{r}$ approaches the cord length in the limit. Similarly the change in $\vec{t}$ as a function of s can be investigated as shown in figure 3.2 and taking the limit:

$$\lim_{\Delta s \to 0} \frac{\Delta \vec{t}}{\Delta s} = \frac{d\vec{t}}{ds} = \kappa \vec{n} \tag{3.2}$$

where: κ Principal curvature.

$\vec{n}$ Principal normal vector.

By definition $\left|\frac{d\vec{t}}{ds}\right| = \kappa$ and therefore $\vec{n}$ is a unit vector. The vectors $\vec{t}$ and $\vec{n}$ are perpendicular, which is seen by applying the product rule to two arbitrary vector functions:

$$(\vec{r}_1 \cdot \vec{r}_2)' = \text{const} \qquad \Rightarrow \qquad \vec{r}_1' \vec{r}_2 + \vec{r}_1 \vec{r}_2' = 0 \tag{3.3}$$

And then by substituting $\vec{r}_1 = \vec{r}_2 = \vec{t}$ it becomes clear that $\vec{t}$ and $\vec{n}$ are orthogonal, since one end up having:

$$2\vec{t}\vec{t}' = 0 \tag{3.4}$$

More comments on the nature of curvature are given later. Lastly a third vector is introduced:

$$\vec{b} = \vec{t} \times \vec{n} \tag{3.5}$$

where: $\vec{b}$ Binormal vector.

These vectors, $\vec{t}$, $\vec{n}$, and $\vec{b}$, designated tangent vector, normal vector, and binormal vector, constitute the *Frenet-Serret* frame or alternatively just the *Frenet* frame. The Frenet frame is according to Anca Ignat [2000] a common choice of reference system in mechanics of spatial rods. It should be emphasised that as the frame travels along the curve the orientation of $\vec{t}$, $\vec{n}$, and $\vec{b}$ changes and therefore are functions of s and that all three vectors are unity and mutually orthogonal.

The rotation around $\vec{t}$ of this frame along the curve is denoted the torsion. By considering the angular change, $\Delta\vartheta$, of the binormal vector as a function of s an expression for torsion can be obtained:

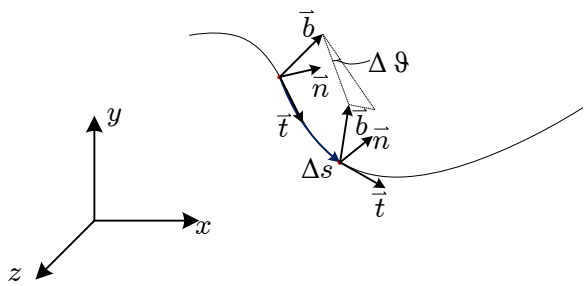

Figure 3.3: *Illustration of the angle formed by the binormal vector over the distance Δs along the curve.*

$$\lim_{\Delta s \to 0} \frac{\Delta\vartheta}{\Delta s} = \tau \tag{3.6}$$

where: τ Torsion.

$\Delta\vartheta$ Angle formed by $b(s)$ and $b(s+\Delta s)$.

This motivates for stating the *Frenet-Serret equations* which constitutes a basic set of identities in differential geometry for spatial curves. To fully derive those the properties of the derivative of $\vec{b}$ is further investigated. Since it is known that $\vec{t} \cdot \vec{b} = 0$, then by taking the derivative:

$$\frac{d\vec{t}}{ds}\vec{b} + \vec{t}\frac{d\vec{b}}{ds} = 0 \tag{3.7}$$

Substitution of equation (3.1) yields:

$$\kappa \vec{n}\vec{b} + \vec{t}\frac{d\vec{b}}{ds} = 0 \tag{3.8}$$

Since the vectors $\vec{b}$ and $\vec{n}$ are orthogonal equation (3.8) reduces to:

$$\vec{t}\frac{d\vec{b}}{ds} = 0 \tag{3.9}$$

Evidently $\frac{d\vec{b}}{ds}$ is parallel to $\vec{n}$ since it is orthogonal to both $\vec{t}$ and $\vec{b}$. As this is the case, the definition of torsion given in equation (3.6) can be rewritten to:

$$\frac{d\vec{b}}{ds} = -\tau\vec{n} \tag{3.10}$$

Remark that a negative sign is introduced. This is only just by definition and therefore somehow arbitrary. Torsion can be both positive and negative whereas curvature is solely positive or zero. Remarks on the understanding of torsion is given later.

Finally the last of the Frenet-Serret equations are derived by considering $\vec{n}$ as the cross product of $\vec{b}$ and $\vec{t}$ and taking the derivative:

$$\vec{n} = \vec{b} \times \vec{t} \qquad \Rightarrow \qquad \frac{d\vec{n}}{ds} = \frac{d\vec{b}}{ds} \times \vec{t} + \vec{b} \times \frac{d\vec{t}}{ds} = -\tau\vec{n} \times \vec{t} + \kappa\vec{b} \times \vec{n} \tag{3.11}$$

Then, since $\vec{t} = -\vec{b} \times \vec{n}$ and $\vec{b} = -\vec{n} \times \vec{t}$, (3.11) reduces to:

$$\frac{d\vec{n}}{ds} = -\kappa\vec{t} + \tau\vec{b} \tag{3.12}$$

The Frenet-Serret equations can now be stated as:

$$\frac{d\vec{t}}{ds} = \kappa\vec{n} \tag{3.13a}$$

$$\frac{d\vec{b}}{ds} = -\tau\vec{n} \tag{3.13b}$$

$$\frac{d\vec{n}}{ds} = -\kappa\vec{t} + \tau\vec{b} \tag{3.13c}$$

These equations relates the base vectors for the Frenet frame to the curvature and torsion. This means that for two differential functions for τ and κ the curve is completely defined by the solution to the Frenet-Serret equations.

A vector is now introduced to describe the full curvature-twist property of a spatial curve. This is denoted the *Darboux vector*. The following general expression is taken initially:

$$\vec{\omega} = \omega_1\vec{t} + \omega_2\vec{n} + \omega_3\vec{b} \tag{3.14}$$

A closer look into the components of the Darboux vector gives an appealing interpretation of twist and curvature. First it is noted that the cross product of equation (3.14) with $\vec{t}$ yields:

$$\vec{\omega} \times \vec{t} = \omega_1 \vec{t} \times \vec{t} + \omega_2 \vec{n} \times \vec{t} + \omega_3 \vec{b} \times \vec{t} \tag{3.15}$$

The LHS can be interpreted as the linear velocity $\frac{\partial \vec{t}}{\partial s}$, a discussion and a proof of this is found in appendix A. The result in this appendix is an important tool when working with multiple rotating frames. From here it follows that:

$$\frac{\partial \vec{t}}{\partial s} = \kappa \vec{n} = -\omega_2 \vec{b} + \omega_3 \vec{n} \tag{3.16}$$

Due to the linear independence of $\vec{b}$ and $\vec{n}$ it can be concluded that $\omega_2 = 0$. Which leads to $\omega_3 = \kappa$. Similarly by taking the cross product of equation (3.14) and $\vec{b}$:

$$\vec{\omega} \times \vec{b} = \omega_1 \vec{t} \times \vec{b} + \omega_2 \vec{n} \times \vec{b} + \omega_3 \vec{b} \times \vec{b} \qquad \Rightarrow \tag{3.17}$$

$$-\tau \vec{n} = -\omega_1 \vec{n} + \omega_2 \vec{t} \tag{3.18}$$

Which again confirm that $\omega_2 = 0$ and additionally that $\omega_1 = \tau$. Therefore the Darboux vector can finally stated as:

$$\vec{\omega} = \tau \vec{t} + \kappa \vec{b} \tag{3.19}$$

The Darboux vector is a helpful tool to understand the nature of curvature and torsion of a spatial curve. It shows that the twist τ is a measure of how much the Frenet frame rotates around the tangent vector, and that the curvature κ is the rotation of the Frenet frame around the binormal vector.

Now when the description of the initial geometry is in place, one must be able to describe the deflections and rotations when the rod experiences deformation. The total displacement can be partitioned into a translational component and a rotational component. The translational component, illustrated in figure 3.4, can be written:

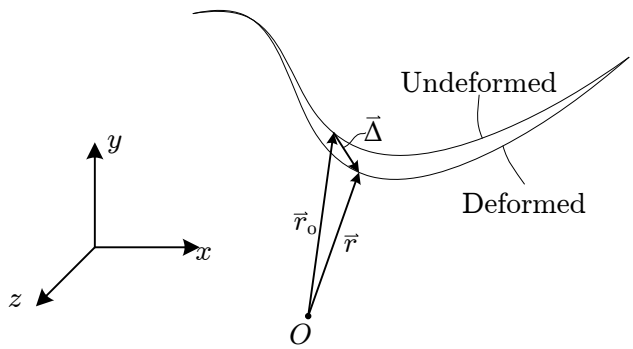

Figure 3.4: *A deformed and undeformed rod where a point is separated by the displacement vector.*

$$\vec{\Delta} = u\vec{i}_0 + v\vec{j}_0 + w\vec{k}_0 \tag{3.20}$$

where: $\vec{\Delta}$ Translation vector when the rod deforms.

u, v, w Translation in x, y, z respectively.

Subscript zero refers to the undeformed geometry. Remark also that $\vec{\Delta}$ is defined in the principal frame. Similarly the rotational components is defined as:

$$\vec{\theta} = \alpha\vec{i}_0 + \beta\vec{j}_0 + \gamma\vec{k}_0 \tag{3.21}$$

where: $\vec{\theta}$ Rotational vector when the rod deforms.

α, β, γ Angles of rotation.

Identically the curvature for the undeformed rod in the principal frame is defined as:

$$\vec{\Omega}_0 = p_0\vec{i}_0 + q_0\vec{j}_0 + r_0\vec{k}_0 \tag{3.22}$$

where: p_0, q_0, r_0 Principal curvatures.

From figure 3.4 it is seen that:

$$\vec{r} = \vec{r}_0 + \vec{\Delta} \tag{3.23}$$

And similarly:

$$\vec{\Omega} = \vec{\Omega}_0 + \delta\vec{\Omega} \tag{3.24}$$

where: $\vec{\Omega}$ Curvature-twist vector of the deformed rod.

$\delta\vec{\Omega}$ Change in curvature-twist from the undeformed to deformed geometry.

To express the changes in curvature $\delta\vec{\Omega}$, the interpretation provided by the Darboux vector is helpful since this states that the curvature and twist are measures of rotation around the binormal and tangential vector respectively. Thus the changes in curvature is the derivative of the rotation vector wrt. s. Hence, using the result from appendix A, $\delta\vec{\Omega}$ can be expressed by:

$$\delta\vec{\Omega} = \frac{\partial\vec{\theta}}{\partial s} = \frac{\partial\vec{\theta}_1}{\partial s} + \vec{\Omega}_0 \times \vec{\theta} \tag{3.25}$$

Here the change in curvature and twist is fully defined by the rotations due to deformations.

To determine the internal forces $Q_{\vec{i}}$, $Q_{\vec{j}}$, and $N_{\vec{k}}$ expression for the strains $\gamma_{\vec{k}\vec{i}}$, $\gamma_{\vec{k}\vec{j}}$, and $\varepsilon_{\vec{k}\vec{k}}$ must be known. However, one must be careful to distinguish between deformation and due to shear and bending. This is illustrated in figure 3.5. The strains can be written:

$$\gamma_{\vec{k}\vec{i}} = \frac{\partial u}{\partial s} - \beta \tag{3.26}$$

$$\gamma_{\vec{k}\vec{j}} = \frac{\partial v}{\partial s} - \alpha \tag{3.27}$$

$$\varepsilon_{\vec{k}\vec{k}} = \frac{\partial w}{\partial s} \tag{3.28}$$

Which in vector notation can be written:

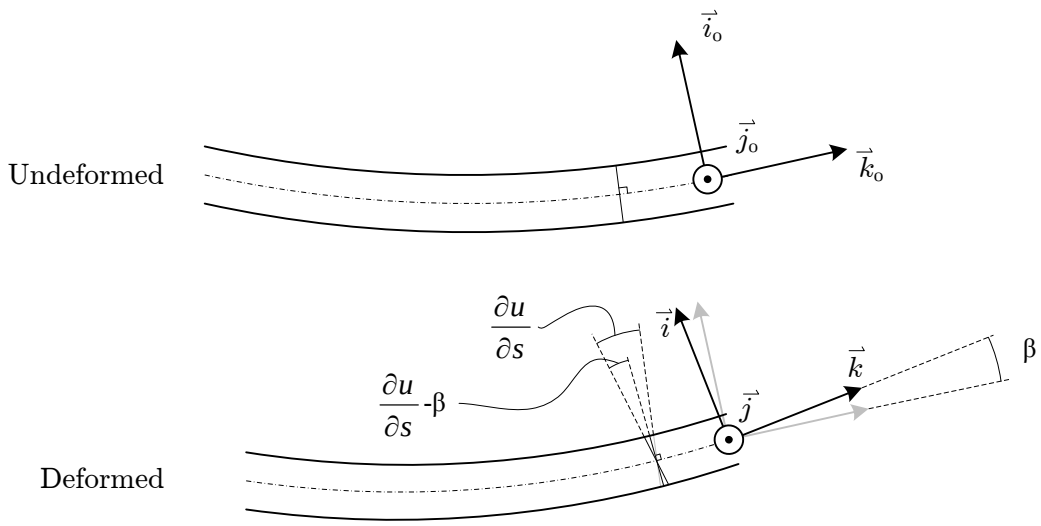

Figure 3.5: *A rod before and after deformation. The principal frame and cross sectional normal from the undeformed rod is transferred to the deformed rod in grey.*

$$\vec{\epsilon} = \frac{\partial \Delta}{\partial s} + \vec{k}_0 \times \vec{\theta} \tag{3.29}$$

$$= \frac{\partial \Delta_1}{\partial s} + \vec{\Omega}_0 \times \vec{\Delta} + \vec{k}_0 \times \vec{\theta} \tag{3.30}$$

In this section the geometrical features of a spatial curve has been investigated, and expressions for strains and changes in curvature are obtained. This makes formula (3.25) and (3.30) the main results from this section.

3.2 Equilibrium and Constitutive relations for spatial rods

The equilibrium equations must be derived from the global coordinate system since equilibrium must be achieve on a global level. The derivations is done in accordance with figure 3.6 for the force and moment equilibrium, respectively. By considering a small piece of a spatially curved rod subjected to body forces and moments, and internal forces and moments the following equilibrium equations are derived:

$$\vec{F} + \frac{\partial \vec{F}}{\partial s} ds - \vec{F} + \vec{f} ds = \rho A \frac{\partial^2 \vec{\Delta}}{\partial t^2} ds \qquad \Rightarrow \tag{3.31}$$

$$\frac{\partial \vec{F}}{\partial s} + \vec{f} = \rho A \frac{\partial^2 \vec{\Delta}}{\partial t^2} \qquad \Rightarrow \tag{3.32}$$

$$\frac{d\vec{F}_1}{ds} + \vec{\Omega}_0 \times \vec{F} + \vec{f} = \rho A \frac{d^2 \vec{\Delta}}{dt^2} \tag{3.33}$$

where:

$\vec{F}$	Internal forces.
$\vec{f}$	Body forces on the rod.
ρ	Density of rod.
A	Cross sectional area of rod.

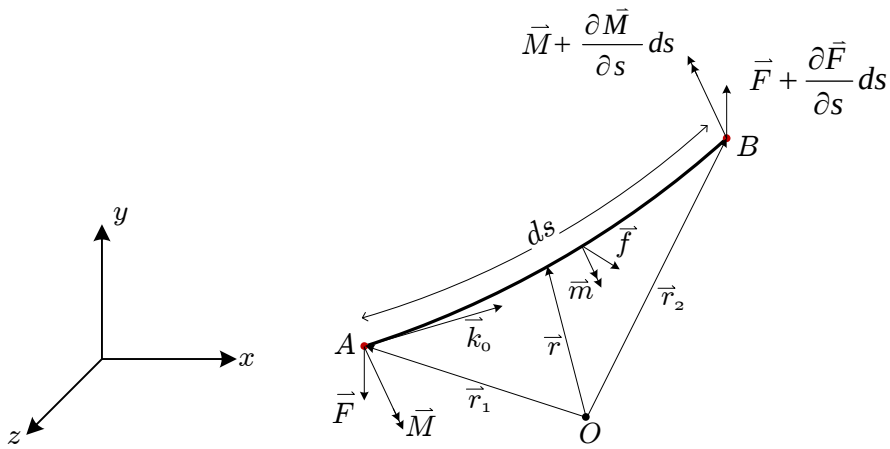

Figure 3.6: *An incremental piece of the rod with internal forces and moments, and body forces and moments.*

By performing moment equilibrium about point B the following is obtained:

$$\vec{M} + d\vec{M} - \vec{M} + \left(-\vec{k}_0 ds\right) \times \left(-\vec{F}\right) + \vec{m} ds = \rho \underline{I} \frac{d^2\vec{\theta}}{dt^2} ds \qquad \Rightarrow \tag{3.34}$$

$$\frac{d\vec{M}}{ds} + \vec{k}_0 \times \vec{F} + \vec{m} = \rho \underline{I} \frac{d^2\vec{\theta}}{dt^2} \qquad \Rightarrow \tag{3.35}$$

$$\frac{d\vec{M}_1}{ds} + \vec{\Omega}_0 \times \vec{M} + \vec{k}_0 \times \vec{F} + \vec{m} = \rho \underline{I} \frac{d^2\vec{\theta}}{dt^2} \tag{3.36}$$

where: $\vec{M}$ Internal moments.

$\vec{m}$ Body moments on the rod.

$\underline{I}$ Area moment of inertia of rod.

Constitutive relations are introduced according to the linear theory of elasticity, i.e.:

$$\vec{M} = \underline{J} \delta \vec{\Omega} \tag{3.37}$$

$$\vec{F} = \underline{K} \vec{\epsilon} \tag{3.38}$$

where: $\underline{J}$ Bending and torsion stiffness matrix.

$\underline{K}$ Shear and Extension stiffness matrix.

The stiffness are defined in the framework of Timoshenko theory as:

$$\underline{J} = \text{diagonal}(EI_x, EI_y, GI_z) \tag{3.39}$$

$$\underline{K} = \text{diagonal}(\lambda GA, \lambda GA, EA) \tag{3.40}$$

where: E Youngs modulus.

G Shear modulus.

I_x, I_y, I_z	Principal moments of inertia.
λ	Shear coefficient.

Similar expressions can be found in G. Karami [1990] or B. Tabarrak [1988].

3.3 Formulation of the Governing Equations

By combining the constitutive relations and the expression for change in curvature and strain the first set of governing equations are obtained:

$$\frac{M_x}{J_x} = \frac{\partial \alpha}{\partial s} + q_0\gamma - r_0\beta \tag{3.41a}$$
$$\frac{M_y}{J_y} = \frac{\partial \beta}{\partial s} + r_0\alpha - p_0\gamma \tag{3.41b}$$
$$\frac{M_z}{J_z} = \frac{\partial \gamma}{\partial s} + p_0\beta - q_0\alpha \tag{3.41c}$$
$$\frac{F_x}{K_x} = \frac{\partial u}{\partial s} + q_0 w - r_0 v - \beta \tag{3.41d}$$
$$\frac{F_y}{K_y} = \frac{\partial v}{\partial s} + r_0 u - p_0 w + \alpha \tag{3.41e}$$
$$\frac{F_z}{K_z} = \frac{\partial w}{\partial s} + p_0 v - q_0 u \tag{3.41f}$$

By expanding the equilibrium equations a second set of governing equations are obtained:

$$\rho A\frac{\partial^2 u}{\partial t^2} = \frac{\partial F_x}{\partial s} + q_0 F_z - r_0 F_y + f_x \tag{3.42a}$$
$$\rho A\frac{\partial^2 v}{\partial t^2} = \frac{\partial F_y}{\partial s} + r_0 F_x - p_0 F_z + f_y \tag{3.42b}$$
$$\rho A\frac{\partial^2 w}{\partial t^2} = \frac{\partial F_z}{\partial s} + p_0 F_y - q_0 F_x + f_z \tag{3.42c}$$
$$\rho I_x\frac{\partial^2 \alpha}{\partial t^2} = \frac{\partial M_x}{\partial s} + q_0 M_z - r_0 M_y - F_y + m_x \tag{3.42d}$$
$$\rho I_y\frac{\partial^2 \beta}{\partial t^2} = \frac{\partial M_y}{\partial s} + r_0 M_x - p_0 M_z + F_x + m_y \tag{3.42e}$$
$$\rho I_z\frac{\partial^2 \gamma}{\partial t^2} = \frac{\partial M_z}{\partial s} + p_0 M_y - q_0 M_x + m_z \tag{3.42f}$$

These equations are completely general for a linear elastic rod that curves in space.

It seems reasonable that the majority of spatial rods will be of circular cross-section and therefore the principal frame is not uniquely defined by the inertial axis. In this case the principal frame is chosen to coincide with the Frenet frame, i.e. $\vec{t}$ and $\vec{k}_0$, $\vec{n}$ and $\vec{i}_0$, and $\vec{b}$ and $\vec{j}_0$ coincides. Regarding the curvature this means that the Darboux vector can be directly adopted to the principal frame, i.e. $p_0 = 0$, $q_0 = \kappa$, and $r_0 = \tau$.

3.4 Lamé type representation of governing equations

Equations of the *Lamé type* are stated solely in terms of kinematical variables, i.e. only by displacements and rotations. By recasting (3.41) in terms of forces and moments these can be

inserted in (3.42) to give the general Lamé type equations for a spatially curved rod. This is a straight forward task with the following result:

$$\begin{aligned}\rho I_x \frac{\partial^2 \alpha}{\partial t^2} =& m_x - K_y\left(\alpha - wp_0 + ur_0 + \frac{\partial v}{\partial s}\right) - I_y E r_0\left(-\gamma p_0 + \alpha r_0 + \frac{\partial \beta}{\partial s}\right)\\ &+ GI_z q_0\left(\beta p_0 - \alpha q_0 + \frac{\partial \gamma}{\partial s}\right) + I_x E\left(\gamma\frac{\partial q_0}{\partial s} - \beta\frac{\partial r_0}{\partial s} - r_0\frac{\partial \beta}{\partial s} + q_0\frac{\partial \gamma}{\partial s} + \frac{\partial^2 \alpha}{\partial s^2}\right)\end{aligned} \tag{3.43a}$$

$$\begin{aligned}\rho I_y \frac{\partial^2 \beta}{\partial t^2} =& m_y + K_x\left(-\beta + wq_0 - vr_0 + \frac{\partial u}{\partial s}\right) + I_x E r_0\left(\gamma q_0 - \beta r_0 + \frac{\partial \alpha}{\partial s}\right)\\ &- GI_z p_0\left(\beta p_0 - \alpha q_0 + \frac{\partial \gamma}{\partial s}\right) + I_y E\left(-\gamma\frac{\partial p_0}{\partial s} + \alpha\frac{\partial r_0}{\partial s} + r_0\frac{\partial \alpha}{\partial s} - p_0\frac{\partial \gamma}{\partial s} + \frac{\partial^2 \beta}{\partial s^2}\right)\end{aligned} \tag{3.43b}$$

$$\begin{aligned}\rho I_z \frac{\partial^2 \gamma}{\partial t^2} =& m_z - I_x E q_0\left(\gamma q_0 - \beta r_0 + \frac{\partial \alpha}{\partial s}\right) + I_y E p_0\left(-\gamma p_0 + \alpha r_0 + \frac{\partial \beta}{\partial s}\right)\\ &+ GI_z\left(\beta\frac{\partial p_0}{\partial s} - \alpha\frac{\partial q_0}{\partial s} - q_0\frac{\partial \alpha}{\partial s} + p_0\frac{\partial \beta}{\partial s} + \frac{\partial^2 \gamma}{\partial s^2}\right)\end{aligned} \tag{3.43c}$$

$$\begin{aligned}A\rho \frac{\partial^2 u}{\partial t^2} =& f_x - K_y r_0\left(\alpha - wp_0 + ur_0 + \frac{\partial v}{\partial s}\right) + K_z q_0\left(vp_0 - uq_0 + \frac{\partial w}{\partial s}\right)\\ &+ K_x\left(w\frac{\partial q_0}{\partial s} - v\frac{\partial r_0}{\partial s} - r_0\frac{\partial v}{\partial s} + q_0\frac{\partial w}{\partial s} - \frac{\partial \beta}{\partial s} + \frac{\partial^2 u}{\partial s^2}\right)\end{aligned} \tag{3.43d}$$

$$\begin{aligned}A\rho \frac{\partial^2 v}{\partial t^2} =& f_y + K_x r_0\left(-\beta + wq_0 - vr_0 + \frac{\partial u}{\partial s}\right) - K_z p_0\left(vp_0 - uq_0 + \frac{\partial w}{\partial s}\right)\\ &+ K_y\left(-w\frac{\partial p_0}{\partial s} + u\frac{\partial r_0}{\partial s} + r_0\frac{\partial u}{\partial s} - p_0\frac{\partial w}{\partial s} + \frac{\partial \alpha}{\partial s} + \frac{\partial^2 v}{\partial s^2}\right)\end{aligned} \tag{3.43e}$$

$$\begin{aligned}A\rho \frac{\partial^2 w}{\partial t^2} =& f_z - K_x q_0\left(-\beta + wq_0 - vr_0 + \frac{\partial u}{\partial s}\right) + K_y p_0\left(\alpha - wp_0 + ur_0 + \frac{\partial v}{\partial s}\right)\\ &+ K_z\left(v\frac{\partial p_0}{\partial s} - u\frac{\partial q_0}{\partial s} - q_0\frac{\partial u}{\partial s} + p_0\frac{\partial v}{\partial s} + \frac{\partial^2 w}{\partial s^2}\right)\end{aligned} \tag{3.43f}$$

The nature of wave propagation in a spatially curved rod with Timoshenko kinematics lies within the solution of (3.43). The governing equations reduces down to the formulation for a Timoshenko beam presented in Shames and Dym [2003] if all curvatures and their derivatives are set to zero. Thus these equations can be seen as generalisations of the conventional governing equations for straight beams

Chapter

4

Investigation of wave propagation in regular helical spring

This section presents a study of wave propagation in a regular helical spring. Through this the dispersion equation is derived, using nondimensional variables, and the dispersion diagram with modal for varies frequencies are presented. The dispersion equation is subjected to asymptotic analysis and comparison is made with the dispersion diagram.

Wave propagation in general is essentially a study of the wave number at various frequencies, i.e. the dispersion equation and the corresponding dispersion curves are important milestones in this study.

The mathematical manipulations required to obtain the dispersion equation are quite comprehensive. This calls out for implementation in a symbolic manipulator such as *Mathematica*. Hence this study also serves the purpose of acquiring skills in the use of Mathematica. This is also expected to be very useful in the study of a perturbed helical where the mathematics become even more involved.

4.1 Determination of geometry

The parametric representation of a helix is most easily stated with the angle of revolution as the parameter and then rewritten to have the arc length as the parameter. A helix is then given by:

$$\vec{r}(\phi) = R \begin{Bmatrix} \cos(\phi) \\ \sin(\phi) \\ \phi \tan(\psi) \end{Bmatrix} \tag{4.1}$$

where:

R	Radius of helix.
ψ	Pitch angle.
ϕ	Angle of revolution.

By imagining the wire unwinded the length of the wire is:

$$s^2 = R^2\phi^2 + \phi^2 R^2 \tan^2(\psi) \qquad \Rightarrow \qquad \phi = \frac{s}{R\sqrt{1+\tan^2(\psi)}} \tag{4.2}$$

where: s Arc length.

Substitution yields the following expression for a helix with the desired parameter:

$$\vec{r}(s) = R\begin{Bmatrix} \cos\left(\frac{s}{R\sqrt{1+\tan^2(\psi)}}\right) \\ \sin\left(\frac{s}{R\sqrt{1+\tan^2(\psi)}}\right) \\ \frac{s\tan(\psi)}{R\sqrt{1+\tan^2(\psi)}} \end{Bmatrix} \tag{4.3}$$

The curvature and torsion can now be determined using the Frenet-Serret equations. First the derivatives of $\vec{r}(s)$ are determined:

$$\vec{t} = \frac{d\vec{r}(s)}{ds} = \frac{1}{\sqrt{1+\tan^2(\psi)}}\begin{Bmatrix} -\sin\left(\frac{s}{R\sqrt{1+\tan^2(\psi)}}\right) \\ \cos\left(\frac{s}{R\sqrt{1+\tan^2(\psi)}}\right) \\ \tan(\psi) \end{Bmatrix} \tag{4.4}$$

$$\kappa\vec{n} = \frac{d^2\vec{r}(s)}{ds^2} = \frac{-1}{R(1+\tan^2(\psi))}\begin{Bmatrix} \cos\left(\frac{s}{R\sqrt{1+\tan^2(\psi)}}\right) \\ \sin\left(\frac{s}{R\sqrt{1+\tan^2(\psi)}}\right) \\ 0 \end{Bmatrix} \tag{4.5}$$

where curvature can be determined from the latter. Since $\vec{n}$ is unity, then by taking the length:

$$\kappa = \left|\frac{d^2\vec{r}(s)}{ds^2}\right| = \frac{1}{R(1+\tan^2(\psi))} = \frac{\cos^2(\psi)}{R(\cos^2(\psi)+\sin^2(\psi))} = \underline{\frac{\cos^2(\psi)}{R}} \tag{4.6}$$

For torsion the binormal vector is first determined:

$$\vec{b} = \vec{t}\times\vec{n} = \frac{-1}{R(1+\tan^2(\psi))^{3/2}}\begin{Bmatrix} -\sin\left(\frac{s}{R\sqrt{1+\tan^2(\psi)}}\right)\tan(\psi) \\ \cos\left(\frac{s}{R\sqrt{1+\tan^2(\psi)}}\right)\tan(\psi) \\ 1 \end{Bmatrix} \tag{4.7}$$

Again using the Frenet-Serret equations the torsion is:

$$\tau\vec{n} = \frac{d\vec{b}}{ds} = \frac{\tan(\psi)}{R^2(1+\tan^2(\psi))^2}\begin{Bmatrix} \cos\left(\frac{s}{R\sqrt{1+\tan^2(\psi)}}\right) \\ \sin\left(\frac{s}{R\sqrt{1+\tan^2(\psi)}}\right) \\ 0 \end{Bmatrix} = \frac{\tan(\psi)}{R(1+\tan^2(\psi))}\vec{n} \qquad \Rightarrow \tag{4.8}$$

$$\tau = \frac{\tan(\psi)}{R(1+\tan^2(\psi))} = \underline{\frac{\cos(\psi)\sin(\psi)}{R}} \tag{4.9}$$

4.2 Derivation of dispersion equation

As is seen both curvature and torsion are constants, hence, all spatial derivatives of principal curvatures are removed from the governing equations, and also body forces and moments are ignored.

The solutions are sought within the usual exponential form:

$$u = \mathscr{U} e^{iks-i\omega t} \tag{4.10a}$$
$$v = \mathscr{V} e^{iks-i\omega t} \tag{4.10b}$$
$$w = \mathscr{W} e^{iks-i\omega t} \tag{4.10c}$$
$$\alpha = \mathscr{A} e^{iks-i\omega t} \tag{4.10d}$$
$$\beta = \mathscr{B} e^{iks-i\omega t} \tag{4.10e}$$
$$\gamma = \mathscr{G} e^{iks-i\omega t} \tag{4.10f}$$

where:

k	Wave number.
$\mathscr{U}, \mathscr{V}, \mathscr{W}$	Amplitudes of displacements.
$\mathscr{A}, \mathscr{B}, \mathscr{G}$	Amplitudes of rotations.

This combination of spatial and temporal dependence satisfy the casuality principle, Sorokin [2009].

The solution can now be derived more or less straight forward following this procedure:

1. Insert equation (4.10) in the six governing equations.
2. Collect terms of $\mathscr{U}, \ldots, \mathscr{G}$ and arrange in a matrix-vector system, such as:

$$\vec{M}\{\mathscr{U} \quad \mathscr{V} \quad \mathscr{W} \quad \mathscr{A} \quad \mathscr{B} \quad \mathscr{G}\}^T = \vec{0} \tag{4.11}$$

3. Equate the determinant of the matrix to zero to find the nontrivial solution of the system. The characteristic polynomial is the dispersion equation.

The implementation can be seen in the Mathematica file *Mathematica files » regularHelixDispEq.nb* on the CD in appendix C.

By following the above mentioned procedure the dispersion equation can be derived. To mentioned a few characteristics of it, it can be said that it is of twelfth order in both k and ω, with no odd powers, all coefficients are real, and by algebraic manipulation it is seen that the dispersion equation is satisfied for $\omega = k = 0$. However, when employing a numerical example for a spring (i.e. specifying R, d, E, ν, ρ, and ψ) the dispersion equation is no longer satisfied at $\omega = k = 0$. Only by forcing Mathematica to use a large number of significant digits the condition is approximately fulfilled. This behaviour is believed to be related to the conditioning of the dispersion equation since the coefficients in it contains many products of physical quantities such as stiffness, moments of inertia etc. after taking the determinant. The mix of large and small numbers leads to a bad conditioning of the polynomial.

To overcome this difficulty *nondimensional scalings* are now introduced. The fundamental idea is as follows. Being that the mathematical model represents a physical system it is not sensitive to the system of units in which the solution is found. Therefore transformations

that changes all the dimensional quantities into dimensionless quantities should not affect the correctness of the model. If, after solving, it is desired to know the results in dimensional quantities some backwards substitution can be conducted. The concept is presented in Barenblatt [2003].

The system is based on the following fundamental physical variable:

$$R[=]L \quad d[=]L \quad k[=]L^{-1} \quad \kappa[=]L^{-1} \quad \tau[=]L^{-1} \quad \psi[=]- \quad E[=]ML^{-1}T^{-2} \quad \nu[=]- \quad \rho[=]ML^{-3} \quad \omega[=]T^{-1}$$

Here L, M, and T denotes the units of length, mass and time, respectively. Thus, length, mass, and time constitute the fundamental units for this problem. The dimensional variables can now be used as scalings for the system. Firstly, R will be taken as the scale for all length variable, i.e. all other variables having unit of length can be rewritten:

$$d = \tilde{d}R \qquad k = \frac{\tilde{k}}{R} \qquad \kappa = \frac{\tilde{\kappa}}{R} \qquad \tau = \frac{\tilde{\tau}}{R} \qquad \{\mathscr{U} \quad \mathscr{V} \quad \mathscr{W}\}^T = \{\tilde{\mathscr{U}} \quad \tilde{\mathscr{V}} \quad \tilde{\mathscr{W}}\}^T R \tag{4.12}$$

Where ~denotes nondimenional quantities. So essentially the idea is to replace the dimensional variable by a nondimensional variable times an appropriate factor that ensures that the units are correct. Also the following introduction is expedient:

$$c_0 = \sqrt{\frac{E}{\rho}} \qquad \rightarrow \qquad c_0[=]LT^{-1} \tag{4.13}$$

c_0 Speed of the plane dilatation wave.

Therefore the nondimensional frequency can be introduced as:

$$\omega = \tilde{\omega}\frac{c_0}{R} \tag{4.14}$$

Similarly can quantities such as stiffness and moments of inertia be stated in terms of dimensionless variables, i.e.:

$$E = E(c_0^2, \rho) \qquad G = G(c_0^2, \rho) \qquad K_j = K_j(c_0^2, \rho, R, \tilde{d}) \qquad I_j = I_j(R, \tilde{d}) \tag{4.15}$$

What is left of dimensional quantities is at this stage c_0, ρ, and R. Simply by multiplying the first three governing equations by the factor $\rho\frac{32}{c_0^2R^2\tilde{d}^2\pi}$ and the remaining three by $\frac{8}{\rho c_0^2R\tilde{d}^2\pi}$, then conduct the derivation from the beginning all dimensional variables and very large denominators, powers of $\tilde{d}$ and π are removed from the dispersion equation. The system matrix then becomes:

$$\begin{bmatrix}
-\frac{\left((\nu+1)\tilde{k}^2+\tilde{\kappa}^2+(\nu+1)\left(\tilde{\tau}^2-\tilde{\omega}^2\right)\right)\tilde{d}^2+8\lambda}{2(\nu+1)} & -i\tilde{d}^2\tilde{k}\tilde{\tau} & \frac{i(\nu+2)\tilde{d}^2\tilde{k}\tilde{\kappa}}{2(\nu+1)} & -\frac{4\lambda\tilde{\tau}}{\nu+1} & -\frac{4i\lambda\tilde{k}}{\nu+1} & 0 \\
i\tilde{d}^2\tilde{k}\tilde{\tau} & -\frac{(\nu+1)\left(\tilde{k}^2+\tilde{\tau}^2-\tilde{\omega}^2\right)\tilde{d}^2+8\lambda}{2(\nu+1)} & \frac{1}{2}\tilde{d}^2\tilde{\kappa}\tilde{\tau} & \frac{4i\lambda\tilde{k}}{\nu+1} & -\frac{4\lambda\tilde{\tau}}{\nu+1} & \frac{4\lambda\tilde{\kappa}}{\nu+1} \\
-\frac{i(\nu+2)\tilde{d}^2\tilde{k}\tilde{\kappa}}{2(\nu+1)} & \frac{1}{2}\tilde{d}^2\tilde{\kappa}\tilde{\tau} & -\frac{\tilde{d}^2\left(\tilde{k}^2+(\nu+1)\left(\tilde{\kappa}^2-2\tilde{\omega}^2\right)\right)}{2(\nu+1)} & 0 & 0 & 0 \\
-\frac{\lambda\tilde{\tau}}{\nu+1} & -\frac{i\lambda\tilde{k}}{\nu+1} & 0 & -\frac{\lambda\tilde{k}^2}{\nu+1}-2\tilde{\kappa}^2-\frac{\lambda\tilde{\tau}^2}{\nu+1}+2\tilde{\omega}^2 & -\frac{2i\lambda\tilde{k}\tilde{\tau}}{\nu+1} & \frac{i(\lambda+2\nu+2)\tilde{k}\tilde{\kappa}}{\nu+1} \\
\frac{i\lambda\tilde{k}}{\nu+1} & -\frac{\lambda\tilde{\tau}}{\nu+1} & 0 & \frac{2i\lambda\tilde{k}\tilde{\tau}}{\nu+1} & -\frac{\lambda\tilde{k}^2+\lambda\tilde{\tau}^2-2(\nu+1)\tilde{\omega}^2}{\nu+1} & \frac{\lambda\tilde{\kappa}\tilde{\tau}}{\nu+1} \\
0 & \frac{\lambda\tilde{\kappa}}{\nu+1} & 0 & -\frac{i(\lambda+2\nu+2)\tilde{k}\tilde{\kappa}}{\nu+1} & \frac{\lambda\tilde{\kappa}\tilde{\tau}}{\nu+1} & -2\tilde{k}^2-\frac{\lambda\tilde{\kappa}^2}{\nu+1}+2\tilde{\omega}^2
\end{bmatrix} \tag{4.16}$$

By taking the determinant of this and equate it to zero the dispersion equation is found in a nondimensional form. Not surprisingly the dispersion equation is a very large expression, and are therefore moved to appendix B under section B.1.

The dispersion equation can be solved for various frequencies using a numerical solver in Mathematica and a direct numerical solution for wave numbers is thereby obtained. This solution is exact down to the precision of the solver, and therefore are expected to resemble the real solution to the governing equations in a very precise manner. Hence, the uncertainty of this method originates mainly on the assumption in the theory, i.e. the plain cross-sections assumptions for rods and the linear theory of elasticity.

The direct numerical solution will henceforth be referred to as the *exact solution* even though this, strictly speaking, is an exaggeration.

4.2.1 Dispersion diagram for a helix

Due to the nondimensionalisation the only thing that needs to be specified to obtain the dispersion diagram is:

$$\psi = 0.13 \qquad \wedge \qquad \tilde{d} = 0.184 \qquad \wedge \qquad \nu = 0.3 \qquad \wedge \qquad \lambda = \frac{6(1+\nu)}{7+6\nu} \tag{4.17}$$

The choices of ψ, $\tilde{d}$, and ν allows for comparison of dispersion curves with Sorokin [2009], and the expression for λ is taken from Shames and Dym [2003]. The dispersion diagram for complex and real valued wave numbers, for $\tilde{\omega} < 0.025$, is seen in figure 4.1 and 4.2, respectively. These figures are the standard way of showing the wave numbers in two dimensions where the complex wave numbers are projected to the real plane and vice versa. However, in figure 4.3 the wave number for the low frequency range is shown in 3 dimensions. The plot neatly illustrates how the complex valued wave numbers emerges or disappears when branches meet or bifurcates. The plots can be seen and manipulated by opening the file *Mathematica files » 3D plots of wave number.nb* on the CD in appendix C.

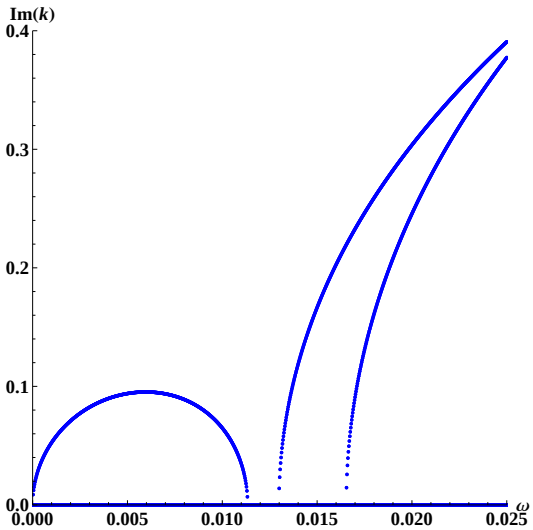

Figure 4.1: *Imaginary part of wave number in the low frequency ranges. Evanescent waves.*

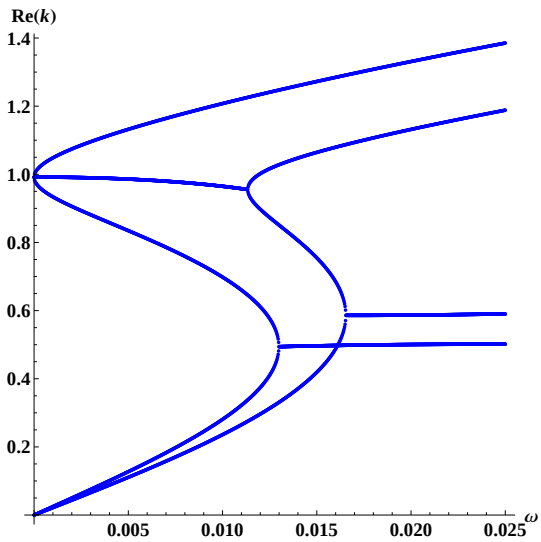

Figure 4.2: *Real part of wave number in the low frequency ranges. Propagating waves.*

Along with figure 4.3 the entire solution can be illustrated in two additional frequency ranges. These are shown in figure 4.4 and 4.5. To a certain extent one can say that figure 4.5 if the full

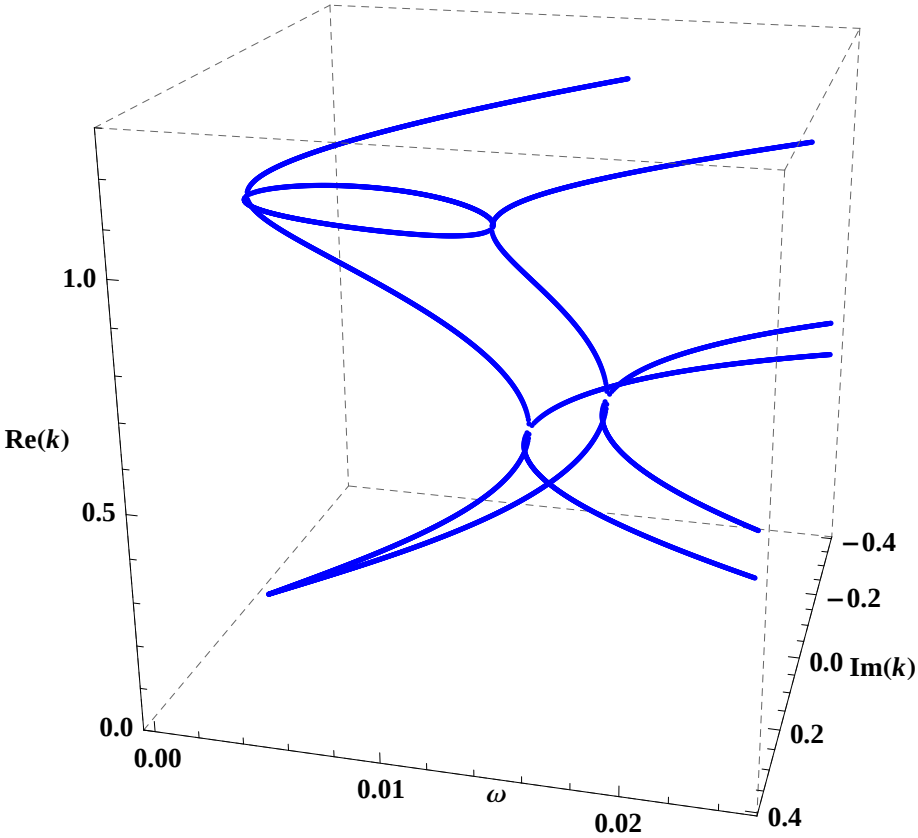

Figure 4.3: *Wave number plotted in the complex space in the low frequency range.*

story of the wave numbers for a helical spring with Timeshenko kinematics, since all waves has cut on. Naturally the plot will change if e.g. pitch angle or $\tilde{d}$ are disturbed, but after six waves has cut on nothing more happens in the dispersion diagram.

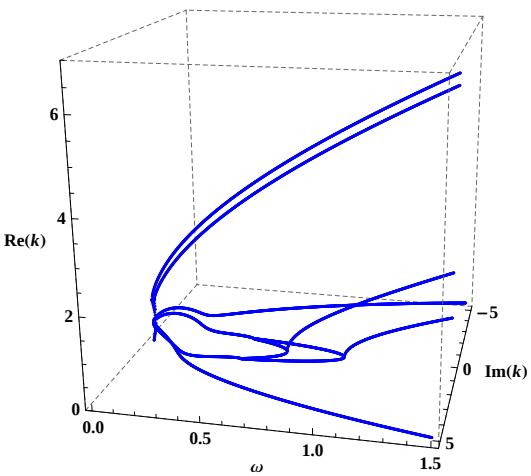

Figure 4.4: *Wave number plotted in the complex space in the mid frequency range, $\tilde{\omega} > 1.5$.*

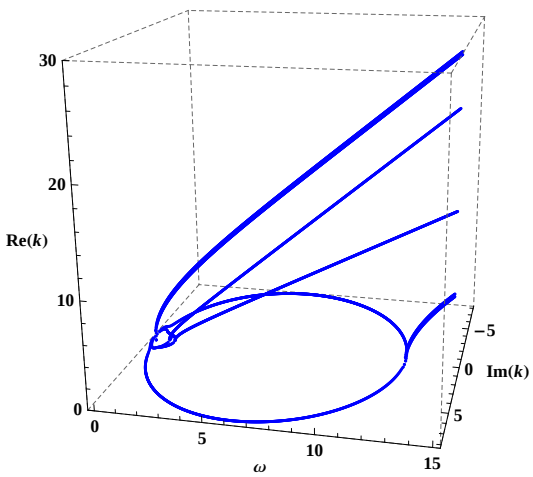

Figure 4.5: *Wave number plotted in the complex space in the high frequency range, $\tilde{\omega} > 15$.*

It should be emphasised that the dispersion equation provides twelve roots since it is of twelfth order in k. However, since they come in pairs of a negative and a positive valued real

part, only wave numbers with positive real parts are included in the plots.

The following comments are given to the dispersion diagrams:

- At sufficiently large frequencies, above $\tilde{\omega} \approx 13$, all waves propagate. I.e. above this frequency two flexural waves, one torsion wave, one axial wave, and two shear waves propagate.
- At low frequencies no wave numbers are purely imaginary. I.e. all evanescent waves consist of a propagating part and an exponentially decaying part.
- There are no crossing of branches, so all roots have multiplicity 1. If the roots to the dispersion equation had multiplicity, the eigenvectors would be linearly dependent, and to overcome this difficulty one of the eigenvectors should be multiplied by ω. In given case this is denoted a *secular term*. This secular term would have represented a growing wave, since it grows with frequency, and therefore becomes instable.
- For the wave numbers shown all phase velocities, $c_{\text{phase}} = \frac{\text{Re}\{\omega\}}{\text{Re}\{k\}}$ Slepyan [2002], are positive. However, the slope of two wave numbers are negative and therefore the group velocity, $c_{\text{group}} = \frac{d\omega}{dk}$ Slepyan [2002], is also negative. This means that two waves, in the low frequency range, propagate in one direction while they convey energy in the opposite direction.
- When waves cut on the phase velocity becomes infinite, since the real part of the wave number is zero. Since the phase velocity is not related to transportation of physically quantity, but merely the propagation of the wave profile it does not need to be bounded.
- When branches bifurcate or meet the slope becomes infinite. Hence, the group velocity is zero. Thus, at cut-on and cut-off frequencies waves do propagate, but energy is not conveyed. This is called a *trapped wave*.

4.2.2 Modal analysis

To get a grip of the modes related to each of the branches and how modes couple *modal coefficients* will now be determined. Indeed, another purpose of this study is to assess the added complexity in modal couplings in the perturbed spring, which will be analysed in the next chapter.

A *modal coefficient* is the mutual relation between the six kinematic variables corresponding to a certain wave number. So effectively it is not the amplitude of oscillations that is determined, but the wave profile.

The branches are numbered as indicated in figure 4.7, and to help keep track of displacements and rotations figure 4.6 is helpful. Also the terms *in-plane* and *out-of-plane* are expedient when discussing the modal vectors. These are defined as:

In-plane: The $\vec{i} - \vec{k}$ plane. I.e. displacements u and w and rotation β are in-plane modes.

Out-of-plane: In direction of $\vec{j}$. I.e. displacement v and rotations α and γ are out-of-plane modes.

These definitions are inspired by a helix with zero pitch angle, i.e. an infinite ring, where the analogy becomes more obvious since the geometry is only in one plane. A helix can thence be seen as an infinite ring where the pitch angle is perturbed.

The method of finding modal coefficients involves expressing either five of the six independent kinematic variables in terms of the remaining one. This means that one row in the matrix

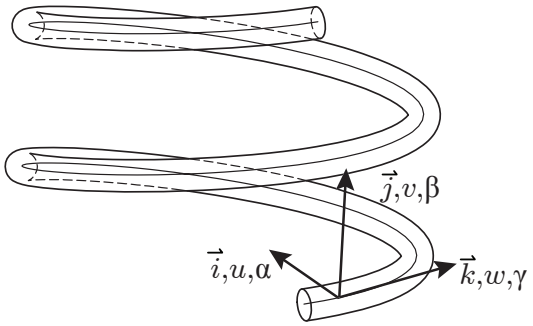

Figure 4.6: *A helical spring with indicated principal frame and corresponding displacement- and rotation components.*

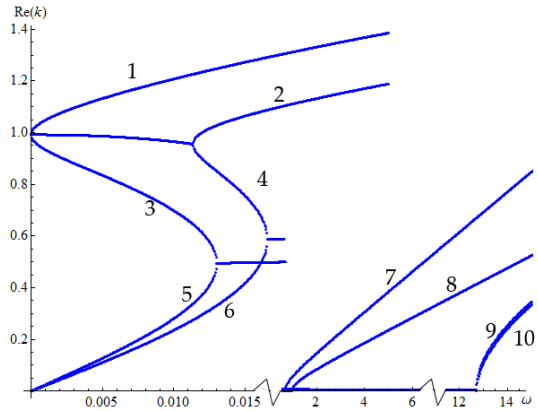

Figure 4.7: *Numbered branches in the dispersion diagram.*

is redundant, and one of the columns must be moved to the RHS in the system of equations. So in principal the following rearrangement must be conducted when expressing the modal vector in terms of the i'th kinematic variable:

$$\begin{bmatrix} m_{1,1} & \cdots & m_{1,i} & \cdots & m_{1,k} \\ \vdots & \ddots & & & \\ m_{j,1} & & \ddots & & \vdots \\ \vdots & & & \ddots & \\ m_{l,1} & & \cdots & & m_{l,k} \end{bmatrix} \begin{Bmatrix} x_1 \\ \vdots \\ x_i \\ \vdots \\ x_k \end{Bmatrix} = \vec{0} \qquad \Rightarrow \tag{4.18}$$

$$\begin{bmatrix} m_{2,1} & \cdots & m_{2,i-1} & m_{2,i+1} & \cdots & m_{1,k} \\ \vdots & \ddots & & & & \\ m_{j,1} & & & & & \vdots \\ \vdots & & & & \ddots & \\ m_{l,1} & & \cdots & \cdots & & m_{l,k} \end{bmatrix} \begin{Bmatrix} x_1 \\ \vdots \\ x_{i-1} \\ x_{i+1} \\ \vdots \\ x_k \end{Bmatrix} = - \begin{Bmatrix} m_{2,i} \\ \vdots \\ m_{j,i} \\ \vdots \\ m_{l,i} \end{Bmatrix} x_i \tag{4.19}$$

The solution to this system will then be of the form:

$$\{x_1 \quad \cdots \quad x_{i-1} \quad x_{i+1} \quad \cdots \quad x_k\}^T / x_i = \{r_1 \quad \cdots \quad r_j \quad \cdots \quad r_{l-1}\}^T \tag{4.20}$$

Where r_j is a modal coefficient. The choice of kinematic variable used for scaling is not immediately clear, and therefore is chosen along the way. The method is applied to all branches having no imaginary part, and plots of the modal coefficients is found both in this section and appendix B.

A common thing for all plots is that square markers indicate real valued modal coefficients, whereas circular markers illustrates purely imaginary modal coefficients. Remark that the phase of the imaginary modal coefficients are shifted by 90° compared to the real ones, which is in good agreement, when observing e.g. α and v or β and u, since the phase shift tells that when the deflection is at its maximum the rotation is zero and vice versa.

It should be pointed out that comparison between quantitative values of displacement and rotations is troublesome. Also the displacements are nondimensional and therefore in principal needs to be multiplied by R. However, this would make the results less general since

no geometric information is specified other than the pitch angle and the ratio $\frac{d}{R}$ at this stage. Consequently the displacement amplitudes are left as nondimensional.

Branch 1 + 2 (figure 4.8 and 4.9): The dominant displacement components are the flexural components u and v. However, as is seen they are of same order, but with equal sign for branch 1 and opposite sign for branch 2. I.e. both of them are flexural wave, but the two are orthogonal modes. These will be referred to as *Flexural waves*.

The impact of the added kinematics of the Timoshenko theory compared to the Bernoulli-Euler theory can be assessed by plotting the shear angle $\Psi = \beta - \frac{\partial u}{\partial s} = \beta - iku$. This can be seen in figure B.1 in appendix B. From here it seems clear that the added kinematics from the Timoshenko theory becomes increasingly important as the frequency grows, which implies that the simpler Bernoulli-Euler theory will not perform well at large frequencies.

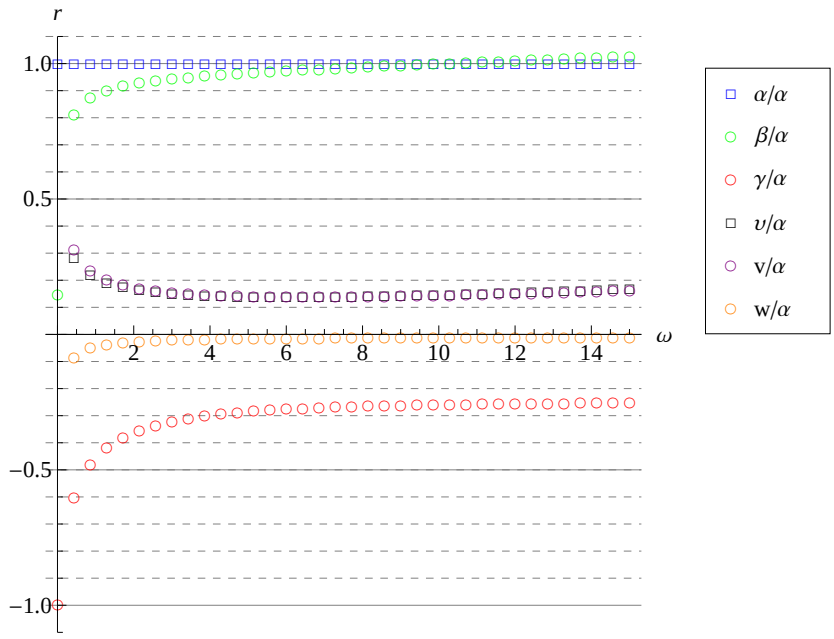

Figure 4.8: *Modal coefficients for branch 1.*

Branch 3 + 4 (figure 4.10 and 4.11): From these plots it is hard to identify any dominant variable. However, for branch 3 the two in-plane displacements u and w are large for low frequencies and for branch 4 the out-of-plane displacement v is the larger one.

Similar to the modal plots for branch 1 and 2, there is a certain amount of orthogonality between the two modes. Out-of-plane displacement v is of course the same, however, in branch 3 the two remaining displacements are positive, whereas they are negative for branch 4.

Branch 5 + 6 (figure 4.12 and 4.13): Again orthogonality between the in- and out-of-plane displacements is seen. For both branches the dominant displacement is seen to be the out-of-plane displacement v and elongation w.

The mode from branch 5 matches the mode of 3 at the highest frequency step. This is not that surprising sine they have the same wave number at the bifurcation. However, as is noted this is not the case for branch 4 and 6. The explanation for this has not been found, but it could constitute an interesting study.

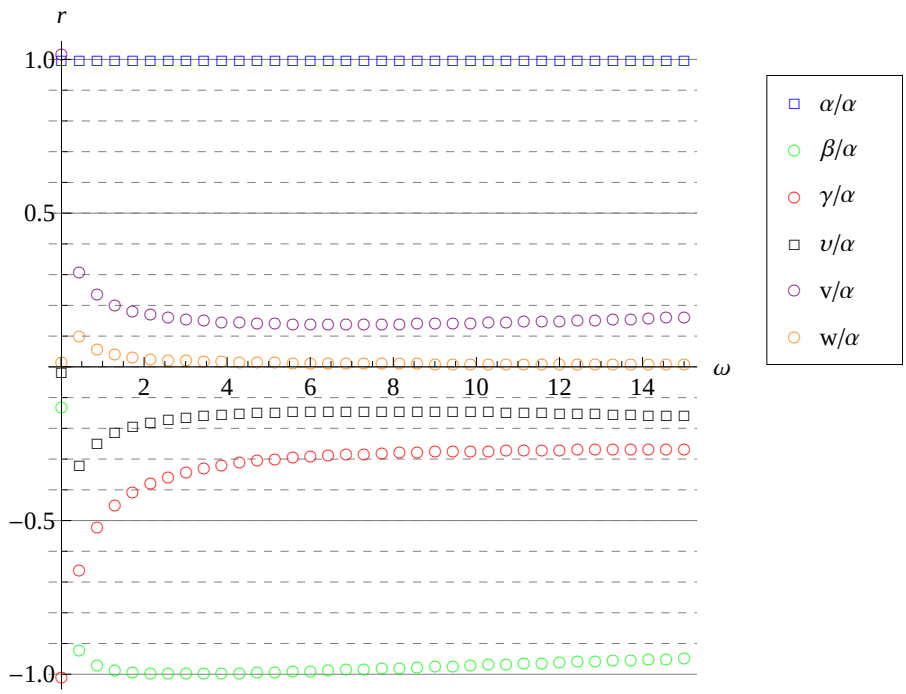

Figure 4.9: *Modal coefficients for branch 2.*

Branch 7 (figure 4.14): In spite of, as earlier stated, direct comparison between rotations and displacement are not doable, then this figure quite clearly implies that this is a wave of dominant torsion, and thence is denoted *Torsional wave*. Zooming in to $-50 < r < 200$ reveals that v is remarkably higher than the other displacement terms, so this couples with the torsion. A plot of this is seen in appendix B figure B.2.

Branch 8 (figure 4.15): Of the displacement terms evidently the axial component is dominant. This couples with the in-plane displacement u, and therefore also the in-plane rotation β. It can thence be concluded that this is an *Axial wave*.

Branch 9 + 10 (figure 4.16 and 4.17): Here the shear angles seems to be dominant, i.e. these are *shear waves* and are direct consequences of the Timoshenko kinematics, and hence could also be denoted *Timoshenko waves*. Like the other pairs of branches the modes can be seen to be orthogonal. A zoom to smaller r values, figure B.3 and B.4, reveals that the displacements u and v are approximately at the same order of magnitude and with the same sign as β and α, respectively.

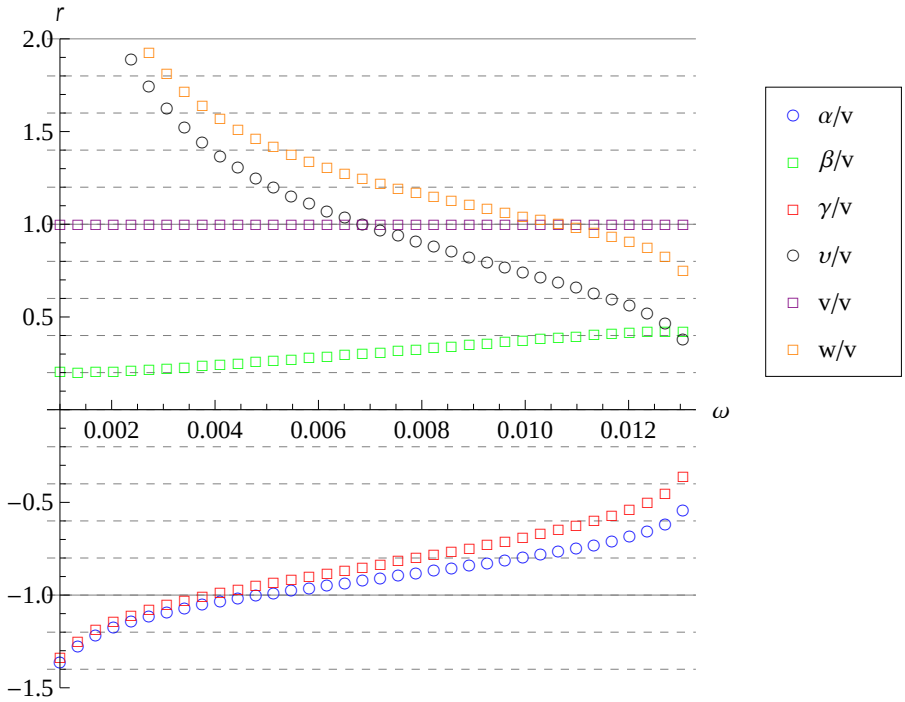

Figure 4.10: *Modal coefficients for branch 3.*

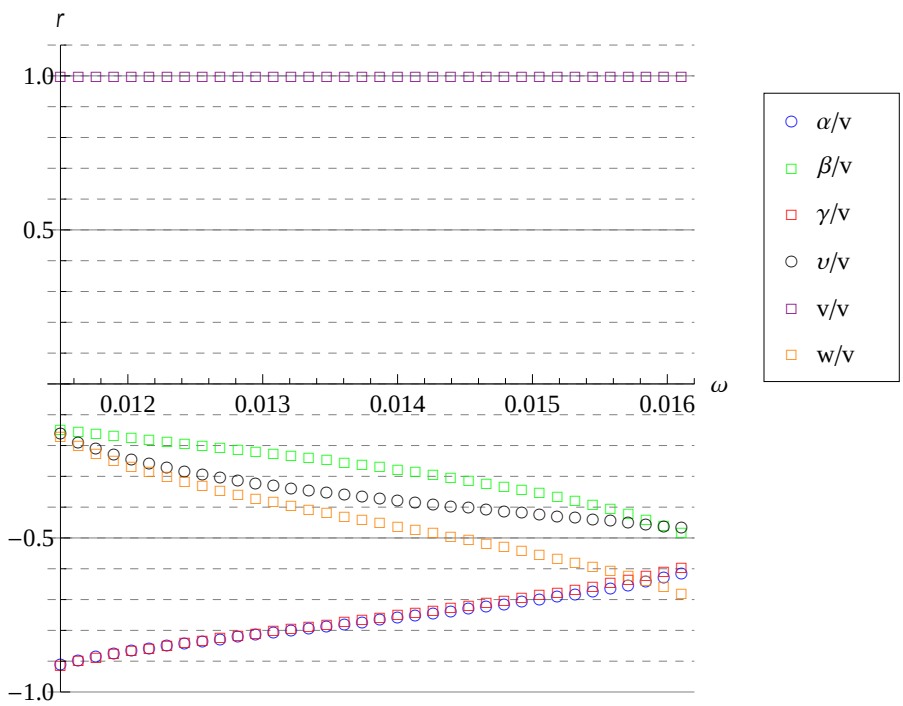

Figure 4.11: *Modal coefficients for branch 4.*

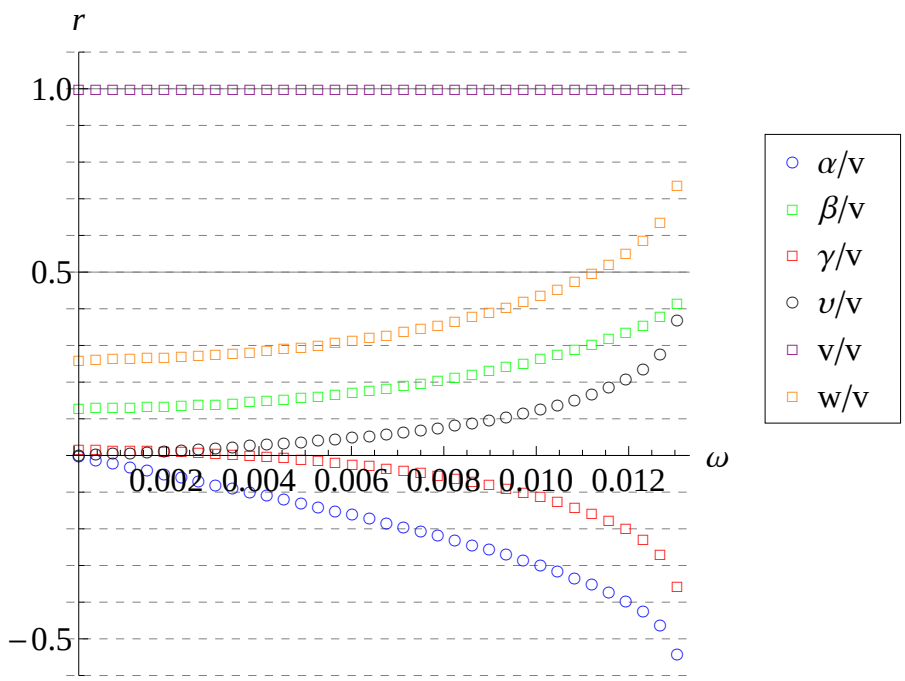

Figure 4.12: *Modal coefficients for branch 5.*

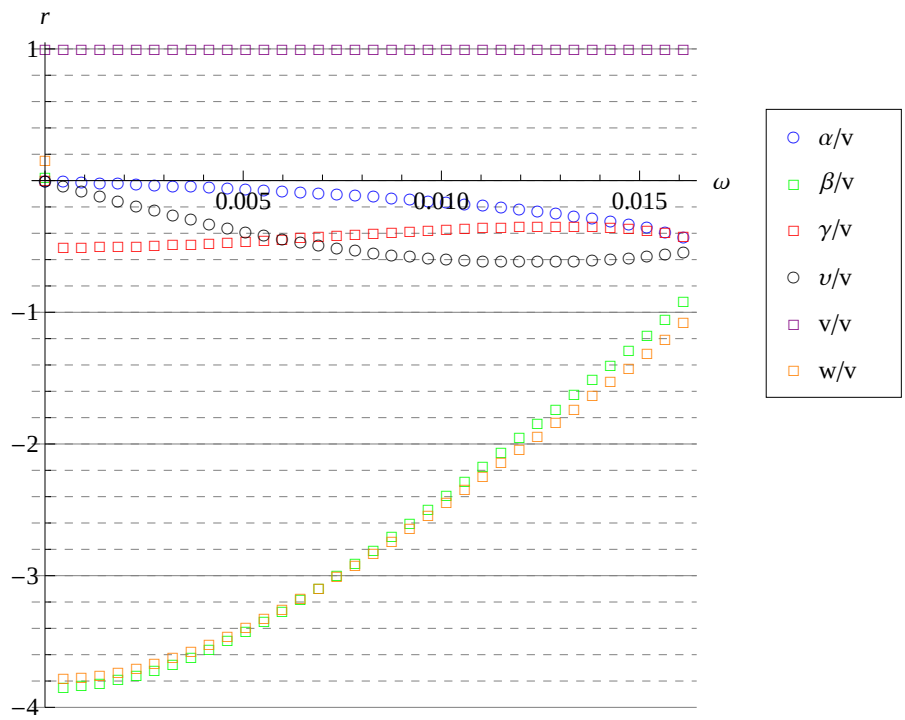

Figure 4.13: *Modal coefficients for branch 6.*

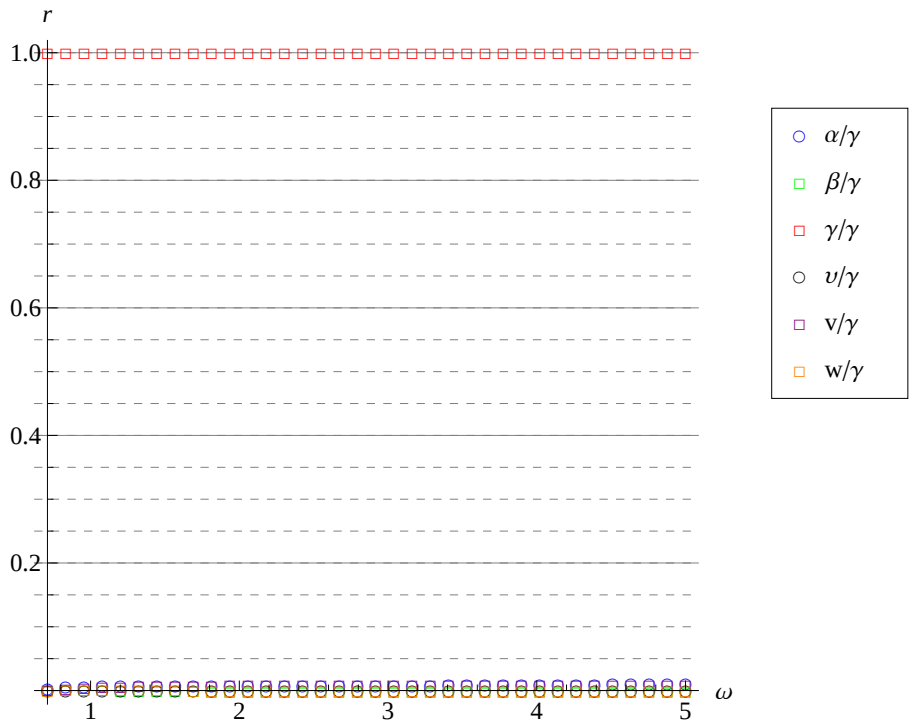

Figure 4.14: *Modal coefficients for branch 7.*

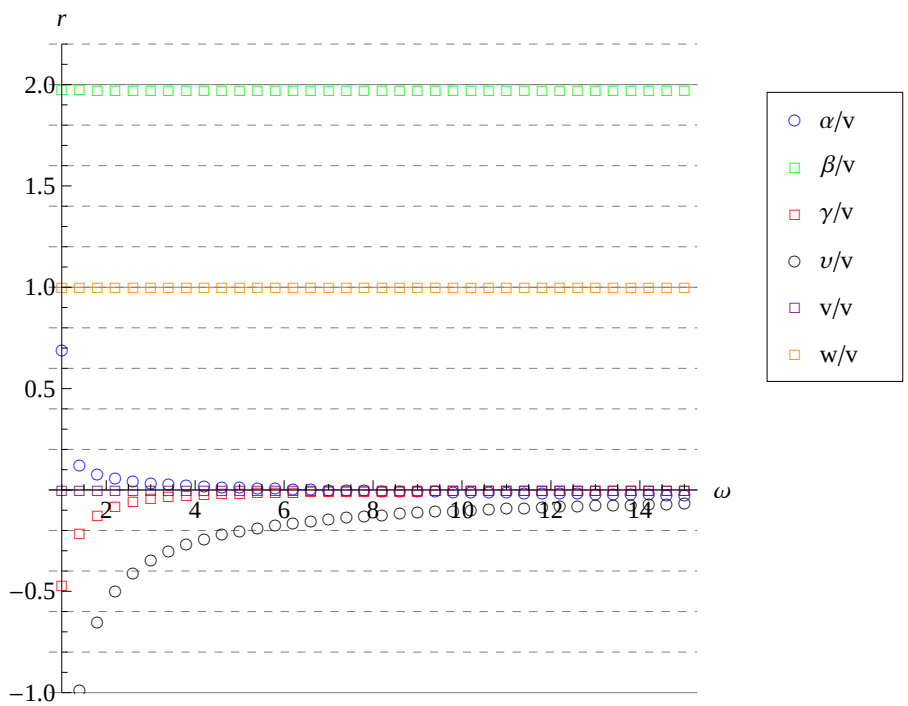

Figure 4.15: *Modal coefficients for branch 8.*

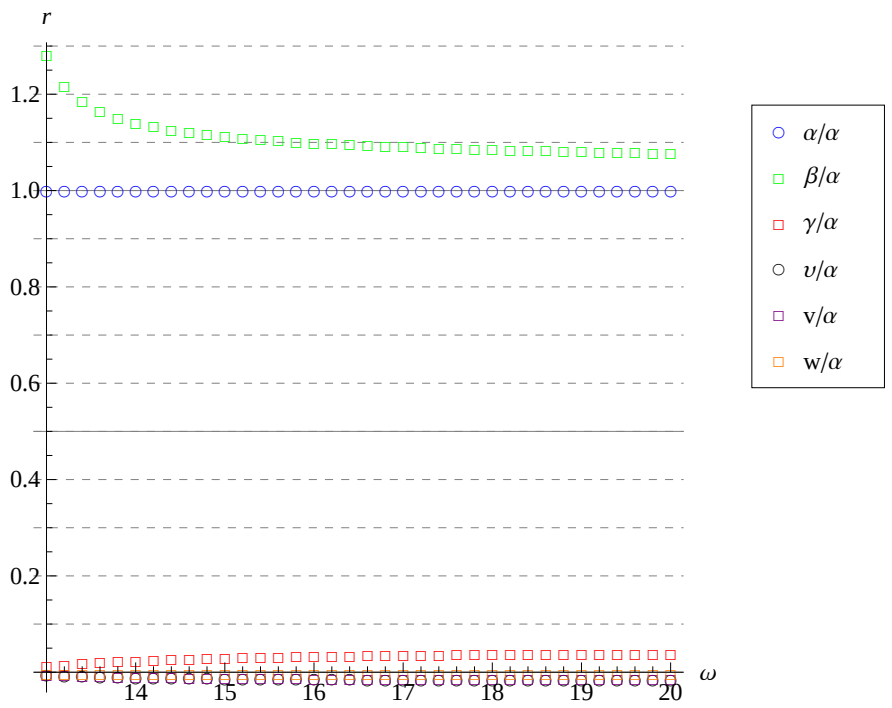

Figure 4.16: *Modal coefficients for branch 9.*

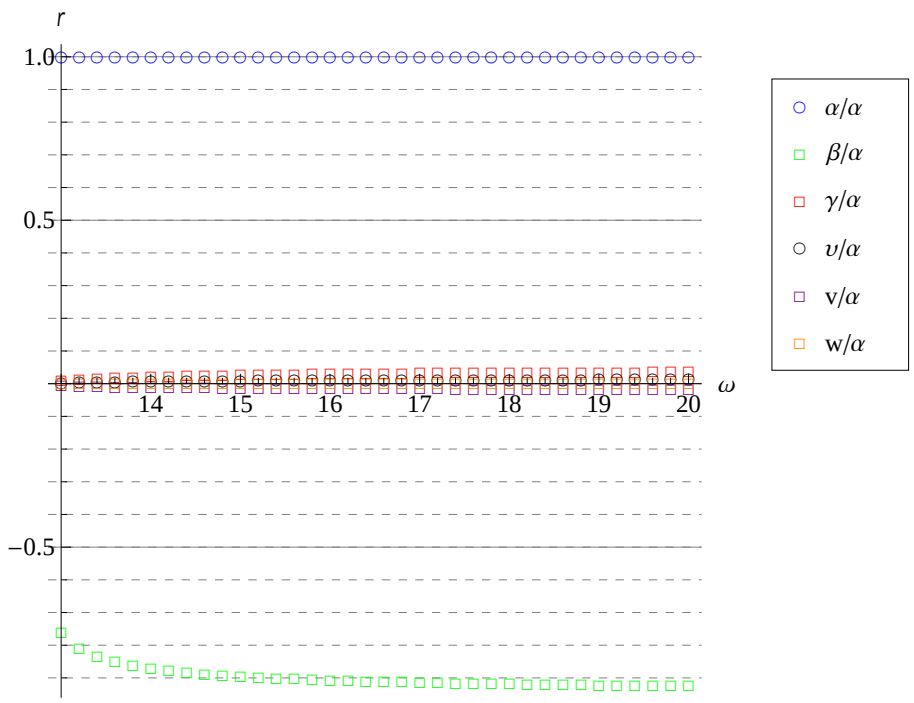

Figure 4.17: *Modal coefficients for branch 10.*

4.3 Asymptotic analysis of dispersion equation

Now when the solution of the dispersion equation is obtained asymptotic analysis is employed to assess which parameters dominate different characteristics of the dispersion equation. Characteristics to be investigated, at this stage, are cut-on frequencies, dependence upon k in high and low frequency ranges.

In *Asymptotic Analysis* or *Perturbation Methods* the basic idea is to approximate the solution of an equation, containing a small parameter, by a power series expansion on this small parameter. One textbook on the topic is *Perturbation Methods* by Hinch [1991].

For an equation $p(x,\epsilon) = 0$ where ϵ is a small parameter the roots can be approximated by a general *perturbation theory expansion*:

$$x = x_0 + \delta_1(\epsilon)x_1 + \delta_2(\epsilon)x_2 + \delta_3(\epsilon)x_3 + \dots \tag{4.21}$$

where: $\delta_i(\epsilon)$ Scalings of ϵ.

x_i Corrections.

Here it is required that $x_i = \mathrm{O}(1)$, and that $1 >> \delta_1 >> \delta_2 >> \dots$. The scalings will be in powers of the small parameter. Hence, the magnitude of each term becomes smaller and smaller. The difficulty mainly lies within determining the scalings and the corrections, and if any *sub-scalings* are needed. To determine the scalings there are two different options. One that involves a certain amount of guessing and a more cumbersome but systematic way. In this section only the first method is applied.

The number of terms necessary to include in the perturbation theory expansion is a matter of what accuracy is desired. In some of the analysis below only one term is included and in others up to four terms.

In general the procedure when applying perturbation methods can be summarised as follows:

1. Rewrite the governing equation using an power expansion.
2. Equate like powers of the small parameter.
3. Determine correction factors.

This procedure do not in any way cover the entire theory of perturbation methods, but merely how it is applied in this chapter.

For the problem at hand there are two parameters that can be considered as small, namely the helix radius to thread diameter $\tilde{d}$ and the torsion $\tilde{\tau}$ since this is proportional to $\sin(\psi)$ which will be small for most springs. $\tilde{d}$ is mainly chosen as the small parameter.

4.3.1 Cut-on frequencies

At a cut-on k is zero which simplifies the dispersion equation. This allows for an analytical solution wrt. $\tilde{\omega}$. The exact solutions shows that zero is a quadruple root and eight additional roots are found. Four of these are distinct, since they come in pairs of positive and negative values. I.e. five distinct cut-on frequencies are obtained. Their values for the spring considered in this section are:

$$\tilde{w}^{(IV)} = 0 \quad \wedge \quad \tilde{w} = \pm 0.695213 \quad \wedge \quad \tilde{w} = \pm 0.983191 \quad \wedge \quad \tilde{w} = \pm 12.7068 \quad \wedge \quad \tilde{w} = \pm 12.723$$

Here the bracketed roman number denotes the multiplicity of the root. The exact solutions along with the reduced dispersion equation is seen in appendix B under section B.3.

To be able to assess the influence of the different parameters of the spring, the above mentioned Perturbation Methods will now be applied. The expectation is to obtain simple expressions for the cut-on frequencies.

In the reduced dispersion equation the following expansion on $\tilde{\omega}$ is suggested:

$$\omega = \omega_0 d^i \tag{4.22}$$

Here ~are omitted for convenience, as will be the case further on. It is expedient to take a look at the exact solutions when guessing values of i. Since two cut-ons are found in the region of $\omega \approx 1$ it seems that $i = 0$ is reasonable, as it establishes $\omega = O(1)$. In this case the leading order term, i.e. the term having the lowest power of the small parameter d in the dispersion equation when applying the expansion, is found as:

$$0 = \frac{64\lambda^2\omega_0^4\left(\kappa^4 - 3\kappa^2\omega_0^2 + 2\omega_0^4\right)}{(1+\nu)^2} d^2 + \dots \tag{4.23}$$

Immediately it is seen that zero is a quadruple root which corresponds to the exact solution. Solving for ω_0 and doing backwards substitution $\omega_0 = \frac{\omega}{d^i}$, the following roots are determined:

$$\omega = \pm\kappa \qquad \wedge \qquad \omega = \pm\frac{\kappa}{\sqrt{2}} \tag{4.24}$$

For the spring considered the numerical values of these are $\omega = \pm 0.983195$ and $\omega = \pm 0.695224$. I.e. the cut-on frequencies of the axial and torsional wave is just a matter of the curvature of the spring.

For the high frequency cut-ons i is chosen as -1 and the leading order term is found to be:

$$0 = \frac{2\omega_0^8\left(-8\lambda + (1+\nu)\omega_0^2\right)^2}{(1+\nu)^2} d^{-6} + \dots \tag{4.25}$$

Here ω can be found:

$$\omega = \pm\frac{\sqrt{2\lambda}}{\sqrt{1+\nu}\,d} \tag{4.26}$$

Where the numerical value is $\omega = \pm 12.6929$. With this one term approximation a nuance is lost since only one root approximate both of the high frequency cut-ons. This implies that a two term approximation is worth attempting. By adding $\omega_1 d^n$ to the asymptotic expansion, chose $n = 1$ the next power of the small parameter is found at d^{-2} as a very large expression. The correction ω_1 can then be found as:

$$\omega_1 = \frac{\kappa\lambda + 2(1+\nu)\tau^2}{8\sqrt{2\lambda(1+\nu)}} \qquad \wedge \qquad \omega_1 = \frac{2\kappa + (\lambda + 2\nu)\tau^2}{8\sqrt{2\lambda(1+\nu)}} \tag{4.27}$$

So the high frequency cut-ons should be approximated by:

$$\omega = \frac{\sqrt{2\lambda}}{\sqrt{1+\nu}d} + \frac{\kappa\lambda + 2(1+\nu)\tau^2}{8\sqrt{2\lambda(1+\nu)}}d \tag{4.28}$$

$$\omega = \frac{\sqrt{2\lambda}}{\sqrt{1+\nu}d} + \frac{2\kappa + (\lambda+2\nu)\tau^2}{8\sqrt{2\lambda(1+\nu)}}d \tag{4.29}$$

This leads to the numerical values $\omega = \pm 12.7068$ and $\omega = \pm 12.723$, so the two term expansion captures the details in this area. From the expressions it is seen that cut-ons are dominated by ν,λ and the small parameter d while κ and τ have only very little influence, but nevertheless constitutes the difference between the two cut-on frequencies.

These results illustrate the advantages of this methods since the approximations, simple as they are, approximate the exact solutions in a precise manner, meanwhile they give a clear picture of how the parameters influence the cut-on frequencies.

4.3.2 High frequency asymptotes

What will be attempted first is just to see what will be the result when suggesting:

$$k = k_0\omega \tag{4.30}$$

and then take the limit $\omega \to \infty$. In principle this corresponds to expanding on the inverse of ω. I.e. the largest power of ω is the leading order term. Hence, to the leading order the dispersion equation is:

$$0 = \cdots - \frac{d^6\left(2+2\nu-k_0^2\right)\left(-1+k_0^2\right)^3\left(2+2\nu-\lambda k_0^2\right)^2}{4(1+\nu)^3}\omega^{12} \tag{4.31}$$

Which has the solutions:

$$k^{(III)} = \pm\omega \qquad \wedge \qquad k = \pm\sqrt{2(1+\nu)}\omega \qquad \wedge \qquad k^{(II)} = \pm\sqrt{\frac{2(1+\nu)}{\lambda}}\omega \tag{4.32}$$

The results shows that the wave numbers are not sensitive to either curvature, torsion, or any other geometrical feature of the spatial curve, but only the material properties and cross sectional geometry of the rod. It seems trustworthy that the explanation is, that the wave length is so short that the waves it do not feel either curvature or torsion, but merely sees the helix thread as a straight rod. At least to the leading order term.

The asymptotic approximations are plotted in figure 4.18, and are superimposed on the real part of the exact solution in figure 4.19 and 4.20. These figures indicate that the asymptotic behaviour develops at very different paces for the different wave numbers. In figure 4.19 it is seen that the asymptotes for the axial and torsion waves are well develop, while the asymptotic solution to the flexural waves is not even near the exact solutions. In figure 4.20 the flexural wave is fully developed and coincides with the asymptotic approximation, and additionally it is seen that the axial and Timoshenko waves share the same asymptote. Furthermore this plot reveals that the torsional wave overshoots its asymptote before settling down.

The conclusion that the propagating waves do not feel the spatial curvature enables comparison with the wave propagating in a straight beam with Timoshenko kinematics. The dispersion equation for a straight rod can be found in Sorokin [2010] as:

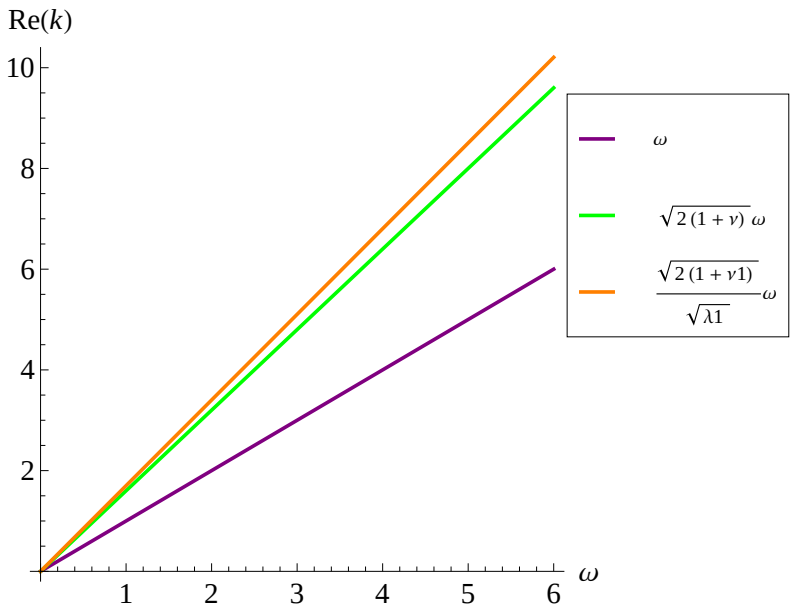

Figure 4.18: *Asymptotes in the high frequency range.*

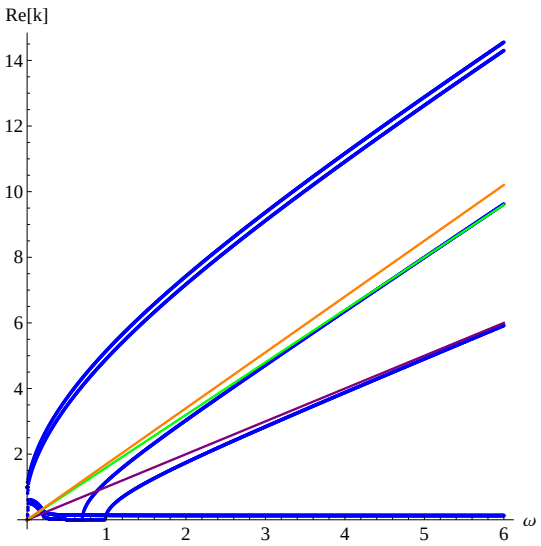

Figure 4.19: *Exact solution and asymptotic expansions for wave number for* $\omega < 6$.

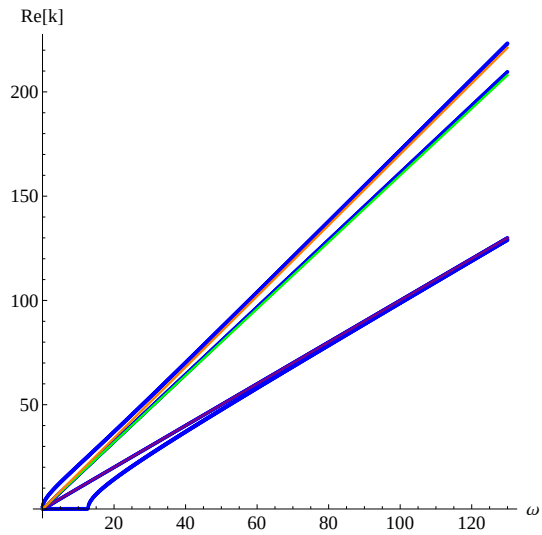

Figure 4.20: *Exact solution and asymptotic expansions for wave number for* $\omega < 130$.

$$k^4 - \left(1 + \frac{2(1+\nu)}{\lambda}\right) k^2\omega^2 - 16\omega^2 + \frac{2(1+\nu)}{\lambda}\omega^4 = 0 \tag{4.33}$$

Which has the solutions:

$$k = \pm\sqrt{\frac{(2+\lambda+2\nu)\omega^2 \pm \sqrt{-4\lambda(1+\nu)\omega^4 + 4(1+\nu)^2\omega^4 + \lambda^2\omega^2\left(64+\omega^2\right)}}{2\lambda}} \tag{4.34}$$

$$= \pm\sqrt{\frac{(2+\lambda+2\nu)\omega^2 \pm \sqrt{64\lambda^2\omega^2 + 4\omega^4 - 4\lambda\omega^4 + \lambda^2\omega^4 + 8\nu\omega^4 - 4\lambda\nu\omega^4 + 4\nu^2\omega^4}}{2\lambda}} \tag{4.35}$$

Here the term $64\lambda^2\omega^2$ can be omitted since it becomes small relative to the others in the limit of $\omega \to \infty$. This enables the factorisation:

$$k = \pm\sqrt{\frac{(2+\lambda+2\nu)\omega^2 \pm \sqrt{(-2+\lambda-2\nu)^2\omega^4}}{2\lambda}} \tag{4.36}$$

$$= \pm\sqrt{\frac{(2+\lambda+2\nu)\omega^2 \pm (-2+\lambda-2\nu)\omega^2}{2\lambda}} \qquad \Rightarrow \tag{4.37}$$

$$k = \pm\omega \qquad \wedge \qquad k = \pm\sqrt{\frac{2(1+\nu)}{\lambda}}\omega \tag{4.38}$$

Also it is known that the axial wave (or free dilatation wave) and shear waves travels at the velocities:

$$c_{\text{dilatation}} = \sqrt{\frac{E}{\rho}} \qquad \wedge \qquad c_{\text{shear}} = \sqrt{\frac{G}{\rho}} = \frac{1}{\sqrt{2(1+\nu)}}c_{\text{dilatation}} \tag{4.39}$$

So in nondimensional form the wave numbers are:

$$k = \pm\omega \qquad \wedge \qquad k = \pm\sqrt{2(1+\nu)}\omega \tag{4.40}$$

Hence it is hereby confirmed that the waves in a helical spring propagate at the same speed as in straight rod at high frequencies which in some sense has been found by taking the limit at high frequencies. It is therefore learning full to go for a more general asymptotic approximation similar to what was done in the previous subsection. Therefore by suggesting expansions on both ω and k as:

$$\omega = \omega_0 d^j \tag{4.41}$$

$$k = K_1 d^n + K_2 d^m + K_3 d^p \tag{4.42}$$

it might be possible to retrieve even more information. It seems evident that j should be chosen as a low number as this will make ω large. Therefore by taking $j = -1$, $n = -1$, $m = 0$, and $p = 1$ the following four function are found via dominant balances:

$$k_1 = \omega - \frac{-\kappa^2}{2\omega} \tag{4.43a}$$

$$k_2 = \sqrt{2(1+\nu)}\omega + \frac{\kappa^2(1+\nu)\left(-(7+5\nu)(\omega d)^2 + \lambda\left(8+(7+5\nu)(\omega d)^2\right)\right)}{2\sqrt{2(1+\nu)}\omega d\left(-\left(1+3\nu+2\nu^2\right)(\omega d)^2 + \lambda\left(-8+\left(1+3\nu+2\nu^2\right)(\omega d)^2\right)\right)}d^{-1} \tag{4.43b}$$

$$k_3 = \sqrt{\frac{(2+\lambda+2\nu)(\omega d)^2 + \sqrt{-4\lambda(1+\nu)(\omega d)^4 + 4(1+\nu)^2(\omega d)^4 + \lambda^2(\omega d)^2\left(64+(\omega d)^2\right)}}{2\lambda}}d \tag{4.43c}$$

$$k_4 = \sqrt{\frac{(2+\lambda+2\nu)(\omega d)^2 - \sqrt{-4\lambda(1+\nu)(\omega d)^4 + 4(1+\nu)^2(\omega d)^4 + \lambda^2(\omega d)^2\left(64+(\omega d)^2\right)}}{2\lambda}}d \tag{4.43d}$$

In all cases K_2 turns out to be zero and K_3 can only be determined for k_1 and k_2 as division by zero occurs for k_3 and k_4. k_1 and k_2 are seen to resemble the previous results to the leading order, but are influenced by the curvature at the first correction. k_3 and k_4 are seen to be identical to the solutions of the straight Timoshenko beam, hence it is known that at very high frequencies they will settle down to the first and last asymptotes in equation (4.32). Plots of the asymptotes (4.43) can be seen in figure 4.21 - 4.23. These plots show that these alternative asymptotic expansions approximate the exact solutions much more accurately, particularly are the flexural and shear wave predicted quite precisely at much lower frequencies. The results also shows that the flexural and shear wave do not distinguish between the helix and the straight rod since equation (4.43c) and (4.43d) are identical to (4.34) for the straight rod. Moreover it is seen that the axial wave given by (4.43a) and the torsional wave (4.43b) to the leading order they still do not feel the geometry of the helix, but to the first correction they fell the in-plane curvature κ. So effectively, it can be concluded that at this level of approximation these waves do not distinguish between an infinite ring and a helix.

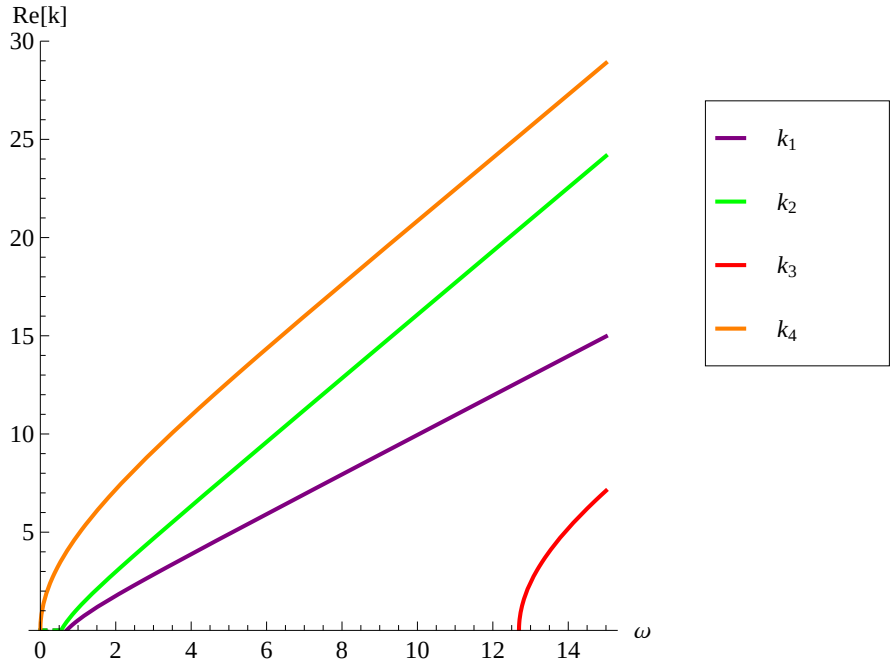

Figure 4.21: *High frequency asymptotes.*

4.3.3 Low frequency asymptotes

The diversity of branches in the low frequency range, figure 4.3, implies that several analyses are required to capture the full picture. This will be done in two stages. First expansion around $k = 0$ is conducted and then around $k \approx 1$ at $\omega = 0$. For the latter a study of the sensitivity to very small pitch angles is presented.

All of the analysis originates from the following scalings:

$$\omega = \omega_0 d^j \tag{4.44}$$

$$k = k_0 d^n \tag{4.45}$$

To capture the branches emerging from zero the scalings $j = 2$ and $n = 1$ are chosen. These leads to the following dominant balance:

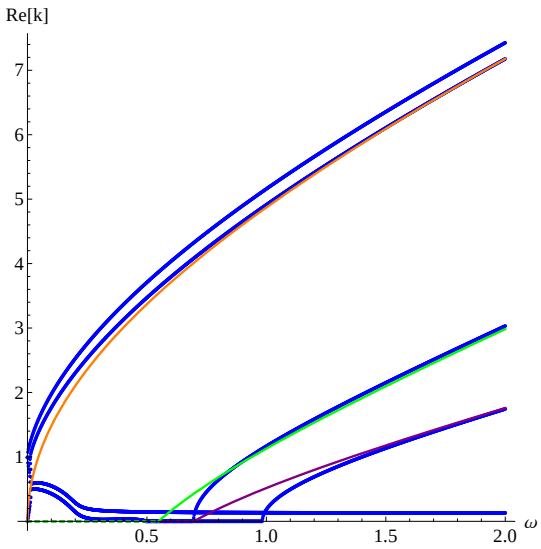

Figure 4.22: *Exact solution and asymptotic expansions for wave number for* $\omega < 2$.

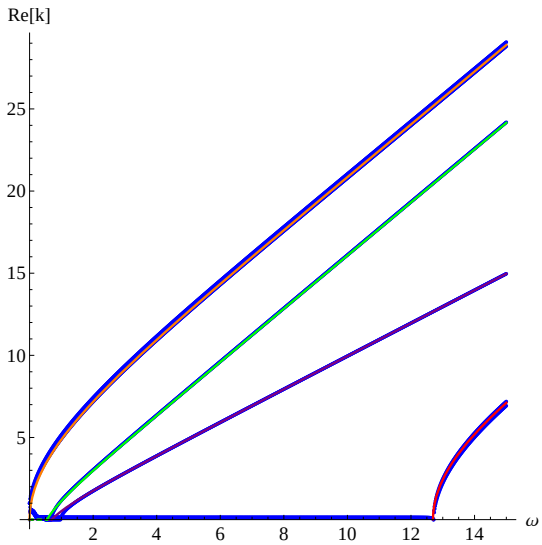

Figure 4.23: *Exact solution and asymptotic expansions for wave number for* $\omega < 15$.

$$0 = \frac{\kappa^4 \lambda^2 \left(k_0^2 - 16\omega_0^2\right)\left(k_0^2 - 16(1+\nu)\omega_0^2\right)}{4(1+\nu)^3} d^{10} + \dots \tag{4.46}$$

Again by solving for the corrections and plugging these into the posed expansions yields:

$$k = \pm \frac{4\omega}{d} \tag{4.47a}$$

$$k = \pm \frac{4\sqrt{(1+\nu)}\omega}{d} \tag{4.47b}$$

A plot of these reveals that they fit well to the exact solution for low frequencies. Plots are seen in figure 4.24 and 4.25. The result proves that these wave numbers do not depend on geometry apart from the small parameter d.

In Wittrick [1966] a straight elastic rod analogy is made to determine the velocity of an axial and a torsion wave in a helix. In the paper the velocity of the wave that elongate the equivalent rod travels with the speed $V = \frac{d}{4R\sqrt{1+\nu}}\sqrt{\frac{E}{\rho}}$ along the helix thread. This result matches the phase velocity of the wave number in (4.47b) if determined in dimensional variables. The wave twisting the equivalent rod travels with the velocity $V' = \frac{d}{4R}\sqrt{\frac{E}{\rho}}$ along the helix thread, which is identical to the phase velocity that can be determined from (4.47a). As it intuitively seems trustworthy that elongation of a spring causes torsion on a local level and vice versa, the analogy is in agreement with these approximations and the modal analysis.

Now the attention is turned to the branches emerging from $k \approx 1$, in figure 4.3. This will turn out to be particularly challenging since an *inner scaling* is required. However, first it is noted that by solving the dispersion equation wrt. k for $\omega = 0$ the following roots are found:

$$k^{(IV)} = 0 \qquad \wedge \qquad k^{(IV)} = \pm\sqrt{\kappa} \tag{4.48}$$

I.e. it is known from the beginning that the expansion must be able to return $k = \sqrt{\kappa}$ at $\omega = 0$. By posing the regular perturbation theory expansions (4.44) and (4.45) where $j = 1$ and $n = 0$ a dominant balance is found as:

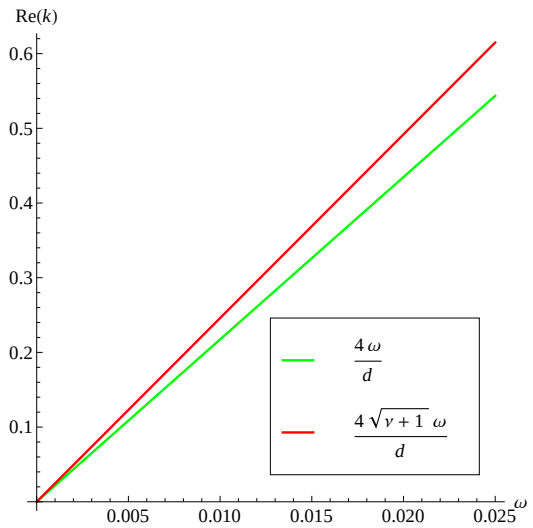

Figure 4.24: *Asymptotic expansions in the low frequency range.*

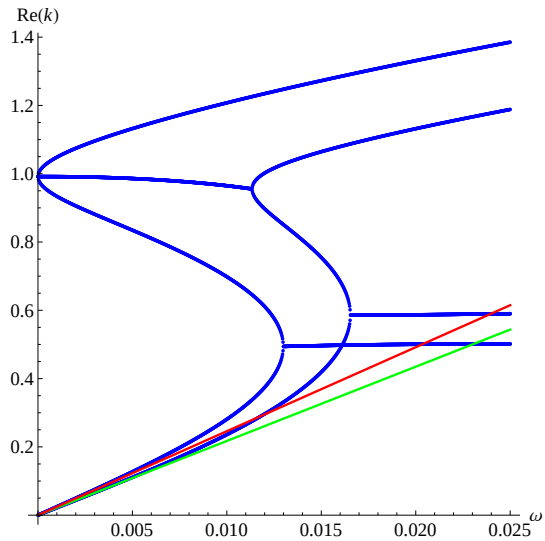

Figure 4.25: *Asymptotic expansions and exact solution in the low frequency range.*

$$
\begin{aligned}
0 = \lambda^2 \Big(& k_0^{12} - 4k_0^{10}\kappa + 256\kappa^4(1+\nu)\omega_0^4 - 16k_0^2\kappa^2(2+\nu)\omega_0^2\left(\kappa^4 + 2\kappa^2\tau^2 + \tau^4 - 16\omega_0^2\right) \\
& + 2k_0^8\left(3\kappa^4 + 6\kappa^2\tau^2 + 3\tau^4 - 16\omega_0^2\right) - 4k_0^6\left(\kappa^6 + 3\kappa^4\tau^2 + \tau^6 + 48\tau^2\omega_0^2 + \kappa^2\left(3\tau^4 + 4(-2+\nu)\omega_0^2\right)\right) \\
& + k_0^4\left(\kappa^8 + 4\kappa^6\tau^2 + \left(\tau^4 - 16\omega_0^2\right)^2 + \kappa^4\left(6\tau^4 + 32(1+\nu)\omega_0^2\right) + 4\kappa^2\left(\tau^6 - 24\nu\tau^2\omega_0^2\right)\right)\Big) d^4 + \dots
\end{aligned}
\tag{4.49}
$$

At this stage what is found is a dominant part of the dispersion equation when the wave number is close to unity and the frequency is small. The scalings used so far are denoted the *outer scalings*. This polynomial is still to large to give any simple expression for the wave number. Therefore an additional expansion is now suggested. This time the expansion is made on k with ω as the small parameter due to the outer scaling:

$$
k_0 = K_0 + K_1\omega_0^{1/2} + K_2\omega_0 + K_3\omega_0^{3/2} + \dots \tag{4.50}
$$

The choice of expanding in fractional powers of ω_0 is inspired by the exact solution, since this has similarities to a polynomial. When posing this *singular perturbation theory expansion* and equating powers of the small parameter the following leading order term is found:

$$
0 = d^4 K_0^4\left(K_0^2 - \kappa\right)^4 \lambda^2 \omega_0^0 + \dots \qquad \Rightarrow \qquad K_0^{(IV)} = 0 \qquad \wedge \qquad K_0^{(IV)} = \pm\sqrt{\kappa} \tag{4.51}
$$

Which is as concluded initially. Proceeding to the next power of ω and using only the positive root $K_0 = \sqrt{\kappa}$ from the previous level, the next dominant balance is:

$$
0 = \dots + 4\kappa^2\lambda^2\left(-32\tau^2\left(\kappa^2(2+\nu) + 2\tau^2\right) + 4\kappa^2 K_1^4\right)\omega_0^2 + \dots \qquad \Rightarrow \tag{4.52}
$$

$$
K_1 = \pm i\mathcal{K}_1 \qquad \wedge \qquad K_1 = \pm\mathcal{K}_1 \tag{4.53}
$$

$$
\text{where} \qquad \mathcal{K}_1 = 2^{3/4}\left(\frac{\tau^2}{\kappa}(2+\nu\kappa)\right)^{1/4} \tag{4.54}
$$

To obtain these expressions a certain amount of simplification is necessary. Here the two relations $\kappa^2+\tau^2=\kappa$ and $\kappa^3+\kappa\tau=\kappa^2$ come in particularly handy. Immediately the next power of ω_0 is identified:

$$0=\cdots+16K_1\kappa^{3/2}\lambda^2\left(-32\tau^2\kappa\,(3+\nu\kappa)+4K_1^2K_2\kappa^{5/2}+6\kappa^2K_1^4\right)\omega_0^{5/2}+\ldots \qquad \Rightarrow \tag{4.55}$$

$$K_2^{(II)}=-\mathscr{K}_2 \qquad \text{for} \qquad K_1=\pm\mathscr{K}_1 \qquad \wedge \qquad K_2^{(II)}=\mathscr{K}_2 \qquad \text{for} \qquad K_1=\pm i\mathscr{K}_1 \tag{4.56}$$

$$\text{where} \qquad \mathscr{K}_2=\frac{\sqrt{2}\nu\tau}{\sqrt{2+\kappa\nu}} \tag{4.57}$$

It presents no difficulties to proceed with the next term in the singular perturbation theory expansion, however, the correction becomes a large expression and therefore it is not presented here, but the next balance is found at power ω_0^3 which produces four roots: $K_3=\pm\mathscr{K}_3$ and $K_3=\pm i\mathscr{K}_3$.

The scaled wave numbers can then be written as:

$$k_0=K_0\pm\mathscr{K}_1\sqrt{\omega_0}-\mathscr{K}_2\omega_0\ \pm\mathscr{K}_3\omega_0^{3/2} \qquad \wedge \qquad k_0=\mathscr{K}_0\pm i\mathscr{K}_1\sqrt{\omega_0}+\mathscr{K}_2\omega_0\ \pm i\mathscr{K}_3\omega_0^{3/2} \tag{4.58}$$

Returning to unscaled variables yields:

$$k=K_0\pm\mathscr{K}_1\frac{\sqrt{\omega}}{\sqrt{d}}-\mathscr{K}_2\frac{\omega}{d}\pm\mathscr{K}_3\frac{\omega^{3/2}}{d^{3/2}} \qquad \wedge \qquad k=K_0\pm i\mathscr{K}_1\frac{\sqrt{\omega}}{\sqrt{d}}+\mathscr{K}_2\frac{\omega}{d}\pm i\mathscr{K}_3\frac{\omega^{3/2}}{d^{3/2}} \tag{4.59}$$

Obviously these represent propagating and evanescent waves respectively due to the imaginary terms in the latter expansion. Plots of these are seen in figure 4.26 through to 4.29 where the two first figures are plotted with an expansion truncated after $\mathscr{K}_2$ and the last two includes $\mathscr{K}_3$. Here it seems quite evident that including four terms in the expansion remarkably improves the validity range of the asymptotic approximation.

The corrections in the expansion indicates that the wave numbers are dependent in the curvature and torsion in a quite complex manner, but to the leading order term κ is the dominant parameter.

Now the case of very small pitch angles are considered. The starting point is the dominant balance found from the previous outer scaling, i.e. equation (4.49), however, this time the small parameter in the inner scaling is τ. Therefore the following scalings are suggested for the inner expansion:

$$k_0=K_0+K_1\tau^i \tag{4.60a}$$

$$\omega_0=\Omega_0\tau^m \tag{4.60b}$$

On top of this it is important to notice that curvature and torsion are not independent, and a coupling between the two should therefore be build in to the dominant balance. Here the identity $\kappa^2-\kappa+\tau^2=0$ will be used. By posing an expansion:

$$\kappa=\kappa_0+\kappa_1\tau+\kappa_2\tau^2+\kappa_3\tau^3+\kappa_4\tau^4+\ldots \tag{4.61}$$

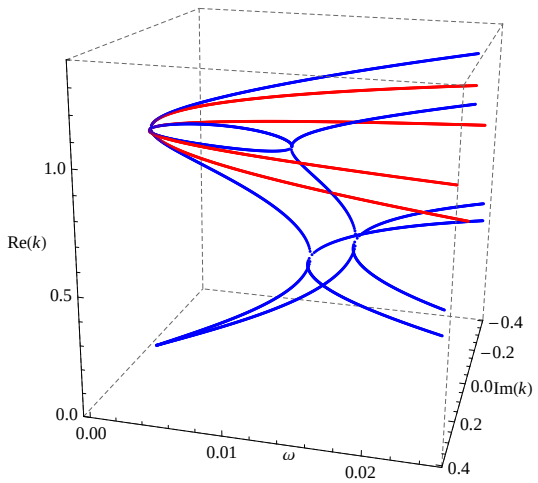

Figure 4.26: *Exact dispersion curves and asymptotic expansions (red curve) truncated after $\mathcal{K}_2$, front view.*

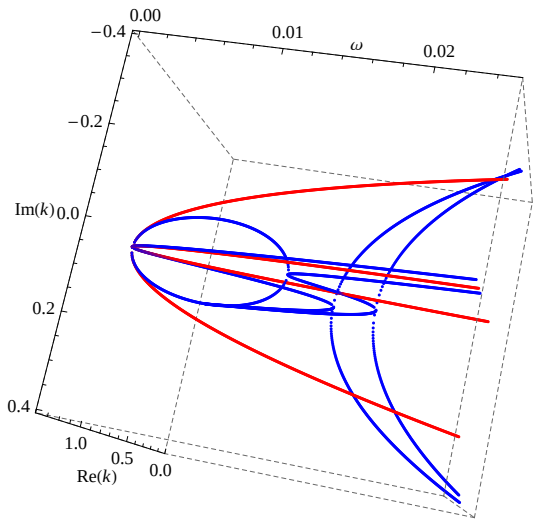

Figure 4.27: *Exact dispersion curves and asymptotic expansions (red curve) truncated after $\mathcal{K}_2$, top view.*

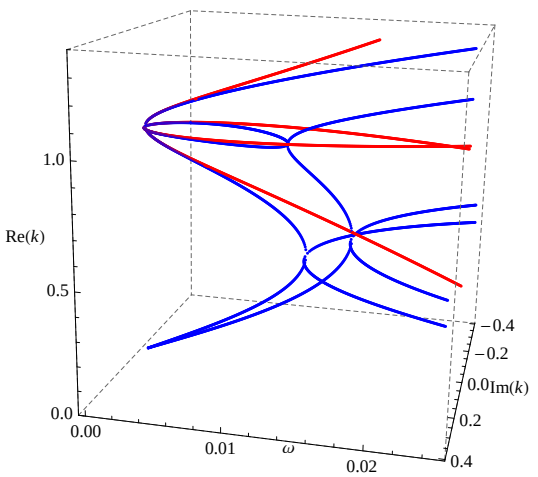

Figure 4.28: *Exact dispersion curves and asymptotic expansions (red curve) including $\mathcal{K}_3$, front view.*

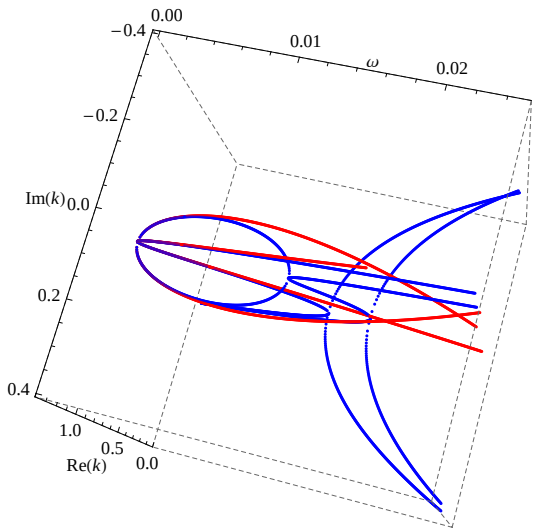

Figure 4.29: *Exact dispersion curves and asymptotic expansions (red curve) including $\mathcal{K}_3$, top view.*

and following the procedure of inserting this, equate powers of τ, and then determine the corrections, the following result is obtained:

$$\kappa = 1 - \tau^2 - \tau^4 \tag{4.62}$$

By substituting this into equation (4.49), and use the inner scalings in (4.60) with $i = m = 1$ a dominant balance is found. When equating powers of the small parameter it is found that $K_0 = 1$ which is also expected since this is an unperturbed root. Meanwhile the correction K_1 is found to be:

$$K_1 = \pm\sqrt{2}\sqrt{(4+\nu)\omega_0^2 \pm \omega_0\sqrt{\left(4+2\nu+\nu^2\omega_0^2\right)}} \tag{4.63}$$

And in unscaled variables k reads:

$$k = 1 \pm \sqrt{2}\sqrt{(4+\nu)\left(\frac{\omega}{\tau d}\right)^2 \pm \frac{\omega}{\tau d}\sqrt{\left(4+2\nu+\nu^2\left(\frac{\omega}{\tau d}\right)^2\right)}\tau} \tag{4.64}$$

$$= 1 \pm \sqrt{2}\sqrt{(4+\nu)\left(\frac{\omega}{d}\right)^2 \pm \frac{\tau\omega}{d}\sqrt{\left(4+2\nu+\nu^2\left(\frac{\omega}{\tau d}\right)^2\right)}} \tag{4.65}$$

A few numerical examples are shown in figure 4.30 through to 4.34. Remark that the asymptotic approximation do not allow for zero valued pitch angle, and therefore figure 4.33 is generated with a very small pitch angle rather than just zero. The plots implies that the two-term approximation for k for low frequencies (below $\omega \approx 0.03$) resembles quite well the real and imaginary part of the exact solution. In figure 4.34 a plot for the exact and approximated solution with $\psi = 0.13$ is shown. Qualitatively this captures the behaviour in this region of the $k-\omega$ space very well, but quantitatively it breaks down at a low frequency. The precision can as usual be increased by adding another term in the expansion for k, however, when trying this it quickly becomes clear that the expressions become very large, and the easy interpretation is therefore no longer available.

From the figures it is clear that a change in pitch angle drastically determines when the evanescent wave emerging from $\omega = 0$ cuts on. This mechanism is seen in formula (4.65) as the competition between the first and second term below the outer radical. Here the first term will for very low frequencies be the smaller until the frequency is sufficiently large so that the quadratic term wins over the linear term. However, when the pitch angle is made smaller the range of frequencies in which the first term is smaller than the second term as τ decreases. In addition the dominans of the first term for very small pitch angles is also why the branches of propagating waves appears as straight lines in the dispersion diagram, since it becomes linear when removing the square root.

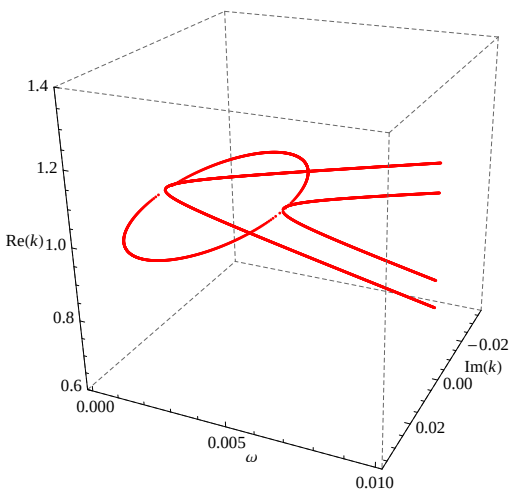

Figure 4.30: *Asymptotic approximation in the low frequency range for* $\psi = 0.05\,rad$.

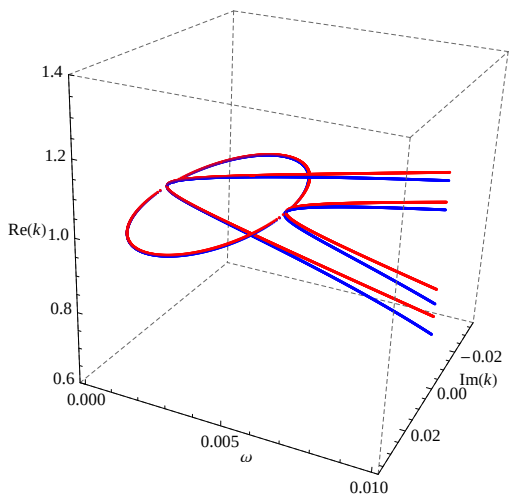

Figure 4.31: *Asymptotic approximation (red curve) and exact solution (blue curve) for* $\psi = 0.05\,rad$.

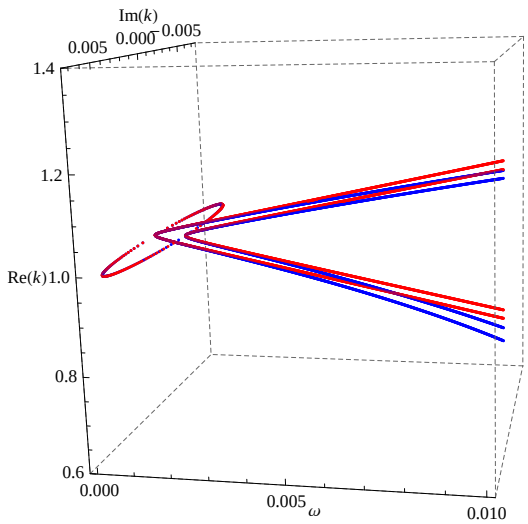

Figure 4.32: *Asymptotic approximation (red curve) and exact solution (blue curve) in the low frequency range for* $\psi = 0.01\,rad$.

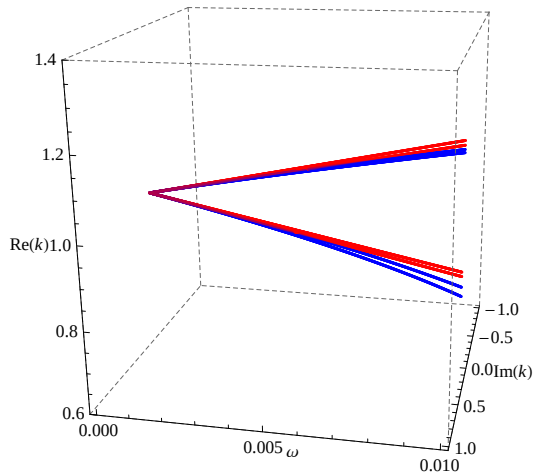

Figure 4.33: *Asymptotic approximation (red curve) and exact solution (blue curve) in the low frequency range for* $\psi = 0.0001\,rad$.

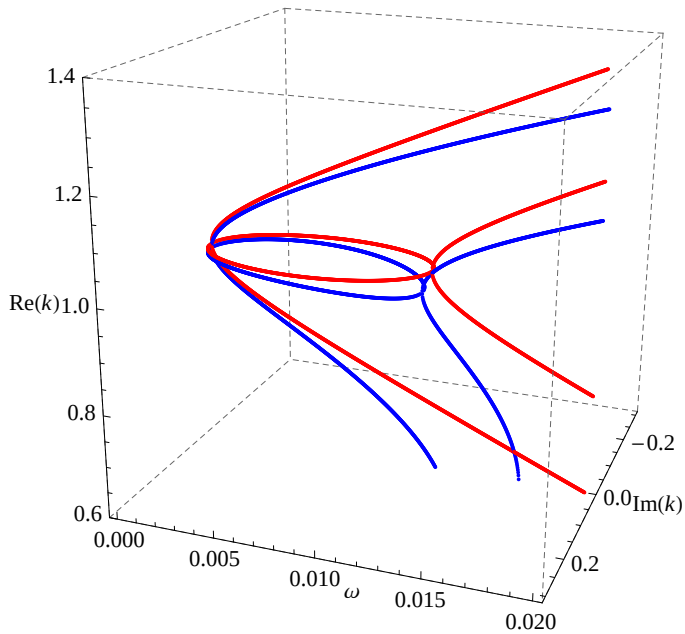

Figure 4.34: *Asymptotic approximation (red curve) and exact solution (blue curve) for* $\psi = 0.13\,rad$.

4.4 Final remarks

The aim of the work presented in this chapter was to introduce and familiarise with the methods and techniques involved in the study of wave propagation. Through that exercise the following experiences are drawn regarding methods:

- Even though all derivations are conducted analytically, the procedure is sensitive to the conditioning of the dispersion equation. Therefore in the following more advanced analysis care must be taken on this issue. To keep working in nondimensional variables is therefore prudent. This method also enables much broader options for comparison with

different geometries and material properties.

- One must be very much aware when doing asymptotic analysis. Several pitfalls must be avoided such as forgetting to return from scaled to unscaled variables and to assess which scalings are appropriate in different regions of the $k-\omega$ space. In spite of these difficulties the method must be said to robustly produce neat explicit approximations for wave numbers, whose exact expressions are unknown.

- The use of software such as Mathematica is essential, as the expressions are so large that it seems virtually impossible to handle this without appropriate software.

When it comes to the actual results of the analysis it is concluded that:

- Wave propagation in a helical has inherent strong couplings in the low frequency range, but at sufficiently high frequency the waves decouple and therefore propagate as in a straight rod.

In the next chapter a corrugated spring is analysed using similar techniques, however, the methods are more complex since it involves solutions on *multiple scales*.

Chapter

5

Investigation of wave propagation in perturbed helical spring

In this section a helical spring of irregular shape is considered. The aim is to take the first step towards assessing the influence of irregular geometry on the wave propagation and modal coupling. First some geometry considerations are presented, thereafter the method for solving which is along the lines of perturbation methods.

The perturbation of a helical spring can of course be done on several parameters. In this chapter the radius is chosen as the perturbed parameter. As is expected the mathematics become even more involved compared to the previous chapter and consequently many expressions are not presented in their explicit form.

5.1 Determining the geometry

The radius will be perturbed to be periodic with s. When doing this an important issue is whether the perturbation of the radius causes perturbations of any other parameter. I.e. does a change in radius implicitly entail a change in pitch angle.

A similar approach as for the parametrisation as in chapter 4 could be taken. This would involve the following function with the angle of revolution as the parameter:

$$\vec{r}(\phi) = \begin{Bmatrix} (\overline{R} + \eta \sin(\zeta\phi)) \cos(\phi) \\ (\overline{R} + \eta \sin(\zeta\phi)) \sin(\phi) \\ \phi \tan(\psi) \end{Bmatrix} \tag{5.1}$$

where:

$\overline{R}$	Mean radius.
η	Corrugation, change in radius for perturbed spring.
ζ	Corrugation rate.

Then establish a relation between ϕ and s which allows for rewriting (5.1). It turns out to be troublesome to establish this relation as it requires integration of $\sqrt{\sin()}$. Alternatively one could also just suggest:

$$\vec{r}(s) = \begin{Bmatrix} (\overline{R} + \eta \sin(\zeta s)) \cos\left(\frac{s}{\overline{R}\sqrt{1+\tan^2(\psi)}}\right) \\ (\overline{R} + \eta \sin(\zeta s)) \sin\left(\frac{s}{\overline{R}\sqrt{1+\tan^2(\psi)}}\right) \\ \frac{s\tan(\psi)}{\sqrt{1+\tan^2(\psi)}} \end{Bmatrix} \tag{5.2}$$

The question is now what the difference is between 5.1 and 5.2. This can be revealed by studying the pitch angle on a local level. Let ψ_a denote the actual pitch angle of a spring. Then the actual pitch angle of a spring generated using formula (5.1) is:

$$\tan(\psi_a) = \frac{z(\phi)}{R(\phi)\phi} = \frac{\overline{R}\phi\tan(\psi)}{\overline{R} + \eta\sin(\zeta\phi)} \tag{5.3}$$

So, the actual pitch angle of the spring varies with ϕ. The specified pitch ψ and the actual ψ_a coincides in the trivial case where either one of the perturbations η or ζ are zero. The similar test for the parametrisation in (5.2) reveals the following:

$$\sin(\psi_a) = \frac{z(s)}{s} = \frac{\tan(\psi)}{\sqrt{1+\tan(\psi)}} = \frac{\sin(\psi)}{\sqrt{\sin^2(\psi)+\cos^2(\psi)}} = \sin(\psi) \tag{5.4}$$

So this parametrisation will ensure that the pitch angle is constant and equals the specified one. The disadvantages of this parametrisation is though that it gets harder to keep track of how many windings a spring with a specified s has revolved. This will turn out to be important in the following chapter. Even so, the parametrisation in (5.2) is adopted in the following.

Calculating the curvature and torsion for this spring is done using the exact same procedure as in section 4.1, but the intermediate steps are much more cumbersome and likewise are the results. However, by imposing smallness of the rate of modulation ζ (i.e. ignoring terms having ζ^2 as a factor) the results simplifies to:

$$\kappa(s) = \frac{\cos^2(\psi)}{\overline{R}^2}\left(\overline{R} + \eta\sin(\zeta s)\right) \qquad \wedge \qquad \tau = \frac{\sin(\psi)\cos(\psi)}{R} \tag{5.5}$$

So, with this approximation, the curvature are influenced by the perturbation while it only has a higher order influence on the torsion.

These expressions are substituted into the governing equations and these are nondimensionalised exactly as in the previous chapter. Consequently a set of second order linear differential equations with spatially varying coefficients are obtained. The spatially varying coefficient compose a new challenge, which must be handled somehow.

It turns out convenient when representing the sine function in the perturbation as exponential functions, i.e. using $\sin(\zeta s) = \frac{1}{2i}\left(e^{i\zeta s} - e^{-i\zeta s}\right)$.

5.2 Methods for solving

The wave propagation in the perturbed spring is expected to be a composition of two different processes. An analogy can be drawn to a weakly damped oscillator with one degree of freedom, say a pendulum with a small damping. Here the oscillations of the pendulum happens on a fast time scale while the drift and decay in amplitude happens over a much longer time scale. The

fact that the full solution can be decomposed into two distinct processes, will be utilised in this chapter.

For the perturbed spring, where the geometry has a slow variation in space compared to the conventional helix, it is expected that wave length is of order of a short scale while the drift or decay in amplitude happens over a much longer scale. The obvious choice of methods for this prototypical example, suggested by *Perturbation Methods*, is the *Method of Multiple Scale* and the *WKB-approximation*. In the literature some examples of wave propagation in corrugated wave guides can be found where the above mentioned method has been applied, e.g. Peake [2005]. The methods are not restricted to small modulations, but to small modulation rates. In other words; the corrugation of the helix radius are allowed to be large just as long as it happens over a large distance.

In the following these methods are explained in a more detail, and how they can be applied to the problem at hand.

5.2.1 Method of multiple scales

The core of these methods lies within the introduction of a short and a long scale which are treated as independent of one another. This can be both short/fast and long/slow scales in space and in time.

The idea is to related the short length scale S_s and the long length scale S_l to the actual length scale s via the small parameter like:

$$S_s = s \qquad \wedge \qquad S_l = \zeta s \tag{5.6}$$

where: S_s Short scale.

S_l Long scale.

To embed this in the governing equations the chain rule must be applied to define derivatives wrt. s. Thus:

$$\frac{\partial}{\partial s} = \frac{\partial S_s}{\partial s}\frac{\partial}{\partial S_s} + \frac{\partial S_l}{\partial s}\frac{\partial}{\partial S_l} = \frac{\partial}{\partial S_s} + \zeta\frac{\partial}{\partial S_l} \tag{5.7}$$

$$\frac{\partial^2}{\partial s^2} = \frac{\partial^2}{\partial S_s^2}\left(\frac{\partial}{\partial S_s} + \zeta\frac{\partial}{\partial S_l}\right) + \zeta\frac{\partial^2}{\partial S_l^2}\left(\frac{\partial}{\partial S_s} + \zeta\frac{\partial}{\partial S_l}\right) = \frac{\partial^2}{\partial S_s^2} + 2\zeta\frac{\partial^2}{\partial S_s \partial S_l} + \zeta^2\frac{\partial^2}{\partial S_l^2} \tag{5.8}$$

After applying these definitions to the governing equations the standard procedure of perturbation method must be followed. So, one must equate powers of the small parameter and then hopefully the terms that caused the need for methods of multiple scale are removed from the leading order balance, and instead found at the first correction.

For the problem of the perturbed helix the solution is sought as power expansions on the small parameter. So for instance:

$$\alpha(S_s, S_l) = \alpha_0(S_s, S_l) + \zeta\alpha_1(S_s, S_l) + \zeta^2\alpha_2(S_s, S_l) + \dots \tag{5.9}$$

And likewise for the remaining kinematic variables. Now, proceeding to equating powers of ζ the terms in the governing equations independent of ζ still contains the spatially varying curvature. The presence of spatially varying coefficients was what caused the need for the method of multiple scales, and it must be concluded, for the time being, that this method is

insufficient in this context. It seems that if the perturbation had been chosen differently, say just a constantly increasing radius, the extraction of the slowly varying part from the leading order would have been successful. However, alternative methods must be suggested.

An essential points in the method of multiple scales is establishing the *secularity condition*. This is omitted in this subsection, but will be presented in the following.

5.2.2 The WKB-approximation

What will now be attempted is the so-called *WKB*-appproximation or *WKB*-method. Indeed this is a method utilising multiple scales, however, with the advantage that it can handle differential equations with spatially varying coefficients that is known, but not specified initially. The WKB-method can handle the canonical equation:

$$\frac{d^2 y}{ds^2} + g^2(\epsilon s)s = 0 \tag{5.10}$$

This example is adopted from Peake [2005], but a similar example is represented in Hinch [1991]. Here ϵ is a small parameter and g is a function that do not need to be specified at this stage. Particular to the WKB-method is that the short length scale is now chosen as a function $\theta(x)$ and the long scale is chosen as before. Remark that the derivative $\frac{\partial\theta}{\partial x}$ will be another function $f(X_l)$ of the long length scale since ϵ will be pulled out in front. These definitions are embedded in the governing equation using:

$$\frac{\partial}{\partial s} = f(S_l)\frac{\partial}{\partial\theta} + \epsilon\frac{\partial}{\partial S_l} \tag{5.11}$$

And similarly for the two times derivative. Then, by posing a power expansion as the solution to (5.10), the dominant balance is found as:

$$f^2(S_l)\frac{\partial^2 y_0}{\partial\theta^2} + g^2(\epsilon s)y_0 = 0 \tag{5.12}$$

In this case the obvious thing to do is setting $f = g$, an the solution can then be found in the exponential form $y_0(\theta) = a_0 e^{i\theta} + b_0 e^{-i\theta}$. An important point is here that the amplitude a_0 might be a function of the long length scale. The next level in the asymptotic series can be found as:

$$f^2\frac{\partial^2 y_1}{\partial\theta^2} + \kappa^2 y_1 = -2f\frac{\partial^2 y_0}{\partial S_l\partial\theta} - \frac{\partial f}{\partial S_l}\frac{\partial y_0}{\partial\theta} = \left(-2fi\frac{\partial a_0}{\partial S_l} - i\frac{\partial f}{\partial S_l}a_0\right)e^{i\theta} \tag{5.13}$$

Note here that the complementary solution to (5.13) is contained in the RHS. These are called *secular* terms since, from the theory of elementary differential equations, a particular solution of the form $y_1(\theta) = a_1\theta e^{i\theta}$ is found. As mentioned in chapter 4 this resembles an instable wave as it will keep grow on the short scale. According to Peake [2005] this resonant behaviour is well known, and should not be regarded as a feature of any real physical system. Therefore a *secularity condition* or *solvability condition* is introduced to avoid the secular behaviour:

$$-2fi\frac{\partial a_0}{\partial S_l} - i\frac{\partial f}{\partial S_l}a_0 = 0 \tag{5.14}$$

The solution to the secularity condition provides an expression for the amplitude in the leading order term a_0 that allows the solution to the first correction to be valid. After solving for a_0 the

solution of (5.10) is known to the leading order, where the function g affect both the amplitude and the wave number to drift on the long scale as opposed to the conventional method of multiple scales where only the amplitude will feel the slow change in the leading order.

The concept of identifying secular terms and eliminating these are not specific to the WKB-method, but appears in the same way in the conventional method of multiple scales, as mentioned earlier.

The WKB-method turns out to be difficult to apply to the problem of a perturbed helix. The root of the problem is that the governing equations are not of the canonical form in (5.10), thus the choice of setting $f = g$ does not turn out as convenient as it does in the example by Peake [2005]. Hinch [1991] presents a method to transform more general equations to the canonical form using. This technique does not have the similar effect when applied to the six governing equation, and therefore further work needs to be done before the WKB-approximation can be applied. The result from the attempt with the WKB-method can be seen in *Mathematica files » WKB.nb*.

5.2.3 Necessary restrictions on perturbation

After having concluded that neither the conventional method of multiple scales or WKB-method can be applied to solve the perturbed helical spring problem, the corrugation η is now restricted to be small. This provides new options for the conventional method of multiple scales. This alters the small parameter in equation (5.6)-(5.9) to be η rather than ζ. Remark that this dies not relax the assumptions on ζ since this was already restricted to be small when deriving (5.5).

It is not regarded as impossible to apply the WKB-method to this problem. It most likely require that one is able to find the right transformation that will provide an option for choosing the function f or other alternative that can provide a breakthrough.

5.3 Finding the solution on multiple scales

The derivation can be followed in the *Mathematica files » multipleScales.nb*. *Part 1* is trivial operations and in *Part 2* the different length scales are introduced.

Restricting η to be small provides a dominant balance exactly as for the conventional helix. In mathematical notations this can be sketched as

$$\underline{L}\begin{Bmatrix} u_0 \\ \vdots \\ \gamma_0 \end{Bmatrix} = \vec{0} \tag{5.15}$$

where: $\underline{L}$ Differential operator.

Here $\underline{L}$ is the same operator as the one resulting in the system matrix for the conventional helix. In the Mathematica file this corresponds to *Part 3*. Hence, at this stage it is known that the solution to the leading order is identical to the solution of the conventional helix while being aware that the amplitudes will be a function of the long scale.

It is now convenient to introduce the modal coefficients, by doing this only one unknown amplitude is left in the system. Hence equation (5.15) is then rewritten to:

$$\underline{L}\begin{Bmatrix} 1 \\ M_{v_0} \\ \vdots \\ M_{\gamma_0} \end{Bmatrix} u_0 = \vec{0} \tag{5.16}$$

where: M_m Modal coefficient linking the m'th variable to u_0.

The general solution to the leading order is therefore:

$$u_0 = \mathscr{U}_0 e^{ik_0 s - i\omega t} + \mathscr{U}_0^* e^{-ik_0 s - i\omega t} \tag{5.17}$$

where: $\mathscr{U}_0^*$ Complex conjugate of $\mathscr{U}_0$.

For convenience the complex conjugated terms are included. Indeed the same could have been done for the solutions in the previous chapter and then having introduced the casuality principle later.

Proceeding to the next level, *Part 4* in the Mathematica, the dominant balance can be partitioned into a system as sketched below:

$$\underline{L}\begin{Bmatrix} u_1 \\ \vdots \\ \gamma_1 \end{Bmatrix} = \sum_{j=1}^{6} \underbrace{\left(\vec{V}_j^{sd} + \vec{V}_j^{r1} e^{i\zeta s} + \vec{V}_j^{r2} e^{-i\zeta s}\right)}_{\mathscr{U}_{0,j}, M_{m,j}} e^{ik_{0,j} s} + \underbrace{\left(\vec{V}_j^{sd,*} + \vec{V}_j^{r1,*} e^{i\zeta s} + \vec{V}_j^{r2,*} e^{-i\zeta s}\right)}_{\mathscr{U}_{0,j}^*, M_{m,j}^*} e^{-ik_{0,j} s} \tag{5.18}$$

where: $\vec{V}^{sd}$ Vector containing only slow derivatives of amplitudes.

$\vec{V}^{r1}$ Vector containing coefficients of $e^{i\zeta s}$.

$\vec{V}^{r2}$ Vector containing coefficients of $e^{-i\zeta s}$.

j Mode.

Conceptually this is similar to equation (5.13). Remark in equation (5.18) the wave number on the RHS is known from the leading order, but the leading order amplitudes are broad along to the first order balance, and must be determined at this stage. The vectors on the RHS of (5.18) are quite cumbersome, but they contain $\mathscr{U}_{0,j}, M_{m,j}$ and their complex conjugated, ζ, $k_{0,j}$, ω and the system parameters κ, τ, d, λ, and ν.

Since the LHS at this order is identical as to the leading order it is known that the complementary solution to (5.18) will be of the same form as (5.17). Being that the RHS still contains some spatially varying coefficients these must be handled to somehow be contained in a secularity condition and through that being forced to vanish. Hence a condition for solvability must be provoked before proceed. This approach is along the same lines as presented in both V. Krylov [1997] and S.V.Sorokin [2003].

A choice of ζ must be attempted and followed by an identification of secular terms. The obvious thing to do is choosing ζ as a multiple of a wave number or a combination of different wave numbers. Say $\zeta = 2k_p$ (where $p = 1, 2, \ldots$ or 6) then by adding the exponentials on the RHS of (5.18) it is seen that every:

$$\vec{V}_{j\neq p}^{sd} e^{ik_{0,j\neq p} s} \qquad \wedge \qquad \vec{V}_{j\neq p}^{sd,*} e^{-ik_{0,j\neq p} s} \tag{5.19}$$

term is secular. This is found as *Part 5* in the Mathematica file. For the terms where $j = p$ these additional terms are also resonant:

$$\vec{V}^{sd}_{j=p} e^{ik_{0,p}s} + \vec{V}^{r1,*}_{j=p} e^{ik_{0,p}s} \qquad \vec{V}^{sd,*}_{j=p} e^{-ik_{0,p}s} + \vec{V}^{r2}_{j=p} e^{-ik_{0,p}s} \tag{5.20}$$

So for this choice of ζ the secularity conditions are:

$$\vec{V}^{sd}_{j\neq p} = 0 \tag{5.21a}$$

$$\vec{V}^{sd,*}_{j\neq p} = 0 \tag{5.21b}$$

$$\vec{V}^{sd}_{j=p} + \vec{V}^{r1,*}_{j=p} = 0 \tag{5.21c}$$

$$\vec{V}^{sd,*}_{j=p} + \vec{V}^{r2}_{j=p} = 0 \tag{5.21d}$$

Condition (5.21a) and (5.21b) states that derivatives of amplitudes wrt. slow scales are zero. This means that the waves with wave number different from twice the corrugation rate ζ will not feel the modulation and be just as for the conventional helix to the leading order. However, the two remaining secularity conditions will cause an impact on the wave with the wave number the modulation rate is chosen after. To ensure these secular terms are zero one just take the complementary determinants of the system, so in the differential operator $\underline{L}$ one column is replaced by the secularity conditions (5.21c) and (5.21d) and the determinants are taken. This originates from *Cramer's rule* from elementary linear algebra. In general terms this states that a variable x_i in a linear system $\underline{A}\vec{x} = \vec{b}$ can be determined from the principal determinant $det(A)$ and a complementary determinant $det(A_i(\vec{b}))$ (column i is replaced by vector b) via the relation $det(A)x_i = det\left(A_i(\vec{b})\right)$. The principal determinant is zero since it satisfies the dispersion equation, so the complementary determinants must also vanish, where the complementary determinant is formed by (5.21c) and (5.21d). This is done in *Part 6* in Mathematica. This yields the two differential equations:

$$C_1 \frac{\partial U_0}{\partial S_s} + C_2 U_0^* = 0 \tag{5.22a}$$

$$C_3 \frac{\partial U_0^*}{\partial S_s} + C_4 U_0 = 0 \tag{5.22b}$$

Here the constants $C_1 - C_4$ are cumbersome expressions containing around 5,600 to 8,200 terms! By substituting the complex conjugate out of equation (5.22a) and (5.22b) a second order equation is obtained:

$$\frac{\partial^2 U_0}{\partial S_s^2} - \frac{C_2 C_4}{C_1 C_3} U_0 = 0 \tag{5.23}$$

This equation will have a solution of the form:

$$U_0(S_s) = C_0 e^{\xi S_s} + C_0^* e^{-\xi S_s} \quad \text{where} \quad \xi = \sqrt{\frac{C_2 C_4}{C_3 C_4}} \tag{5.24}$$

Here the positive root will cause decay for negative s and the negative root will cause decay for positive s provided that ξ is real, otherwise they will drift. The definition of the slow time

scale ($S_s = \eta s$) can now be reintroduced so that the solution is given explicitly. For the first displacement the solution to the p'th mode for the perturbed helical spring can be stated as:

$$u_p(s) = \mathscr{U}_{0,p} e^{(ik_p - \xi\eta)s} e^{-i\omega t} \tag{5.25}$$

The propagation of the wave is thus governed by the sign and magnitude of $\frac{C_2C_4}{C_3C_4}$. If it is negative ξ becomes complex and the amplitude will drift with of the slow scale, but the amplitude of oscillations remains the same. If $\frac{C_2C_4}{C_3C_4}$ then ξ is real and the wave will attenuate with s like an evanescent wave.

This solution is to the leading order and have one slow scale. Indeed it is doable to increase the accuracy of the solution, by increasing the number of terms in the expansion. However, to keep being able to have the freedom to avoid secular terms one needs to introduce additional superslow scales. According to Hinch [1991] the solution is valid for $s \lesssim O(\eta^{-n})$ when the long scales in the solution are defined up to $S_n = \eta^n s$. This restriction will turn out to be important later.

An informative study is to investigate how lack of perfectly tuned corrugation will affect the wave propagation. This can be done by introducing a *detuning parameter* in the modulation of the spring. So instead of choosing just $\zeta = 2k_p$ then take:

$$\zeta = 2k_p + \sigma\eta \tag{5.26}$$

where: σ Detuning parameter.

The detuning parameter should be seen as an error in the corrugation that enables an assessment of what tolerance can be accepted in the corrugation of the spring.

The secular terms in (5.21c) and (5.21d) works out as:

$$\vec{V}^{sd}_{j=p} + \vec{V}^{r1,*}_{j=p} e^{i\sigma\eta} = 0 \tag{5.27}$$

$$\vec{V}^{sd,*}_{j=p} + \vec{V}^{r2}_{j=p} e^{-i\sigma\eta} = 0 \tag{5.28}$$

Taking the complementary determinants and combining the two first order differential equations gives:

$$\frac{\partial^2 U_0}{\partial S_s^2} - i\sigma \frac{\partial U_0}{\partial S_s} - \frac{C_2C_4}{C_1C_3} U_0 = 0 \tag{5.29}$$

This has the solution:

$$\xi = \frac{i\sigma \pm \sqrt{-\sigma^2 + 4 * \frac{C_2C_4}{C_1C_3}}}{2} \tag{5.30}$$

This equation contains additional information compared to equation (5.24). It states that depending in the size of $\frac{C_2C_4}{C_1C_3}$ there is a range of acceptable slack in the precision of the corrugation that can be allowed and the wave will still decay.

The above analyses can also be conducted with a choice of $\zeta = k_p \pm k_g$. The secular terms will then be collected from both mode p and g, four complementary determinants are taken

from which two second order modulation equations wrt. $\mathscr{U}_{0,p}$ and $\mathscr{U}_{0,g}$ can be stated . The result will be that both mode p and g is affected somehow.

In any case numerical examples needs to be employed to check what effect the corrugation will have on the wave propagation. A few examples of this is presented in the next chapter where results for the analysis of a conventional helix and the perturbed helix are compared against results generated from a finite element approach.

Chapter

6

Waveguide finite element analysis

In this chapter a numerical approach is taken to predict the wave propagation in the helical spring. This is done using the stiffness and inertia properties determined via finite element software. Comparison will be made between results from the two analytical solutions and the one obtained in this chapter.

The concept of the Waveguide Finite Element[1] method is to utilise finite element procedures to determine stiffness and inertia properties of a periodic structure. A period of a corrugated helix can be seen in figure 6.1. The stiffness and inertia properties are afterwards imported in a mathematical software, where they can be post processed. The advantage is that tricky geometry is easily handled, but explicit information of dependence of geometrical features on stiffness is lost, while the restriction is that the structure needs to be periodic. The basics in the method is well summarised in D. Duhamel [2005].

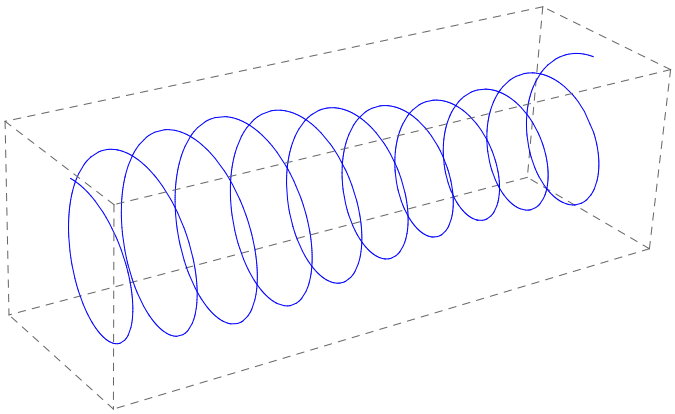

Figure 6.1: *A period of corrugated helical spring.*

6.1 The concept of Waveguide Finite Element

The practical execution of a waveguide finite element analysis can be conducted using *ANSYS* for the finite element related parts and *MatLab* for handling the matrices.

After the geometry and mesh is generated in ANSYS, a *Block Lanczos* modal analysis is performed. This is per se not interesting, but it allows for creating text files with stiffness and

[1] Abbreviated WFE

inertia properties in *Harwell-Boeing* format. This is imported in MatLab where the stiffness- and mass matrix are constructed in sparse format[2].

The manipulations of the matrices are as follows. First one determines the dynamic stiffness matrix:

$$\left(\underline{K}+\omega^2\underline{M}\right)\vec{U}=\vec{F} \qquad \Rightarrow \tag{6.1}$$

$$\underline{S}\vec{U}=\vec{0} \tag{6.2}$$

where:

$\underline{K}$	Stiffness matrix determined from FE-software.
$\underline{M}$	Mass matrix determined from FE-software.
$\vec{U}$	Nodal degrees of freedom.
$\vec{F}$	External forces on period.
ω	Excitation frequency.
$\underline{S}$	Dynamic stiffness matrix.

Assuming the external degrees of freedom are the first and last six entries in $\vec{U}$, which is the case for the spring, then condensation of internal degrees of freedom can be conducted by defining these submatrices:

$$\begin{bmatrix} \underline{S}_{RR} & \underline{S}_{IR} & \underline{S}_{LR} \\ \underline{S}_{RI} & \underline{S}_{II} & \underline{S}_{LI} \\ \underline{S}_{RL} & \underline{S}_{IL} & \underline{S}_{LL} \end{bmatrix} \begin{Bmatrix} \vec{u}_R \\ \vec{u}_I \\ \vec{u}_L \end{Bmatrix} = \begin{Bmatrix} \vec{f}_R \\ \vec{0} \\ \vec{f}_L \end{Bmatrix} \tag{6.3}$$

The subscripts refer to *RIGHT*, *INTERNAL*, and *LEFT* nodes of the substructure shown in figure 6.2. Following the example from Cook et al. [2002] the condensation results in:

$$\begin{bmatrix} \underline{S}_{11} & \underline{S}_{12} \\ \underline{S}_{21} & \underline{S}_{22} \end{bmatrix} \begin{Bmatrix} \vec{u}_L \\ \vec{u}_R \end{Bmatrix} = \begin{Bmatrix} \vec{f}_L \\ \vec{f}_R \end{Bmatrix} \tag{6.4}$$

where

$$\underline{S}_{11}=\underline{S}_{RR}-\underline{S}_{IR}\underline{S}_{II}^{-1}\underline{S}_{RI} \qquad \underline{S}_{12}=\underline{S}_{LR}-\underline{S}_{IR}\underline{S}_{II}^{-1}\underline{S}_{LI} \tag{6.5}$$

$$\underline{S}_{21}=\underline{S}_{RL}-\underline{S}_{IL}\underline{S}_{II}^{-1}\underline{S}_{RI} \qquad \underline{S}_{22}=\underline{S}_{LL}-\underline{S}_{IL}\underline{S}_{II}^{-1}\underline{S}_{LI} \tag{6.6}$$

The structure is now reduced to only be given by the displacements of the end nodes at the specified frequency. The variable Φ is now introduced, and corresponding to figure 6.2 it is state that:

$$u_L\Phi=u_R \tag{6.7}$$

Which originates from a solution in the exponential format so:

$$u_L=Ue^{iks_L} \qquad \wedge \qquad u_R=Ue^{iks_R} \tag{6.8}$$

[2]This is done using some MatLab routines written by Alf Søe Knudsen, AAU

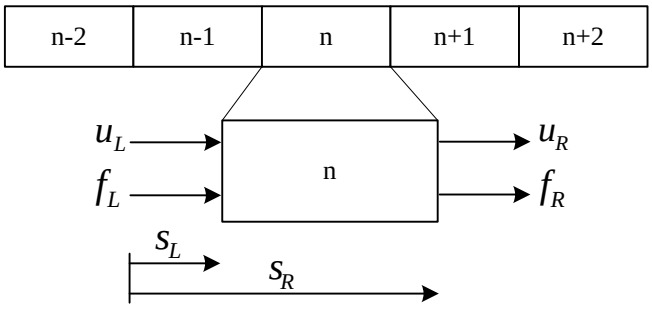

Figure 6.2: *The n'th period of structure with indicated displacements and forces on each face.*

By taking the ratio:

$$\frac{u_R}{u_L} = e^{ik(s_R - s_L)} = e^{ikl} \qquad \Rightarrow \qquad u_R = \Phi u_L \tag{6.9}$$

where: Φ Changes over one period.

l Length of period.

The product kl is denoted the *Bloch parameter* and Φ can then be seen as a measure of the change a wave experience after traversing one period of the structure. Also the forces follows the same relation, but with different sign to ensure equilibrium:

$$f_R = -\Phi f_L \tag{6.10}$$

From the condensed system the following two equations can be found:

$$f_L = \underline{S}_{11}\vec{u}_L + \underline{S}_{12}\Phi\vec{u}_L \tag{6.11}$$
$$-\Phi f_L = \underline{S}_{21}\vec{u}_L + \underline{S}_{22}\Phi\vec{u}_L \tag{6.12}$$

Multiplying (6.11) with Φ and adding the two equations yields:

$$0 = \underline{S}_{21}\vec{u}_L + \underline{S}_{22}\Phi\vec{u}_L + \underline{S}_{11}\Phi\vec{u}_L + \underline{S}_{12}\Phi^2\vec{u}_L \tag{6.13}$$
$$= \left(\underline{S}_{21} + (\underline{S}_{22} + \underline{S}_{11})\Phi + \underline{S}_{12}\Phi^2\right)\vec{u}_L \tag{6.14}$$

This is an polynomial eigenvalue problem, contrary to equation (6.1) which is a conventional eigenvalue problem, since the eigenvalue Φ appears in different powers. Using the build-in solver for polynomial eigenvalue problems in MatLab the values of Φ is obtained and comparison can then be made on the values of $e^{ik_j l}$ for the conventional helix and $e^{(ik_l - \xi)s}$ for the perturbed helix.

6.2 Geometrical considerations

Prior to generating any geometry in ANSYS it is prudent to consider the restrictions on the multiple scales solution. The corrugation rate ζ needs to be small for the approximations of $\kappa(s)$ and τ to be valid. Additionally η needs to be small since the perturbation expansion is

made on this, and according to the discussion of the validity range of the leading order solution (5.25) it must be chosen carefully to ensure that the asymptotic solution can be trusted over one period.

Generation of geometry is straight forward for the conventional helix, however, it turns out to be more tricky for the perturbed helix. The arc length s_l, corresponding to one corrugation, must satisfy:

$$\zeta s_l = 2\pi \tag{6.15}$$

However, this does not necessarily correspond to an the integral number of revolution of the helix thread, which is required by the WFE approach. Otherwise there will be a mismatch of coordinate systems. Hence, any choice of the modulation of ζ will most likely not be appropriate. Immediately there are two options available, either implement a transformation between coordinate systems, or choose a modulation that ensures an integral number of revolution. The latter is a bit artificial since this limits the number of admissible frequencies, but it doesn't make the analysis less comparable and it is the easiest to apply.

From a geometrical relation similar to (4.2) the wave number must satisfy:

$$k = \frac{1}{2n\sqrt{1+\tan^2(\psi)}} \tag{6.16}$$

where n is the number of revolutions. If for instance branch six in figure 4.7 is to correspond to a corrugated spring with $n = 10$ then $k = 0.0495742$ which approximately correspond to a frequency of $\omega = 0.0022697$. In this case the nondimensional length of one period will be $s_l = \frac{\pi}{0.0495742} = 63.37$. Hence the requirement on η is $\eta \lesssim \frac{1}{60}$ for (5.25) to be valid over one period.

6.3 FE Model details

Below is given some relevant parameters employed in the FE model.

Parameters :

$$\begin{aligned} R &= 0.1m \\ \psi &= 0.13 \\ E &= 210GPa \\ \nu &= 0.3 \\ \rho &= 7827kg/m^3 \end{aligned}$$

Values of η and ζ will be defined later. Modelling the spring is done by dividing it into ten sets of 100 key points and then drawing a spline through these.

Element: The beam element *BEAM189* is chosen since this supports Timoshenko beam theory kinematics. In principle this should not be necessary since this is less important at low frequencies, but for the sake of consistency it is included.

Mesh: The corrugated spring model is meshed with 1000 elements and the conventional spring model is meshed with 200 elements.

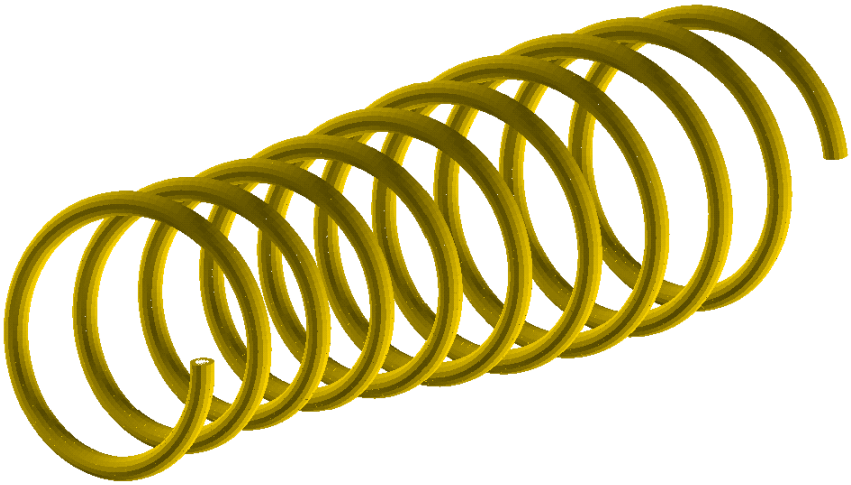

Figure 6.3: *Period of corrugated spring modelled in ANSYS where* $\eta = 1/10$ *and* $\zeta = 2 \cdot 0.0495742$.

A screen shot of the model is seen in figure 6.3. The last node is located in $(x, y) = (0.099472, -0.0093084)$, but was supposed to be in $(x, y) = (0.1, 0.0)$. Whether this precision is sufficiently accurate is not known at this stage, but even so it will be attempted.
The FE model can be made by running the macro *Ansys macros » helix.mac* found on the CD.

6.4 Results and comparison to results from multiple scales analysis

Using the WFE model presented above some results will be generated and compared to the analytical models derived in chapter 4 and 5.

6.4.1 Regular helix

Comparison of the WFE results to the exact analytical results can indicate whether the implementation of the WFE method is correct. Again it is clarified that strictly speaking the results from chapter 4 are not exact, but only approximated by the polynomial solver in Mathematica. However, in the context of comparing with finite element approach it is probably reasonable to regard it as exact.

For the conventional helix the results are compared over a period as shown in figure 6.4. Remark that even though the finite element model is generated using the dimensional quantities it is not necessary to do this for the analytical results since comparison will be made on e^{iks} which in itself is nondimensional and therefore it makes no difference if the variables each are scaled to be dimensional and then multiplied.

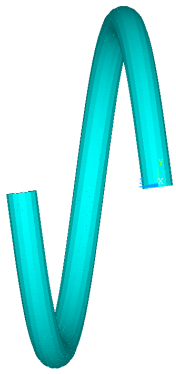

Figure 6.4: *One period of the regular spring modelled in ANSYS.*

When comparing the wave propagation predicted by different methods the most informative quantity to compare would be the wave number over a range of frequencies. However, this turns out to be troublesome for the following reason. Solving for k in $\Phi = e^{ikl}$ requires the use of inverse trigonometric functions which will have many solutions. This is analogous to the fact that the solving for θ in $x = \cos(\theta)$ results in $\theta = \pm\cos^{-1}(x) + 2\pi p$ where p is an integral number. This will require some sort of logic to be implemented in to determine the which one is the right solution. Therefore comparison will just be made between Φ and e^{iks_l}.

In figure 6.5 and 6.6 $Re(\Phi)$ and $Re\left(e^{iks_l}\right)$ is plotted in the frequency ranges $0 < \omega < 0.025$ and $0 < \omega < 1$, respectively.
The plots show that the results from the WFE method approximate the exact solution well in the given frequency ranges. This implies that the method is applicable as a reference for the corrugated spring.

6.4.2 Perturbed helix

In the result presented the corrugation rate ζ is chosen after branch 5 and 6 each for two different frequencies. Indeed it is relevant to compare varies corrugation rates, however, since the models are implemented in three different softwares (Mathematica, ANSYS, and MatLab) then generating a set of results is quite tiresome. The generation of results can be seen in *Mathematica files » multipleScales.nb* under *Part 7*.

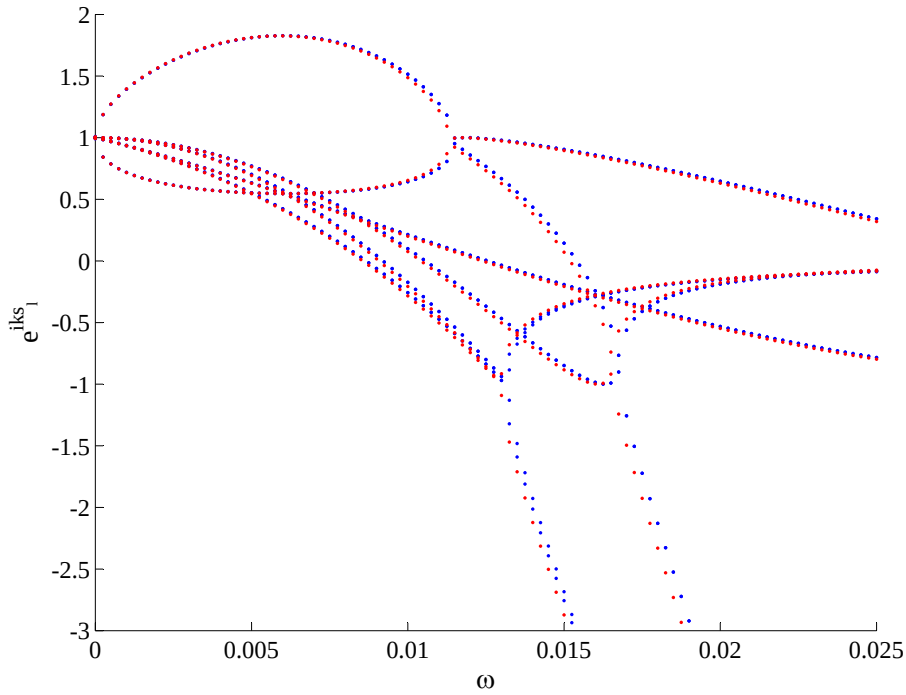

Figure 6.5: *Plot of* $Re(\Phi)$ *(blue dotted curves) from the WFE method and* $Re\left(e^{iks_l}\right)$ *(red dotted curves) from the analytical method for* $\omega < 0.025$.

For these branches some admissible configurations of wave number and frequency are found in table 6.1 along with the arc length and number of revolutions. Being that ξ is purely imaginary for all four corrugations the wave will only drift on the slow scale and not attenuate.

Branch	n	k	s_l	ω	ξ
5	10	0.0495742	63.27	0.0019883	0.111236 i
5	4	0.123945	25.35	0.0048758	0.091289 i
6	10	0.0495742	63.27	0.0022697	0.18968 i
6	4	0.123945	25.35	0.0055687	0.206959 i

Table 6.1: *Parameters for perturbed helix in nondimensional form.*

For a spring of four and ten revolutions the values $Re\left(e^{iks_l}\right)$ are seen in table 6.2 and 6.3 for branch 5, and table 6.4 and 6.5 for branch 6.

Remark that in the case of $\eta = 0$ (the spring is not perturbed) the change over one period of the wave which ζ is chosen after, will be exactly -1 since:

$$e^{ik_j \frac{2\pi}{2k_j}} = e^{i\pi} = -1 \tag{6.17}$$

This will have the effect that over one period of the perturbed helix the amplitude will only drift by a small amount and therefore only deviate slightly from -1.
Both the WFE and the multiple scales solution provide the leading order solution plus a small perturbation, which is as expected. In other words: a small corrugation will have a small impact on the results. What is more remarkable is that the modulated wave is purely real when determined via the WFE method while it is complex when determined via the method of multiple scales. This could imply that the WFE method suggests that the modulated wave decays in the

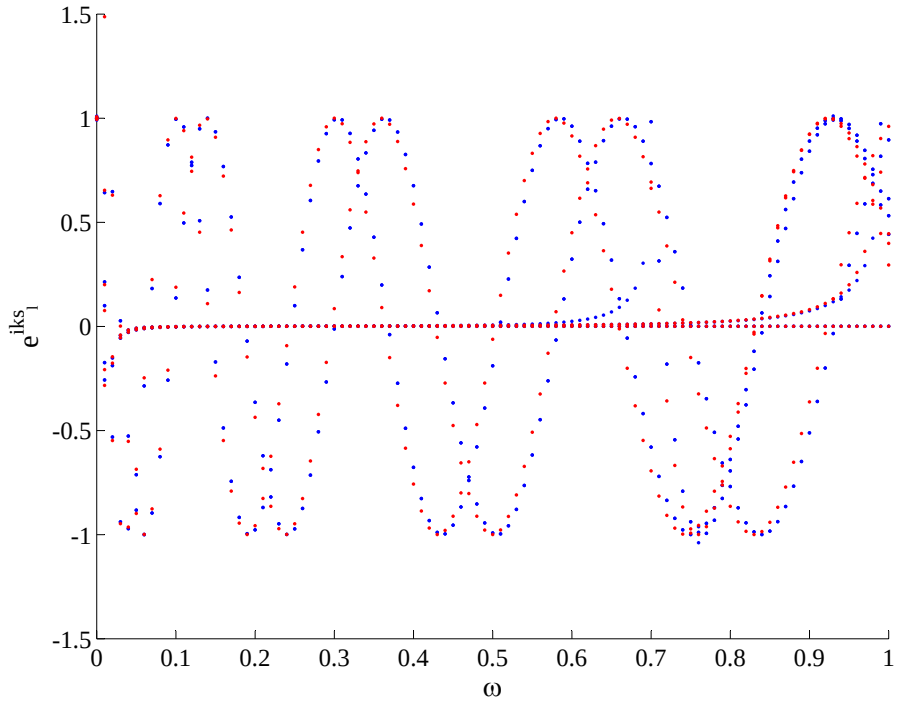

Figure 6.6: *Plot of* $Re(\Phi)$ *(blue dotted curves) from the WFE method and* $Re\left(e^{iks_l}\right)$ *(red dotted curves) from the analytical method for* $\omega < 0.025$.

Branch	WFE	MS
6: $e^{ik_6 s_l}$	$-0.91935+0.39345i$	$-0.91883+0.39466i$
5: $e^{(ik_5-\xi\eta)s_l}$	-0.94341	$-0.995719+0.092421i$
3: $e^{ik_3 s_l}$	$-0.72641+0.68726i$	$-0.72280+0.69106i$
1: $e^{ik_1 s_l}$	$-0.93478-0.35523i$	$-0.93478-0.35523i$

Table 6.2: *Results for spring with four revolutions and* $\eta = 1/25$, $\zeta = 2k_5$ *at* $\omega = 0.0048758$.

Branch	WFE	MS
6: $e^{ik_6 s_l}$	$-0.92188+0.38748i$	$-0.92414+0.38205i$
5: $e^{(ik_5-\xi\eta)s_l}$	-0.97567	$-0.993107+0.1172i$
3: $e^{ik_3 s_l}$	$0.63734+0.77058i$	$0.64384+0.76516i$
1: $e^{ik_1 s_l}$	$0.48491-0.87456i$	$0.49196-0.87062i$

Table 6.3: *Results for spring with ten revolutions and* $\eta = 1/60$, $\zeta = 2k_5$ *at* $\omega = 0.0019883$.

corrugated spring, since the modulus of Φ is no longer one. This surely suggest a discrepancy between the results obtained from the two methods.

For the data sets presented the correctness of the multiple scale solution cannot be confirmed nor can the WFE results, so no firm conclusions can be drawn. The outcome is, to a certain extent, that the validity of the multiple scales solution is questionable and that the assumptions only allows for a very narrow range of admissible design options. More results need to be generated to be able to grasp what the methods predict. The circumstances that might influence the correctness of the solutions in a negative manner are summarised as follows:

1. The lack of precision when making the geometry in ANSYS. This is considered less plausible since there also is a small lack of precision in the FE model for the conventional

Branch	**WFE**	**MS**
6: $e^{(ik_6-\xi\eta)s_l}$	-0.94405	$-0.97807+0.20829i$
5: $e^{ik_5 s_l}$	$-0.89488-0.4463i$	$-0.88998-0.45599i$
3: $e^{ik_3 s_l}$	$-0.38736+0.92193i$	$-0.38261+0.92390i$
1: $e^{ik_1 s_l}$	$-0.79314-0.60905i$	$-0.79023-0.61281i$

Table 6.4: *Results for spring with four revolutions and* $\eta = 1/25$, $\zeta = 2k_6$ *at* $\omega = 0.0055687$.

Branch	**WFE**	**MS**
6: $e^{(ik_6-\xi\eta)s_l}$	-0.97617	$-0.97999+0.1990i$
5: $e^{ik_5 s_l}$	$-0.90511-0.42517i$	$-0.90093-0.43396i$
3: $e^{ik_3 s_l}$	$0.90877+0.41729i$	$0.91084+0.41276i$
1: $e^{ik_1 s_l}$	$0.78744-0.61639i$	$0.79577-0.605598i$

Table 6.5: *Results for spring with ten revolutions and* $\eta = 1/60$, $\zeta = 2k_6$ *at* $\omega = 0.0022697$.

helix where the results are acceptable.

2. The analytical solution is only determined to the leading order which only causes a drift in amplitude for one mode. If higher approximations were included a drift in amplitude on a superslow scale would occur.

3. Dimensional ζ needs to be small for the approximations of curvature and torsion to be valid. It remains unknown how strongly approximations affect the solution in an erroneous manner.

4. Lastly, of course, it should be pointed out that it is likely that some kind of error have occurred during the derivation of the multiple scales solution.

If ignoring the doubt on the validity of the results from the multiple scales solution states that the chosen corrugation is not able attenuate the travelling waves, but will only cause their amplitudes to drift. In the context of minimising noise transmission it would be desirable make the travelling waves decay, however, if the quantity ξ and how it originates was studied in more details information on this subject might become apparent.

Chapter

7

Discussions and conclusions

In this section the findings are summarised and discussed, and the main questions from chapter 2 will be answered.

7.1 Discussions

The work presented in this report shows the challenges of the analytical analysis of structural dynamics, but constitutes only a small part of the huges topic.

The report starts out with a presentation of the theory of dynamics of spatial rods. The product of this part is a set of six governing equations in six kinematic variables. These governing equations are generalisations of the more familiar Timoshenko beam theory for straight rods like presented in Shames and Dym [2003].

7.1.1 Helical spring of regular shape

It is found that for an infinite helical spring of regular shape the dispersion equation can be obtained analytically. The explicit solutions for the wave numbers are not available, but asymptotic analysis can be employed to retrieve dominant terms and thereby obtain explicit approximations for the wave numbers in both a high and low frequency range.

In the following the findings obtained through the asymptotic analysis of the regular spring are summarised and discussed.

Low frequency asymptotes In the low frequency range the branches emerging from $\omega = 0$ are approximated by a perturbation expansion. Via these approximations global extension and torsion waves are identified by comparing the phase velocities with results presented by Wittrick [1966]. This identification is not readily available from the asymptotic analysis, but the elastic rod analogy presented in Wittrick [1966] makes it more obvious.

For the branches emerging from $k \approx 1$ in the dispersion diagram an asymptotic expansion is found where the curvature and torsion appears in all corrections and a dominant parameter is not as easily recognised. In the same region an expansion is made on τ. This analysis provides the same leading order solution in the limit of small pitch angle as the previous solution. This solution also provides a clear explanation on the impact of τ on the cut-on frequency of the evanescent flexural wave.

High frequency asymptotes The approximations found for k at high frequencies can be partitioned by their ranges of validity. One set of simple solutions valid at very high frequencies

and another more intricate set of solutions that approximate the exact solutions at much lower frequencies. It is, however, found that the simple solution is contained in the more advanced solutions in the limit of $\omega \to 0$.

The simple approximations valid at very high frequencies proves that the geometry do not have any effect on the wave number. Meanwhile it is observed that the curvature influence the wave number for the torsion and the axial wave at the first correction in the more accurate solutions for k.

For the flexural and shear waves, the only waves affected by the Timoshenko kinematics, it has been found that the wave numbers can be approximated the same way as for a straight rod.

Cut-on frequencies The asymptotic analysis reveals dominans of curvature on cut-on frequency the torsion and axial wave. The shear waves are mainly governed by the shear coefficient and the thread diameter, and weak impact from curvature and torsion causes the cut-on frequencies to diverge from one another.

Generally it is found that the approximations to the leading order quite precisely resembles the exact solutions. Again this shows the power of having explicit results since they clearly point out how the cut-on frequency can be determined for any spring where the thread diameter to helix radius ratio is small.

7.1.2 Helical spring of irregular shape

The first challenge found during this analysis is a proper description of the geometry. As is seen from section 5.1 perturbing the radius of a helix with the angle of revolution as the parameter has an impact on the pitch angle locally. Perturbing the radius when the arc length acts as the parameter maintains the pitch angle on a local level, but it gets harder to keep track of the number of revolutions associated to a numerical value of the arc length. A restriction of smallness is imposed on the corrugation rate in order to obtain simple expressions for curvature and torsion.

The method of multiple scales is identified as an option for solving the problem, however, it is found that a restriction of smallness on the corrugation η must be employed to make the method of multiple scales applicable. The problem can then be solved by following the standard procedure of perturbation methods.

By choosing a corrugation rate ζ different modulation equations can be found which gives the decay or drift of amplitude on the long length scale. The modulation equation is not unique, but depends on how ζ is chosen. The results presented are in no way exhaustive, but more serves as providing some results for comparison with results from the WFE method.

The results determined from the method of multiple scales shows that for two specific modes the amplitude will drift and not decay. This contradicts the results determined via the WFE method, that implies that the waves will decay. The sources of this discrepancy has not been identified, and therefore it cannot be determined, for the time being, if any of the solutions found are the true solutions.

The apparent impression after comparing results is that the multiple scale solution is so heavily limited by its assumptions, that it is somehow impractical to apply. Nevertheless a systematic method to find a solution for the problem of wave propagation in corrugated spring has been identified.

7.2 Conclusions

The dynamics of spatially curved rods is governed by six linear partial differential equations of second order. In the general case these are coupled and has spatially varying coefficients, but decouples for simple geometries.

The wave propagation can analytically be analysed for a helical spring of regular shape. However, exact explicit expressions for wave numbers are not available, but they can be found by numerically approximate the roots the twelfth order dispersion equation. Alternatively, explicit expressions of the wave numbers can be derived using asymptotic analysis which provides insight in governing parameters and mechanisms. The helical spring has inherent coupling of modes at low frequencies, while they decouple into dominant flexural, torsional, axial, and shear waves at high frequencies.

For a helical spring of irregular shape the problem of free vibrations can be solved using the method of multiple scales. However, the solution as derived in this report is subjected to restrictions that severely limits the range in which the solution is valid. The solution has not been validated. Further work needs to be done to accomplish this.

The Waveguide Finite Element method is well suited to study the wave propagation in periodic structures. The results compare well to the exact results for the regular helix, while discrepancies have been found between the WFE results and the results from the multiple scales solution. Consequently the true solution of the perturbed helical spring remains unknown.

Chapter

8

Future perspectives

Based on the experiences obtained through the project work some alternatives to what has been done will be suggested in this chapter. The suggestions are mainly addressed to the analysis of the perturbed spring as this is the most insufficient part of the project.

It is not known whether it is doable to find the WKB-solution to the problem of the perturbed helix, however, it is expected that it would be much superior than the conventional method of multiple scale. The WKB-approximation in general produces a result where both amplitude and wave number is affected at the leading order level for all waves. Also the influence of the corrugation will most likely appear in a more explicit manner meanwhile might be possible to choose it more arbitrarily and not just select it after a certain wave number before the derivation can be carried on till the end. On basis of this it seems very encouraging to put effort into finding the WKB-solution both for the sake of the present problem as well as generally acquiring skills in the use of the method to tackle future challenges with differential equations having coefficients that varies on a slow scale.

An alternative method to the perturbation methods could be the theory of differential equations with periodic coefficients. This is mentioned in V. Krylov [1997] as Mathieu or Hill equations and should be suited to solve the problem of wave motion in periodic wave guides.

The current analysis it would be desirable to have more robust multiple scale solutions to the perturbed spring. This could be conducted by testing what influence different expressions for curvature and torsion would have on the governing equations. Also it could be interesting to introduce a superslow length scale to obtain higher approximations of the multiple scales solution. As well as an implementation of the coordinate transformation mentioned in chapter 6 in the WFE procedure and thereby allowing for more arbitrarily selected geometry.

Along the same lines as done in chapter 4 it would be relevant to study what is dominant in the modulation parameter ξ. An explicit solution for ξ has been found, but in a very cumbersome form, so the clear picture in what makes it real or complex is not available.

After having met the challenges with establishing geometrical relation it might be relevant to reverse this process. So instead of stating the parametrisation of a spatial curve and determine curvature and torsion, then specify functions for curvature and torsion and then determine the geometry of the corresponding spatial curve by solving the Frenet-Serret equations.

An option that lies beyond the scope of this thesis is to go for more general theories where the plane cross-section hypothesis has not been employed. This involves solutions to the far more general theory of elastodynamics where the high frequency phenomena such as *surface waves* or *Rayleigh waves* can be captured. Basically through this theory one do not impose any displacement field, but try to solve the theory of elasticity. A study like this is might not be very relevant for the understanding of wave propagation in spatial rods, but can serve as a

complementary theory to the Timoshenko type theory of rods and also enrich the knowledge of high frequency phenomena.

In order to produce more practically relevant results an obvious thing is to study vibrations of springs of finite length. This can be done via the boundary integral equations method as mentioned in the beginning, where the free field solution is utilised, and a solution is found that accounts for boundary conditions. Continuing the work on modelling an elastic rod more realistically would also include nonconservative effects such as damping in the material.

Bibliography

Dan Tiba Anca Ignat, Jürgen Sprekels. A model for a general elastic curved rod. *Mathematical Methods in the Applied Sciences*, pages 835–854, November 2000.

M. Farshad H. Yi B. Tabarrak, A.N. Sinclair. On the dynamics of spatially curved and twisted rods - a finite element formulation. *Journal of Sound and Vibration*, pages 315–326, 1988.

Grigiry Isaakovich Barenblatt. *Scaling*. Cambridge University Press, 2003. ISBN 0 521 82657 8.

Robert D. Cook, David S. Malkus, Michael E. Plesha, and Robert J. Witt. *Concepts and Applications of Finite Element Analysis*. John Wiley & Sons, INC, 111 River Street, Hoboken, NJ 07030, 4 edition, 2002. ISBN 9780471356059.

M.J. Brennan D. Duhamel, B.R. Mace. Finite element analysis of the vibrations of waveguides and periodic structures. *Journal of Sound and Vibration*, pages 205–220, 2005.

M. Yazdchi G. Karami, M. Farshad. Free vibrations of spatial rods - a finite element anaylsis. *Communications in applied numerical methods*, 6:417–428, 1990.

E.J. Hinch. *Perturbation Methods*. Cambridge University Press, 1991. ISBN 0 521 37310 7.

John E. Mottershead. Finite elements for dynamical analysis of helical rods. *Int. J. Mech. Sci.*, 22:267–283, 1980.

Nigel Peake. Asymptotic methods in aeroacoustics. Lecture Notes, 2005.

Singiresu S. Rao. *Mechanical Vibrations*. PEARSON, Prentice Hall, 2004. ISBN 0-13-120768-7.

Irving H. Shames and Clive L. Dym. *Energy and Finite Element Methods in Structural Mechanics*. Taylor & Francis Inc, revised edition edition, 2003. ISBN 0891169423.

Leonid I. Slepyan. *Models and Phenomena in Fracture Mechanics*. Springer, 2002. ISBN 3-540-43767.

Sergey V. Sorokin. Linear dynamics of elastic helical springs: asymptotic analysis of wave propagation. *Proceedings of The Royal Society A*, pages 1513–1537, January 2009.

Sergey V. Sorokin. The boundary integral equations method in vibro-acoustics. *RASD 2010*, pages 1–17, 2010.

Murray R. Spiegel. *Theoretical Mechanics*. McGraw-Hill Book Company, 1982. ISBN 0-07-084357-0.

S.V. Grishina S.V.Sorokin. Analysis of wave propagation in sandwich beams with parametric stiffness modulations. *Journal of Sound and Vibration*, pages 1063–1082, 2003.

S.V. Sorokin V. Krylov. Dynamics of elastics beams with controlled distributed stiffness parameters. *Smart Mater. Struct.*, 6:573582, 1997.

W.H. Wittrick. On elastic wave propagation in helical springs. *It. J. Mech. Sci.*, 8:25–47, 1966.

Nomenclature

Latin Letters

α, β, γ	Angles of rotation.
u, v, w	Translation in x, y, z respectively.
$\vec{r}(s)$	Parameter function of spatial curve.
s	Arc length of spatial curve.
κ	Curvature of spatial curve.
τ	Torsion of spatial curve.
$\vec{t}$	Tangential vector.
$\vec{b}$	Binormal vector.
$\vec{n}$	Principal normal vector.
ϕ	Angle of revolution.
ψ	Pitch angle.
R	Radius of helix.
$\Delta\vartheta$	Angle formed by $b(s)$ and $b(s+\Delta s)$.
$\delta\vec{\Omega}$	Change in curvature-twist from the undeformed to deformed geometry.
$\delta p, \delta q, \delta r$	changes in twist and curvature in the principal frame.
p_0, q_0, r_0	Curvatures in principal frame.
$\vec{\Delta}$	Translation vector when the rod deforms.
$\vec{\Omega}$	Curvature-twist vector of the deformed rod.
$\vec{\theta}$	Rotational vector when the rod deforms.
$\underline{I}$	Area moment of inertia of rod.
$\underline{J}$	Bending and torsion stiffness matrix.
$\underline{K}$	Shear and Extension stiffness matrix.
λ	Shear coefficient.
ρ	Density of rod.
$\vec{F}$	External forces on period.
$\vec{f}$	Body forces on the rod.
$\vec{M}$	Internal moments.
$\vec{m}$	Body moments on the rod.
A	Cross sectional area of rod.
c_0	Speed of the plane dilatation wave.
E	Youngs modulus.
G	Shear modulus.
I_x, I_y, I_z	Principal moments of inertia.
$\mathscr{A}, \mathscr{B}, \mathscr{G}$	Amplitudes of rotations.
$\mathscr{U}, \mathscr{V}, \mathscr{W}$	Amplitudes of displacements.
ω	Excitation frequency.
$\mathscr{U}_0^*$	Complex conjugate of $\mathscr{U}_0$.
j	Mode.
k	Wave number.

M_m	Modal coefficient linking the m'th variable to u_0.
$\delta_i(\epsilon)$	Scalings of ϵ.
x_i	Corrections in perturbation expansion.
η	Corrugation, change in radius for perturbed spring.
ζ	Corrugation rate.
σ	Detuning parameter.
$\overline{R}$	Mean radius.
S_l	Long scale.
S_s	Short scale.
$\underline{L}$	Differential operator.
$\vec{V}^{r1}$	Vector containing coefficients of $e^{i\zeta s}$.
$\vec{V}^{r2}$	Vector containing coefficients of $e^{-i\zeta s}$.
$\vec{V}^{sd}$	Vector containing only slow derivatives of amplitudes.
$\underline{K}$	Stiffness matrix determined from FE-software.
$\underline{M}$	Mass matrix determined from FE-software.
$\underline{S}$	Dynamic stiffness matrix.
$\vec{U}$	Nodal degrees of freedom.
Φ	Changes over one period.
l	Length of period.

Appendix

A

Additional proof for derivation of governing equations

In this chapter a proof and a discussion is given for the transformation of derivatives of vectors between rotation coordinate system is given. The result is used throughout chapter 3. Additionally some alternative ways of deriving geometrical relations are given here.

A.1 Derivatives between rotation coordinate systems

The proof is inspired by Spiegel [1982] and originates by considering two frames with coinciding origins. Their axis are denoted XYZ (which is fixed in space) and xyz where the latter frame rotates with an angular velocity $\vec{\omega}$. In the rotating frame a vector $\vec{A}$ is observed and its time derivative is:

$$\left.\frac{d\vec{A}}{dt}\right|_M = \frac{dA_1}{dt}\vec{i} + \frac{dA_2}{dt}\vec{j} + \frac{dA_3}{dt}\vec{k} \tag{A.1}$$

Here M denotes that it is seen from the moving frame. $\vec{i}$, $\vec{j}$, and $\vec{k}$ are basis in the moving frame. If an observer in the fixed coordinate system was to determine the time derivative of A the result would be:

$$\left.\frac{d\vec{A}}{dt}\right|_F = \frac{dA_1}{dt}\vec{i} + \frac{dA_2}{dt}\vec{j} + \frac{dA_3}{dt}\vec{k} + A_1\frac{d\vec{i}}{dt} + A_2\frac{d\vec{j}}{dt} + A_3\frac{d\vec{k}}{ds} \tag{A.2}$$

$$= \left.\frac{d\vec{A}}{dt}\right|_M + A_1\frac{d\vec{i}}{dt} + A_2\frac{d\vec{j}}{dt} + A_3\frac{d\vec{k}}{ds} \tag{A.3}$$

From chapter 3 it is known that a base vector and its derivative will be orthogonal. The derivatives of the base vectors are therefore taken as an arbitrary linear combination of the two remaining, i.e.:

$$\frac{d\vec{i}}{dt} = \alpha_1 \vec{j} + \alpha_2 \vec{k} \tag{A.4a}$$

$$\frac{d\vec{j}}{dt} = \alpha_3 \vec{k} + \alpha_4 \vec{i} \tag{A.4b}$$

$$\frac{d\vec{k}}{dt} = \alpha_5 \vec{i} + \alpha_6 \vec{j} \tag{A.4c}$$

From (A.4a) and (A.4b) it is seen that $\frac{d\vec{i}}{dt} \cdot \vec{j} = \alpha_1$ and $\vec{i} \cdot \frac{d\vec{j}}{dt} = \alpha_4$ respectively. And since $\vec{i} \cdot \vec{j} = 0$ then taking the derivative yields:

$$\vec{i} \cdot \frac{d\vec{j}}{dt} + \frac{d\vec{i}}{dt} \cdot \vec{j} = 0 \tag{A.5}$$

This concludes that $\alpha_4 = -\alpha_1$. By similar reasoning it can be determined that $\alpha_5 = -\alpha_2$ and $\alpha_6 = -\alpha_3$. The system in equations (A.4) can be rewritten to be:

$$\frac{d\vec{i}}{dt} = \alpha_1 \vec{j} + \alpha_2 \vec{k} \tag{A.6a}$$

$$\frac{d\vec{j}}{dt} = \alpha_3 \vec{k} - \alpha_1 \vec{i} \tag{A.6b}$$

$$\frac{d\vec{k}}{dt} = -\alpha_2 \vec{i} - \alpha_3 \vec{j} \tag{A.6c}$$

The last three terms in equation (A.3) is therefore expressed by:

$$A_1 \frac{d\vec{i}}{dt} + A_2 \frac{d\vec{j}}{dt} + A_3 \frac{d\vec{k}}{ds} = A_1 \left(\alpha_1 \vec{j} + \alpha_2 \vec{k}\right) + A_2 \left(\alpha_3 \vec{k} - \alpha_1 \vec{i}\right) + A_3 \left(-\alpha_2 \vec{i} - \alpha_3 \vec{j}\right) \tag{A.7}$$

$$= (-\alpha_1 A_2 - \alpha_2 A_3)\, \vec{i} + (\alpha_1 A_1 - \alpha_3 A_3)\, \vec{j} + (\alpha_2 A_1 + \alpha_3 A_3)\, \vec{k} \tag{A.8}$$

Arranging this in a determinant and substituting $\vec{\omega} = \alpha_3 \vec{i} - \alpha_2 \vec{j} + \alpha_1 \vec{k}$ yields:

$$A_1 \frac{d\vec{i}}{dt} + A_2 \frac{d\vec{j}}{dt} + A_3 \frac{d\vec{k}}{ds} = \begin{vmatrix} \vec{i} & \vec{j} & \vec{k} \\ \omega_1 & \omega_2 & \omega_3 \\ A_1 & A_2 & A_3 \end{vmatrix} = \vec{\omega} \times \vec{A} \tag{A.9}$$

Lastly formula (A.3) can be expressed in a concise way, namely:

$$\left.\frac{d\vec{A}}{dt}\right|_F = \left.\frac{d\vec{A}}{dt}\right|_M + \vec{\omega} \times \vec{A} \tag{A.10}$$

The following points are made regarding this result to emphasise the relevance of this result regarding the derivation of the governing equations:

- The derivative of time t can be replaced by the parameter s.
- The vector $\vec{\omega}$ can be replaced by the principal curvature vector $\vec{\Omega}$ and (A.10)
- The formula can be used to transform vectors between the global and local coordinate systems.
- Cross products such like $\vec{\Omega} \times \vec{t}$ may be seen as the velocity of $\vec{t}$ wrt. the parameter s.

A.2 Alternative proofs of geometrical relations

First a group of kinematical relations that links rotations to displacements. First by taking the scaler version of equation (3.25):

$$p = p_0 + \delta p \tag{A.11a}$$
$$q = q_0 + \delta q \tag{A.11b}$$
$$r = r_0 + \delta r \tag{A.11c}$$

where: $\delta p, \delta q, \delta r$ changes in twist and curvature in the principal frame.

The goal is now to establish formulas that relates α, β, γ, u, v, w and δp, δq, δr in terms of the original geometry, i.e. by use of $\vec{i}_0$, $\vec{j}_0$, $\vec{k}_0$ and p_0, q_0, and r_0.

Returning to equation (3.23) and taking the derivative wrt. s then:

$$\vec{k} = \vec{k}_0 + \frac{d\vec{\Delta}}{ds} \tag{A.12}$$

Here $\vec{k}_0$ is chosen to coincide with $\vec{t}$. As earlier mentioned the base vectors in the principal frame are functions of s and therefore the latter term in equation (A.12) should be differentiated by the product rule as:

$$\frac{d\vec{\Delta}}{ds} = \underbrace{\frac{du}{ds}\vec{i}_0 + \frac{dv}{ds}\vec{j}_0 + \frac{dw}{ds}\vec{k}_0}_{\frac{d\vec{\Delta_1}}{ds}} + u\frac{d\vec{i}_0}{ds} + v\frac{d\vec{j}_0}{ds} + w\frac{d\vec{k}_0}{ds} \tag{A.13}$$

Using the notation introduced here equation (A.12) can now be written as:

$$\vec{k} = \frac{d\vec{\Delta_1}}{ds} + \vec{k}_0 + u\frac{d\vec{i}_0}{ds} + v\frac{d\vec{j}_0}{ds} + w\frac{d\vec{k}_0}{ds} \tag{A.14}$$

By utilising the relations derived in appendix A this is rewritten:

$$\vec{k} = \frac{d\vec{\Delta_1}}{ds} + \vec{k}_0 + \vec{\Omega}_0 \times \vec{\Delta} \tag{A.15}$$

By evaluating the cross product and collecting terms of $\vec{i}_0$, $\vec{j}_0$, and $\vec{k}_0$ the following expression is obtained:

$$\vec{k} = \frac{du}{ds}\vec{i}_0 + \frac{dv}{ds}\vec{j}_0 + \frac{dw}{ds}\vec{k}_0 + \vec{k}_0 + \vec{i}_0(q_0 w - v r_0) - \vec{j}_0(p_0 w - u r_0) + \vec{k}_0(p_0 v - u q_0) \tag{A.16}$$
$$= \left(\frac{du}{ds} + q_0 w - v r_0\right)\vec{i}_0 + \left(\frac{dv}{ds} - p_0 w + u r_0\right)\vec{j}_0 + \left(\frac{dw}{ds} + 1 + p_0 v - u q_0\right)\vec{k}_0 \tag{A.17}$$

From this equation three different relations can be establish by taking the dot product with $\vec{i}_0$, $\vec{j}_0$, and $\vec{k}_0$:

$$\vec{k}\cdot\vec{i}_0 = \frac{du}{ds} + q_0 w - v r_0 \tag{A.18a}$$

$$\vec{k}\cdot\vec{j}_0 = \frac{dv}{ds} - p_0 w + u r_0 \tag{A.18b}$$

$$\vec{k}\cdot\vec{k}_0 = \frac{dw}{ds} + 1 + p_0 v - u q_0 \tag{A.18c}$$

To carry on with these it is necessary to assume small angular changes from the original to the deformed stage. In that case the direction the LHS of (A.18) can be considered as direction cosines since, for equation (A.18c):

$$\cos\left(\vec{k},\vec{k}_0\right) = \frac{\vec{k}\cdot\vec{k}_0}{|\vec{k}||\vec{k}_0|} = \cos(\gamma) \approx 1 \tag{A.19}$$

This is only valid provided that γ is a small quantity. Also note the impotence of $\vec{k}$ and $\vec{k}_0$ being unity vectors and therefore can be cancelled out of the equation. In figure xxx the angles between the two frames are indicated. As well it is illustrated how the direction cosines are approximated. From this figure it is as well seen that the remaining two direction cosines from the equations (A.18) are:

$$\cos\left(\vec{k},\vec{j}_0\right) = \cos\left(-\frac{\pi}{2} - \alpha\right) = -\cos\left(\frac{\pi}{2} + \alpha\right) = -\sin(\alpha) \approx -\alpha \tag{A.20}$$

$$\cos\left(\vec{k},\vec{i}_0\right) = \cos\left(\frac{3\pi}{2} + \beta\right) = \sin(\beta) \approx \beta \tag{A.21}$$

Which leads to the following relations:

$$\beta = \frac{du}{ds} + q_0 w - v r_0 \tag{A.22a}$$

$$-\alpha = \frac{dv}{ds} - p_0 w + u r_0 \tag{A.22b}$$

$$0 = \frac{dw}{ds} + p_0 v - u q_0 \tag{A.22c}$$

This group of kinematical relations originated from the translation balance in equation (3.23). Similarly another group of kinematical relations can be derived from the translational component. By representing formula (A.11) in vector form:

$$\vec{\Omega} = \vec{\Omega}_0 + \delta\vec{\Omega} \tag{A.23}$$

where: $\vec{\Omega}$ Curvature-twist vector of the deformed rod.

$\delta\vec{\Omega}$ Change in curvature-twist from the undeformed to deformed geometry.

As the rod deforms it twist by the angle γ around $\vec{k}_0$ and similar by the amounts α and β around $\vec{i}_0$ and $\vec{j}_0$ respectively. Therefore $\delta\vec{\Omega}$ takes the following form:

$$\delta\vec{\Omega} = \frac{d\vec{\theta}_1}{ds} = \frac{d\alpha}{ds}\vec{i}_0 + \frac{d\beta}{ds}\vec{j}_0 + \frac{d\gamma}{ds}\vec{k}_0 \tag{A.24}$$

Then equation (A.23) can be rewritten to:

$$p\vec{i} + q\vec{j} + r\vec{k} = \left(p_0 + \frac{d\alpha}{ds}\right)\vec{i}_0 + \left(q_0 + \frac{d\beta}{ds}\right)\vec{j}_0 + \left(r_0 + \frac{d\gamma}{ds}\right)\vec{k}_0 \tag{A.25}$$

By projecting this vector equation to the axis of $\vec{i}_0$, $\vec{j}_0$, and $\vec{k}_0$, i.e. taking the dot products, the following three scalar relations can be determined:

$$p = \left(p_0 + \frac{d\alpha}{ds}\right) + \left(q_0 + \frac{d\beta}{ds}\right)\gamma - \left(r_0 + \frac{d\gamma}{ds}\right)\beta \tag{A.26}$$

$$q = -\left(p_0 + \frac{d\alpha}{ds}\right)\gamma + \left(q_0 + \frac{d\beta}{ds}\right) + \left(r_0 + \frac{d\gamma}{ds}\right)\alpha \tag{A.27}$$

$$r = \left(p_0 + \frac{d\alpha}{ds}\right)\beta - \left(q_0 + \frac{d\beta}{ds}\right)\alpha + \left(r_0 + \frac{d\gamma}{ds}\right) \tag{A.28}$$

Since, as discussed earlier, the deformations and rotations will be small, the above equations can be reduced by neglecting products of small quantities and their derivatives, and by including equation (A.11) an expression for he changes in curvature and twist can be found as:

$$p_0 + \delta p = p_0 + \frac{d\alpha}{ds} + q_0\gamma - r_0\beta \qquad \Rightarrow \qquad \delta p = \frac{d\alpha}{ds} + q_0\gamma - r_0\beta \tag{A.29}$$

$$q_0 + \delta q_0 = -p_0\gamma + q_0 + \frac{d\beta}{ds} + r_0\alpha \qquad \Rightarrow \qquad \delta q = \frac{d\beta}{ds} + r_0\alpha - p_0\gamma \tag{A.30}$$

$$r_0 + \delta r_0 = p_0\beta - q_0\alpha + r_0 + \frac{d\gamma}{ds} \qquad \Rightarrow \qquad \delta r = \frac{d\gamma}{ds} + p_0\beta - q_0\alpha \tag{A.31}$$

These constitutes another group of kinematic relations.

In vector notation the three formulas for curvature can be written:

$$\delta\vec{\Omega} = \frac{d\overrightarrow{\theta_1}}{ds} + \vec{\Omega}_0 \times \vec{\theta} \tag{A.32}$$

Appendix

B

Wave propagation in regular infinite helix

This chapter contains additional formulas for the investigation of the regular helix.

B.1 Dispersion equation

The dispersion equation for the regular helix is:

$$
\begin{aligned}
0 = {} & \frac{1}{4(1+\nu)^3}\tilde{d}^2\Big(256\lambda^2\tilde{\omega}^4\left(\tilde{k}^2+\tilde{\kappa}^2-\tilde{\omega}^2\right)\left(\tilde{k}^2+(1+\nu)\left(\tilde{\kappa}^2-2\tilde{\omega}^2\right)\right)+\tilde{d}^4\Big(\tilde{k}^6-2\tilde{k}^4\left(\tilde{\kappa}^2+\tilde{\tau}^2+(2+\nu)\tilde{\omega}^2\right) \\
& -\tilde{\omega}^2\left(\tilde{\kappa}^2+2\tilde{\tau}^2-2\tilde{\omega}^2\right)\left(\tilde{\kappa}^2+(1+\nu)\left(\tilde{\tau}^2-\tilde{\omega}^2\right)\right)+\tilde{k}^2\left(\tilde{\kappa}^4+\tilde{\tau}^4+2(1+2\nu)\tilde{\tau}^2\tilde{\omega}^2+(5+4\nu)\tilde{\omega}^4+\tilde{\kappa}^2\left(2\tilde{\tau}^2-(1+\nu)\tilde{\omega}^2\right)\right)\Big) \\
& \Big(\lambda^2\tilde{k}^6-\lambda\tilde{k}^4\left(2\lambda\tilde{\kappa}^2+2\lambda\tilde{\tau}^2+(4+\lambda+4\nu)\tilde{\omega}^2\right)-\tilde{\omega}^2\Big(2\lambda(1+\nu)\tilde{\kappa}^4+(2+\lambda+2\nu)\tilde{\kappa}^2\left(\lambda\tilde{\tau}^2-2(1+\nu)\tilde{\omega}^2\right) \\
& +\left(\lambda\tilde{\tau}^2-2(1+\nu)\tilde{\omega}^2\right)^2\Big)+\tilde{k}^2\Big(\lambda^2\tilde{\kappa}^4+\lambda^2\tilde{\tau}^4+2\lambda(\lambda-2(1+\nu))\tilde{\tau}^2\tilde{\omega}^2+4(1+\nu)(1+\lambda+\nu)\tilde{\omega}^4 \\
& +\lambda\tilde{\kappa}^2\left(2\lambda\tilde{\tau}^2+(2-\lambda+2\nu)\tilde{\omega}^2\right)\Big)\Big)+16\lambda\tilde{d}^2\tilde{\omega}^2\Big(-2\lambda\tilde{k}^8+\tilde{k}^6\left(-\lambda(-2+\nu)\tilde{\kappa}^2+4\left(-3\lambda\tilde{\tau}^2+(1+\nu+\lambda(2+\nu))\tilde{\omega}^2\right)\right) \\
& +\tilde{\omega}^2\Big((2+\lambda)(1+\nu)\tilde{\kappa}^6-4(1+\nu)\tilde{\omega}^2\left(-\tilde{\tau}^2+\tilde{\omega}^2\right)\left(-\lambda\tilde{\tau}^2+2(1+\nu)\tilde{\omega}^2\right)+\tilde{\kappa}^4\Big(\left(2(1+\nu)^2+\lambda(4+3\nu)\right)\tilde{\tau}^2 \\
& -(1+\nu)(10+3\lambda+4\nu)\tilde{\omega}^2\Big)+\tilde{\kappa}^2\left(3\lambda(1+\nu)\tilde{\tau}^4-2\left(5(1+\nu)^2+\lambda(4+3\nu)\right)\tilde{\tau}^2\tilde{\omega}^2+2(1+\nu)(8+\lambda+6\nu)\tilde{\omega}^4\right)\Big) \\
& +\tilde{k}^4\Big(2\lambda(1+\nu)\tilde{\kappa}^4+\tilde{\kappa}^2\left(-6\lambda\nu\tilde{\tau}^2+(1+\nu)(2+\lambda+2\nu)\tilde{\omega}^2\right)-2\Big(\lambda\tilde{\tau}^4-(2+19\lambda+2\nu+12\lambda\nu)\tilde{\tau}^2\tilde{\omega}^2 \\
& +\left(8+5\lambda+12\nu+4\lambda\nu+4\nu^2\right)\tilde{\omega}^4\Big)\Big)-\tilde{k}^2\Big(\lambda(2+\nu)\tilde{\kappa}^6+2\tilde{\kappa}^4\left(\lambda(2+\nu)\tilde{\tau}^2-(\nu(1+\nu)+\lambda(3+\nu))\tilde{\omega}^2\right) \\
& -2\tilde{\omega}^2\left(\lambda(3+2\nu)\tilde{\tau}^4-\left(6+10\nu+4\nu^2+\lambda(15+14\nu)\right)\tilde{\tau}^2\tilde{\omega}^2+2(1+\nu)(5+\lambda+4\nu)\tilde{\omega}^4\right)+\tilde{\kappa}^2\Big(\lambda(2+\nu)\tilde{\tau}^4 \\
& -2\left(3+4\nu+\nu^2+\lambda(3+4\nu)\right)\tilde{\tau}^2\tilde{\omega}^2+\left(18+5\lambda+32\nu+2\lambda\nu+14\nu^2\right)\tilde{\omega}^4\Big)\Big)\Big)\Big)
\end{aligned}
\tag{B.1}
$$

B.2 Modal analysis

This section contains additional plots to the modal analysis.

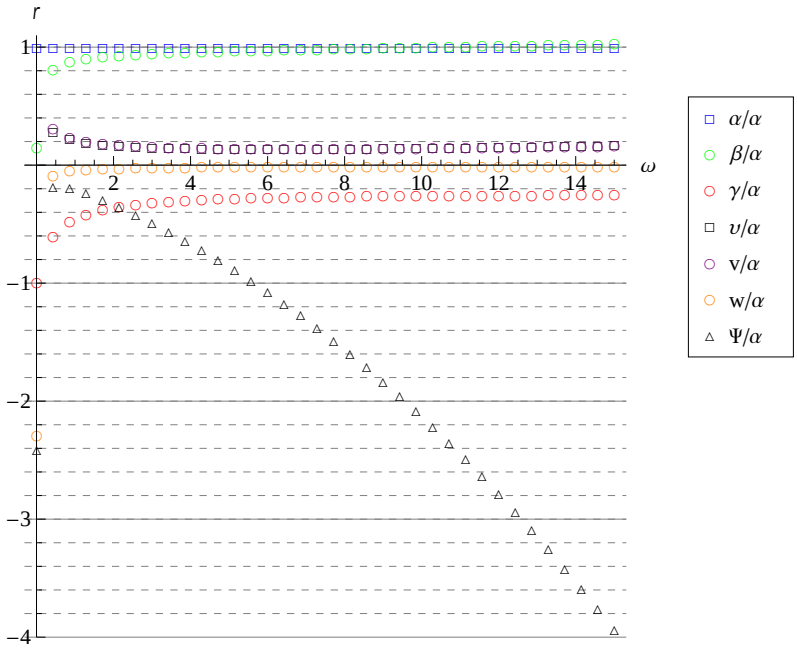

Figure B.1: *Modal coefficients for branch 1, with the shear angle* Ψ *is included.*

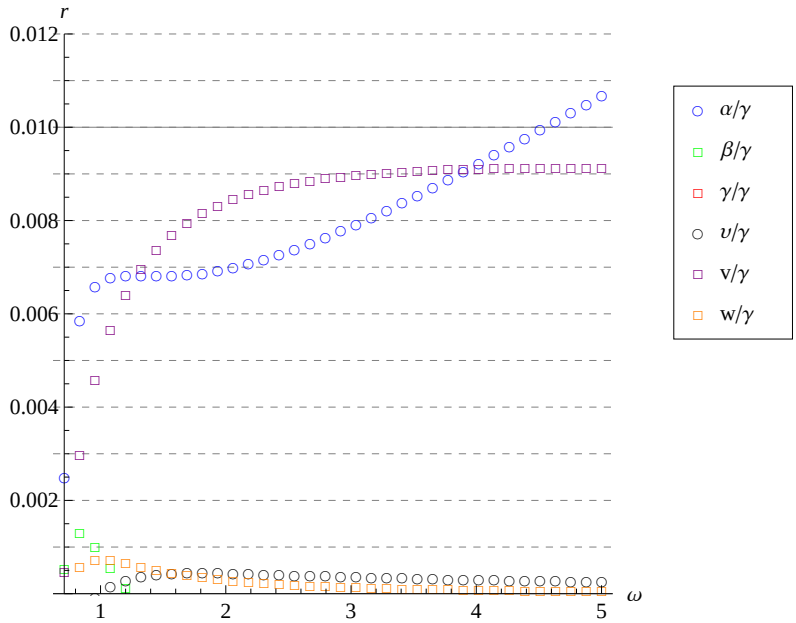

Figure B.2: *Modal coefficients for branch 7, zoomed.*

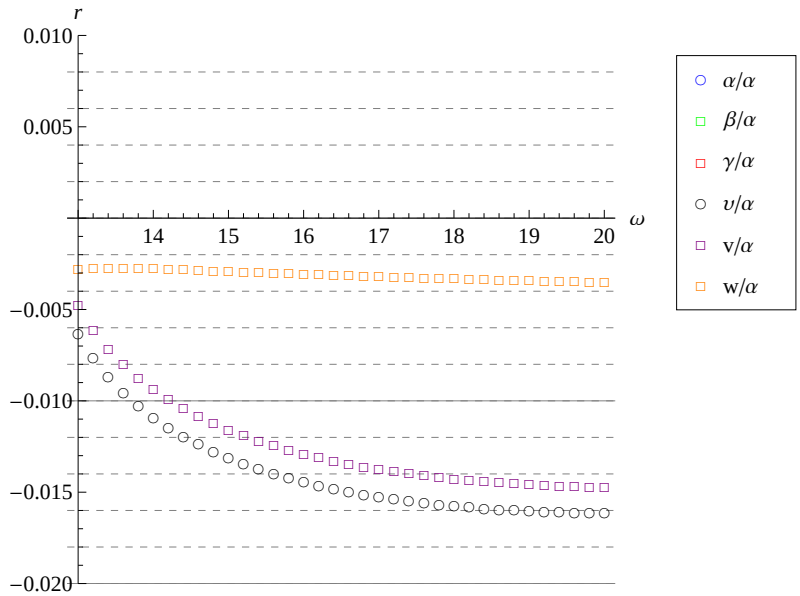

Figure B.3: *Modal coefficients for branch 9, zoomed.*

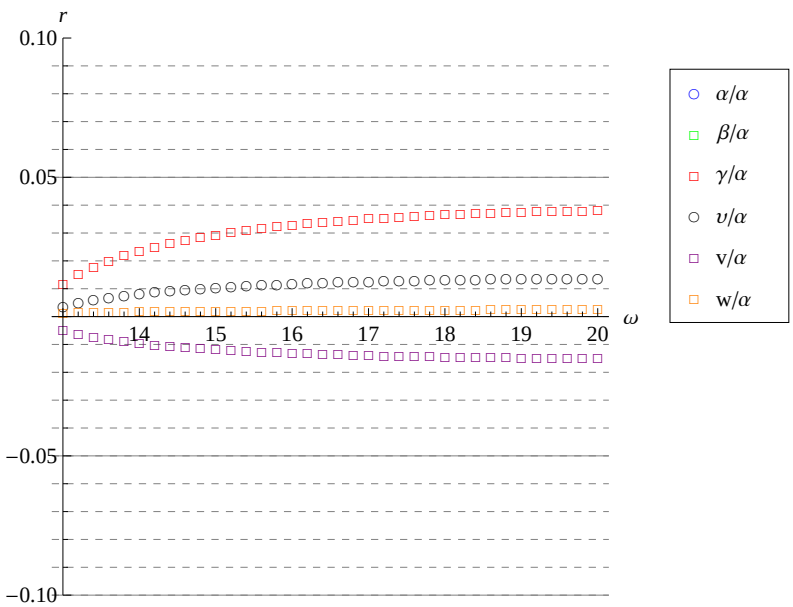

Figure B.4: *Modal coefficients for branch 10, zoomed.*

B.3 Cut-on frequencies

Setting the wave number to zero reduced the dispersion equation to:

$$
\begin{aligned}
0 = {} & \frac{1}{4(1+\nu)^3} d^2\omega^4 \Big(16\kappa^2\lambda + d^2\kappa^4\lambda + 3d^2\kappa^2\lambda\tau^2 + 2d^2\lambda\tau^4 - 2d^2\kappa^2\omega^2 - 32\lambda\omega^2 - 2d^2\kappa^2\lambda\omega^2 \\
& - 2d^2\kappa^2\nu\omega^2 - 4d^2\tau^2\omega^2 - 2d^2\lambda\tau^2\omega^2 - 4d^2\nu\tau^2\omega^2 + 4d^2\omega^4 + 4d^2\nu\omega^4\Big) \\
& \Big(2d^2\kappa^4 + 16\kappa^2\lambda + 2d^2\kappa^4\nu + 16\kappa^2\lambda\nu + 2d^2\kappa^2\tau^2 + d^2\kappa^2\lambda\tau^2 + 4d^2\kappa^2\nu\tau^2 + 2d^2\kappa^2\nu^2\tau^2 + d^2\lambda\tau^4 \\
& + d^2\lambda\nu\tau^4 - 4d^2\kappa^2\omega^2 - 16\lambda\omega^2 - 6d^2\kappa^2\nu\omega^2 - 16\lambda\nu\omega^2 - 2d^2\kappa^2\nu^2\omega^2 - 2d^2\tau^2\omega^2 \\
& - d^2\lambda\tau^2\omega^2 - 4d^2\nu\tau^2\omega^2 - d^2\lambda\nu\tau^2\omega^2 - 2d^2\nu^2\tau^2\omega^2 + 2d^2\omega^4 + 4d^2\nu\omega^4 + 2d^2\nu^2\omega^4\Big)
\end{aligned} \tag{B.2}
$$

Which has the exact solutions:

$$k^{(IV)} = 0 \tag{B.3}$$

$$
\begin{aligned}
k = {} & \pm\frac{1}{2\sqrt{d^2(1+\nu)}}\Big(16\lambda + d^2\left(2\kappa^2(2+\nu) + (2+\lambda+2\nu)\tau^2\right) \pm \Big(\lambda^2\left(16+d^2\tau^2\right)^2 + 4d^4\left(\kappa^2\nu - (1+\nu)\tau^2\right)^2 \\
& - 4d^2\lambda\left(-16+d^2\tau^2\right)\left(-\kappa^2\nu + (1+\nu)\tau^2\right)\Big)^{1/2}\Big)^{1/2}
\end{aligned} \tag{B.4}
$$

$$
\begin{aligned}
k = {} & \pm\frac{1}{2\sqrt{d^2(1+\nu)}}\Big(d^2\kappa^2 + 16\lambda + d^2\kappa^2\lambda + d^2\kappa^2\nu + 2d^2\tau^2 + d^2\lambda\tau^2 + 2d^2\nu\tau^2 \pm \Big(-4d^2\lambda(1+\nu)\Big(d^2\kappa^4 \\
& + 2d^2\tau^4 + \kappa^2\left(16+3d^2\tau^2\right)\Big) + \left(16\lambda + d^2\left(\kappa^2(1+\lambda+\nu) + (2+\lambda+2\nu)\tau^2\right)\right)^2\Big)^{1/2}\Big)^{1/2}
\end{aligned} \tag{B.5}
$$

Appendix

C

CD